Valence transition and superconductivity in the extended periodic Anderson model

Dissertation

zur Erlangung des akademischen Grades
Doctor rerum naturalium (Dr. rer. nat.)

vorgelegt

der Fakultät Mathematik und Naturwissenschaften
der Technischen Universität Dresden

von

M.Sc. Phan Van Nham
geb. am 10 Februar, 1980 in Thaibinh, Vietnam

Dresden, 2009

Institut für Theoretische Physik
Technische Universität Dresden, 01062 Dresden.

Berichterstatter

1. Gutachter: **Prof. Klaus W. Becker**
   Institut für Theoretische Physik
   Technische Universität Dresden, 01062 Dresden.

2. Gutachter: **Prof. Holger Fehske**
   Institut für Physik
   Ernst-Moritz-Arndt-Universität Greifswald, 17487 Greifswald.

3. Gutachter: **Prof. Wolfram Brenig**
   Institut für Theoretische Physik
   Technische Universität Braunschweig, 38106 Braunschweig.

Eingereicht am 05.02.2009

Tag der Verteidigung 04.05.2009

Abstract

In this thesis, an extended periodic Anderson model with an additional local Coulomb repulsion Ufc between localized f electrons and conduction electrons is investigated by use of the projector-based renormalization method (PRM). First, it is shown that the model in one dimension shows a valence transition, which becomes sharper, when the energy of the f level approaches the Fermi level. The transition becomes also enhanced, when the hybridization V between the localized and conduction electrons decreases, for the case that the total number of electrons is fixed. In the two-dimensional case, one finds a similar valence transition behavior. However, in the valence transition regime also a superconducting phase may occur. To investigate this phase, we start from an Hamiltonian which includes small gauge symmetry breaking fields. We derive renormalization equations, from which the superconducting pairing functions are self-consistently determined. Our analytical and numerical results show that d-wave superconductivity becomes dominant in the valence transition regime. This confirms the suggestion by Miyake that valence fluctuations may lead to superconductivity in the Ce based heavy-fermion systems under high pressure.

Kurzfassung

In dieser Arbeit wird mit Hilfe der projektiven Renormierungsmethode (PRM) ein erweitertes periodische Anderson Modell untersucht, das zusätzlich eine Coulomb-Abstoßung zwischen den lokalisierten f-Elektronen und den Leitungselektronen enthält. In einer Dimension zeigt das Modell einen Valenzübergang, wenn sich die Energie des f-Niveaus der Fermienergie nähert. Der Übergang wird ebenfalls schärfer, wenn bei festgehaltener Gesamtelektronenzahl die Hybridisierung V zwischen den lokalisierten und den Leitungselekronen abnimmt. In zwei Dimensionen findet man ein ähnliches Valenzübergangsverhalten. Allerdings kann zusätzlich eine supraleitende Phase im Valenzübergangsgebiet auftreten. Um die supraleitende Phase zu untersuchen, betrachten wir einen Hamiltonoperator mit kleinen zusätzlichen Feldern, die die Eichsymmetrie brechen. Wir leiten Renormierungsgleichungen her, aus denen sich die supraleitenden Paarfunktionen selbstkonsistent bestimmen lassen. Unsere analytischen und numerischen Reultate zeigen, dass im Valenzübergangsgebiet d-Wellen-Supraleitung dominiert. Dies bestätigt eine Vermutung von Miyake, dass Valenzfluktuationen in Ce-basierten Schwerfermionensystemen bei hohen Drücken zur Supraleitung führen können.

Contents

List of Figures

Chapter 1

Introduction

Superconductivity was first discovered in 1911 by Heike Kamerlingh Onnes [1] while he was studying the resistance of mercury. At the temperature of 4.2K, he observed that the resistance suddenly disappeared and became unmeasurable in a small temperature regime. For some decades later there was no theoretical understanding of the superconducting mechanism except the classical interpretation of London's equations of the Meissner effect [2]. Only in 1950, the first phenomenological theory of superconductivity was proposed by Landau and Ginzburg [3]. This theory, which is called Ginzburg-Landau theory of superconductivity, had great success in explaining the macroscopic properties of superconductors. In particular, Abrikosov [4] showed that the Ginzburg-Landau theory predicts the division of superconductors into the two categories now referred to as Type I and Type II superconductors. Seven years later, the complete microscopic theory of superconductivity was finally proposed by Bardeen, Cooper and Schrieffer (BCS) [5]. The BCS theory explained the superconducting current as a superfluid of Cooper pairs, i.e., pairs of electrons interacting through the exchange of phonons. This theory is successfully applied to most superconducting elements which are now called conventional superconductors.

Since the discovery of the high temperature superconductors [6] as well as of superconductivity in heavy fermion systems [7], physicists realized that the BCS theory

is not always applicable. These compounds are called unconventional superconductors. After years of debate and experimental measurements, now it is believed that the pairing symmetry in the unconventional superconductors has not always s-wave symmetry as in the conventional superconductors but also d-wave or other more complex symmetries. Therefore, the discovery of new mechanisms for superconductivity in the unconventional superconductors has been one of the most attractive problems in condensed matter physics. Investigating the phase diagrams that express the dependence of the ordering temperatures (magnetic, superconducting, etc.) on external control parameters (pressure, composition, etc.) of the unconventional superconductors shows that superconductivity is often closely linked to magnetism. In particular, a number of studies in f-electron systems showed that the superconducting state is often located close to the threshold of magnetism [8, 9]. These findings suggest that the mechanism that forms Cooper pairs can be of magnetic origin. That means, an electron, which carries its own magnetic moment, will produce a large polarization of its surroundings. This polarization produces a local magnetic field which can be felt by a second electron. If the relative orientation of the spins is appropriate, an attractive interaction will occur.

While the magnetic superconducting mechanism in the f-electron systems is still controversially discussed, the new discovery of superconductivity in Ce-based narrow-band metals [10, 13, 11, 14, 15] under high pressure has shown that the superconducting picture is more complicated. As an example, let us look at the pressure dependence of the superconducting critical temperatures of $CeCu_2(Si_{1-x}Ge_x)_2$ [16] as shown in Fig. 1.1. At small pressure, the Ce $4f$ orbitals are singly occupied and carry a static moment which is subject to long-range antiferromagnetic order (open circles for $x = 0.1$ and open squares for $x = 0.25$). When the pressure is increased, the hybridization between the $4f$ orbitals and conduction bands is enhanced which leads to dynamical frustration (Kondo spin-flips) and suppresses long-range order. The first superconducting dome emerges close to the edge of the antiferromagnetic state. So, one believes that magnetically mediated pairing may induce superconductivity (red dome). Further increasing the hybridization between the localized and conduction electrons by increasing the hydrostatic pressure leads the

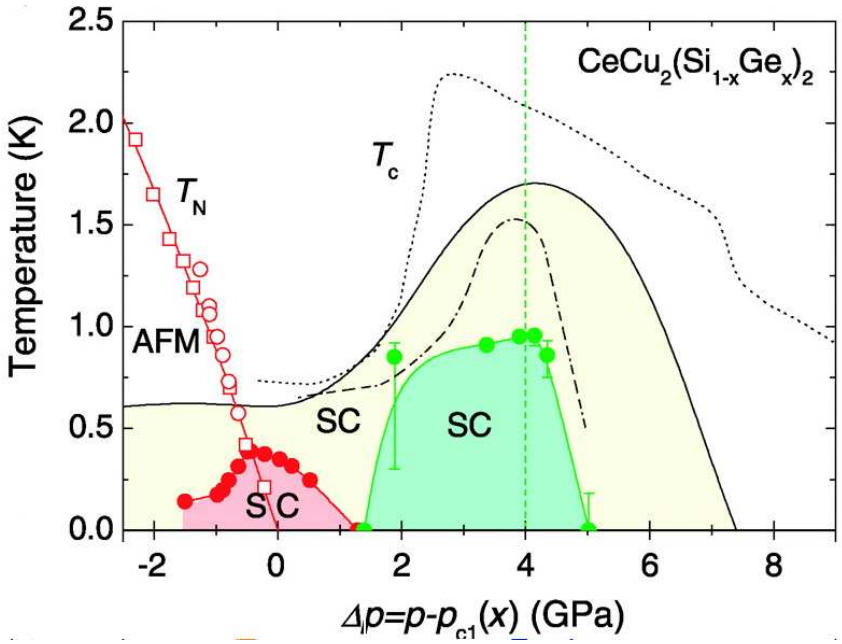

Figure 1.1: Experimental phase diagram of $CeCu_2(Si_{1-x}Ge_x)_2$, which shows antiferromagnetic (AFM) and superconducting (SC) transition temperatures versus relative pressure $\Delta p = p - p_{c1}$ (p_{c1} is the critical pressure at which magnetic order is fully suppressed). Open symbols show the AFM transition temperature (T_N) for $x = 0.1$ (circles, $p_{c1} = 1.5$GPa) and for $x = 0.25$ (squares, $p_{c1} = 2.4$GPa). Closed circles show the SC transition temperature (T_c) for $x = 0.1$. T_c is also shown for $x = 1$ (solid line, $p_{c1} = 11.5$GPa) and for $x = 0$ (dotted line from [10] and dashed-dotted line from [11], $p_{c1} = 0.4$GPa). The approximate location of the volume collapse observed in [12] is indicated by a vertical dashed line at $\Delta p = 4$GPa.

systems to an intermediate valence state. That means, the $4f$ electrons delocalize through stronger hybridization with ligand states and occupy wider energy bands at the Fermi energy. The transition from the integer valence to the intermediate valence configuration may proceed through a first-order phase transition that involves a collapse of the unit cell volume with no change in lattice symmetry (green dashed vertical line). In this regime, a second superconducting dome opens with a higher critical temperature than the former one. It is believed that here the superconductivity may be mediated by the valence fluctuations. For small doping, $x = 0.1$ (closed symbols), the two superconducting domes are

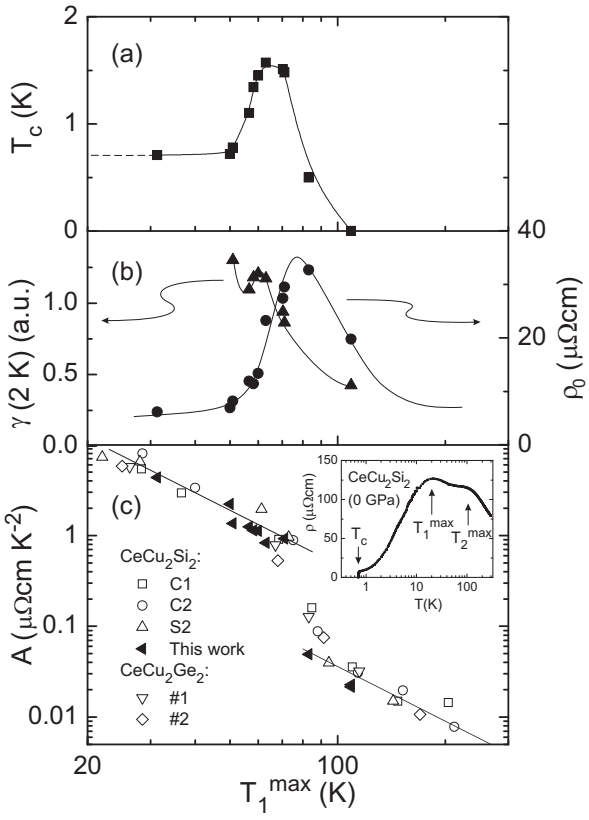

Figure 1.2: (a) Bulk superconducting transition temperature T_c, (b) residual resistivity ρ_0, Summerfield coefficient γ, and (c) prefactor A of the resistivity law $\rho \sim AT^2$ are shown for $CeCu_2Si_2$ and $CeCu_2Ge_2$ as function of $T_1^{\max}$. The meaning of $T_1^{\max}$ is explained in the text.

completely separated. On the other hand, in the case of $x = 1$ (solid line), or un-doping, $x = 0$ (dotted line [10] or dashed dotted line [12]), the two domes are smeared out and overlap. Nevertheless, the secondary dome is still dominant and has a maximum value at a pressure close to p_v, at which the volume collapse was observed [17].

In order to bring forward more evidence that valence fluctuations mediate superconductivity in the Ce-based heavy fermion under high pressure, the dependence of key properties of $CeCu_2Si_2$ on $T_1^{\max}$, i.e., the temperature value defined in the inset of Fig. 1.2(c), at which the resistivity ρ shows its maximum, is presented in Fig. 1.2 [12]. According to reference [12], $T_1^{\max}$ depends linearly on the external pressure in the second superconducting dome. Therefore the key properties in Fig.1.2 as function of $T_1^{\max}$ and as function of the external pressure are identical [12]. Comparison of Fig. 1.2(a) and Fig. 1.2(b) shows that in the regime of $T_1^{\max}$, at which the superconducting critical temperature reaches its maximum, the residual resistivity ρ_0 becomes enhanced. Moreover, the coefficient A of the T^2 law of the resistivity ρ decreases rapidly in the same $T_1^{\max}$ regime, see Fig. 1.2(c).

Since A scales as $(m^*/m)^2$ in the strongly correlated limit, one has [18],

$$\frac{m^*}{m} = \frac{1 - n_f/2}{1 - n_f}, \tag{1.1}$$

where n_f being the f-occupation number of the Ce ions. We see that the rapid decrease of A in Fig. 1.2(c) is related to the sharp change of the Ce valence. Note that the gain in the residual resistivity ρ_0 can be understood as a many-particle effect which enhances the impurity potential. It also is proportional to the valence susceptibility $-(\partial n_f/\partial \epsilon_f)_\mu$, where ϵ_f is the atomic f level of the Ce ion and μ is chemical potential [19]. Thus the enhancement of ρ_0 close to the peak of T_c in the high pressure regime of heavy fermion compounds can directly be related to the degree of sharpness of the valence change.

The abrupt change of the valence of Ce ion in the heavy fermion systems under high pressure was qualitatively described by including a large Coulomb repulsion U_{fc} (represented by pink arrows in Fig. 1.3) between localized f and conduction electrons [20]. Increasing the applied pressure the localized electron energy ϵ_f is shifted closer to the Fermi level E_F. There will be a point in which the effective f-level reaches the Fermi level $\epsilon_f + n_f U_{fc} \approx E_F$ and the f-band will start to become empty. Here, n_f is again the average occupation of the localized electrons. Therefore, on an individual $4f$ hole site, the repulsion caused by U_{fc} disappears and the density of conduction electrons will increase, as shown in Fig. 1.3(b). This extra screening of the conduction electron density is not strictly localized on the atom, but extends onto the neighboring sites. The f electrons on Ce atoms in the neighborhood of the hole site will feel an increased repulsion (represented by the thicker pink arrows). Thus it would be energetically favorable to transfer the f electrons into the delocalized conduction band. This self-reinforcing tendency to transfer electrons from the localized to conduction bands explains intuitively the abrupt change in n_f for larger Coulomb repulsion U_{fc} [21, 22].

The origin of superconductivity mediated by the valence fluctuations in the heavy fermion systems is illustrated in Figs. 1.3(c-d). Due to the applied pressure, an isolated pair of $4f^0$ holes, separated by two lattice positions with an intervening filled $4f^1$ site, can occur. It is accompanied by their clouds of conduction electrons which will overlap at

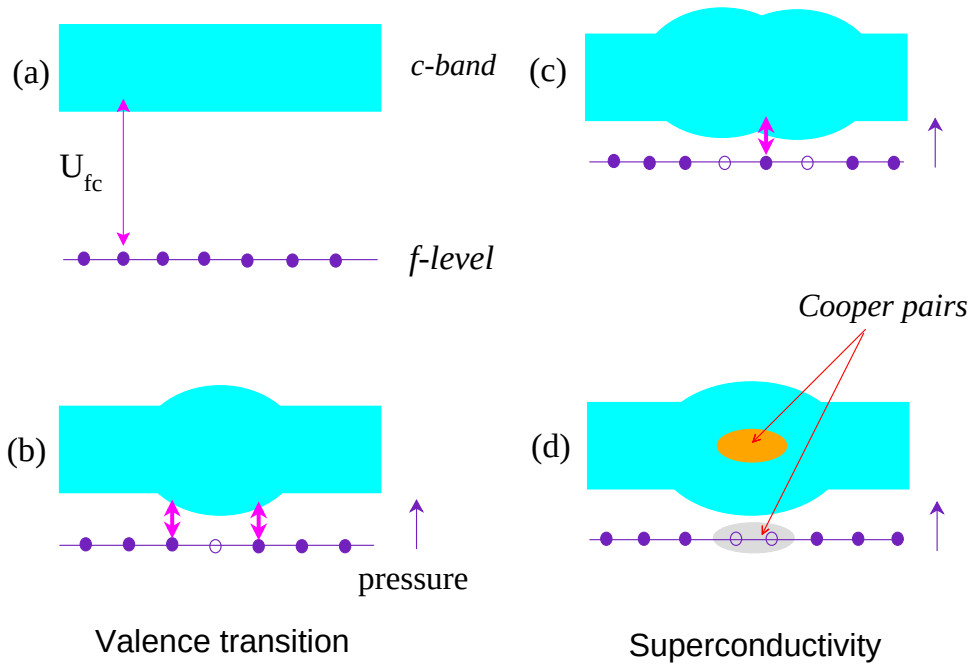

Figure 1.3: Graphical representation of valence transition of f electrons in the presence of Coulomb repulsion U_{fc} with conduction electrons. (a) f-level is far below the Fermi level and all sites are filled. (b) Under high pressure, the f-level reaches the Fermi level and the f electrons start to transfer into the conduction band. Empty $4f^0$ sites will be screened by the conduction electrons. (c) and (d) show how an attraction can raise, which forms Cooper pairs of $4f$ holes and conduction electrons as well.

the intermediate site and further increase the Coulomb repulsion at that point. It would therefore be energetically favorable for the two $4f$ holes to move on neighboring sites. Thus, an attractive interaction between $4f$ holes results. The attractive interaction between localized holes is equivalent to that of conduction electrons. A couple of conduction electrons as well as of localized holes can be considered as Cooper pairs. This argument gives an intuitive understanding of the origin of the valence-fluctuation mechanism of superconductivity.

The origin of superconductivity mediated by enhanced charge fluctuations caused by repulsive interaction in a multiband systems was first proposed as a possible mechanism

of superconductivity in high-T_c cuprates [23]. Motivated by further study of this mechanism [24, 25], the relationship between valence fluctuation and superconductivity in heavy fermion systems was initially put on a theoretical footing by Miyake in 1998 by including an extra term which represents the Coulomb repulsion U_{fc} between the localized-f and the conduction-c electrons into the periodic Anderson model (PAM) [26]. Solving this extended periodic Anderson model (EPAM) in three dimensions by a slave-boson mean-field approximation, the authors in [21] found that valence fluctuations were considerably enhanced by a moderate strength of U_{fc} when the Coulomb repulsion between localized electrons on the same site was assumed to be infinitely large. The valence fluctuations occur if the f-electron level ϵ_f is tuned relative to the Fermi level. In a mean-field approximation, this special value of ϵ_f is of the order of half of the bandwidth. Associated with the rapid valence change, d-wave superconductivity was found. Thus the authors pointed out the possibility of superconductivity caused by valence fluctuations. This scenario could explain various properties found in $CeCu_2Si_2$, at least qualitatively [27]. Solving the one-dimensional EPAM by use of the density matrix renormalization group (DMRG), the authors in [22] also obtained the valence instability. However, it occurred when U_{fc} was larger than the conduction bandwidth and the f-electron energy ϵ_f was deeper than the lower bound of the conduction band. In this case, only singlet pairing superconducting correlation functions were considered by assuming that the investigated system can be described in analogy to the single-band Tomonaga-Luttinger liquid. The obtained results showed that in the sharp valence transition regime, the superconducting correlation functions for singlet pairing become dominant. This once more affirmed that the EPAM can be used as a possible explanation of superconductivity due to the valence fluctuations.

Recently, the EPAM has also been studied in the dynamical mean field theory (DMFT), combined with exact diagonalization for infinite dimensions [28]. The obtained results are in agreement with the ones found by the DMRG method. The work was done by the same group for the EPAM in two dimensions by applying the fluctuation-exchange approximation. It showed that in the weak coupling region (modest strength of U_{fc}), a charge density

wave was also instable which may cause superconductivity as well [29]. Therefore, it is still unclear whether in the weak coupling or in the strong coupling regime, superconductivity due to the valence fluctuations occurs in the EPAM. That means, other possible theoretical methods should also be used to study this problem.

In this thesis, we use a recently developed projector based renormalization method (PRM) [30] to investigate the valence transition and superconductivity of the EPAM. The PRM derives a solvable effective Hamiltonian by deriving and solving renormalization equations using unitary transformations. The method has already been used to study the valence transition in the PAM [31]. There, in the case of a fixed chemical potential, a drastic change of the f-occupation from integral to mixed valence is found. This transition can possibly be explained as a collapse of the large Fermi surface of the heavy fermion state which incorporates not only the conduction electrons but also the localized electrons. Nevertheless, due to the complicated process of deriving the renormalization equations for the strongly correlated systems, various approximations had to be applied and no solution could be obtained for degeneracy $\nu_f = 2$. To overcome these restrictions and simplify the renormalization process we use an extended version of the PRM based on choosing a suitable generator [32, 33]. For this generator, we can restrict ourselves to second order renormalization contributions during the unitary transformations, and instead of difference equations we obtain differential equations which can easily be solved.

The thesis is organized as follows. In the next chapter we briefly describe the EPAM, which is the PAM including the Coulomb repulsion between conduction and localized electrons. Chapter 3 introduces the PRM. Its application to the EPAM is left to chapter 4. The numerical results for one-dimensional case are presented in chapter 5. There, we discuss the renormalized dispersion relation of the conduction electrons as well as the valence transition. Analytic calculations of the superconducting energy gaps and superconducting pairing functions based on the results of the PRM are presented in chapter 6. In chapter 7, we discuss the numerical results for d-wave superconducting energy gaps in two dimensions. Finally, chapter 8 contains our conclusions.

Chapter 2

Extended periodic Anderson model (EPAM)

As discussed in the introductory chapter, there are strong indications for an interrelation of superconductivity and the abrupt change in the valence of the Ce ion in the Ce-based heavy fermion systems under high pressure. Therefore, the extended periodic Anderson model (EPAM) was proposed in [26] with the expectation that the Coulomb interaction between the conduction electrons and the localized electrons can explain the abrupt change in Ce f occupation. That model is described as follows

$$\begin{aligned}\mathcal{H} = &(\varepsilon_f - \mu)\sum_{i,m} f^\dagger_{im} f_{im} + \sum_{\mathbf{k},m}(\varepsilon_{\mathbf{k}} - \mu) c^\dagger_{\mathbf{k}m} c_{\mathbf{k}m} \\ &+ \frac{1}{\sqrt{N}}\sum_{\mathbf{k},i,m} V_{\mathbf{k}}\left(f^\dagger_{im} c_{\mathbf{k}m}\, e^{\mathrm{i}\mathbf{k}\mathbf{R}_i} + \text{h.c.}\right) + U_{fc}\sum_{i,m,m'} n^c_{im} n^f_{im'} + U_f \sum_{\substack{i \\ m\neq m'}} n^f_{im} n^f_{im'}.\end{aligned} \tag{2.1}$$

Here $f^\dagger_{im}$ (f_{im}) and $c^\dagger_{\mathbf{k}m}$ ($c_{\mathbf{k}m}$) are creation (annihilation) operators of f-electrons at site i and conduction electrons with wave vector $\mathbf{k}$, respectively. Angular momentum and spin indices of the electrons are combined into the index m (of degeneracy ν_f) which is assumed to be equal for f and c electrons for simplicity. The excitation energies of f and conduction electrons are denoted by ε_f and $\varepsilon_{\mathbf{k}}$. The chemical potential is μ which is used for adjusting the total electron density. N is number of lattice sites and the Fourier

transformation of c operators is defined by

$$c^\dagger_{\mathbf{k}m} = \frac{1}{\sqrt{N}} \sum_i c^\dagger_{im} e^{i\mathbf{k}\mathbf{R}_i}. \tag{2.2}$$

A hybridization of strength $V_\mathbf{k}$ between localized and delocalized electrons is described by the third term. In general, $V_\mathbf{k}$ may depend on $\mathbf{k}$ [34, 35], but for simplification a $\mathbf{k}$-independent V is used. The last two terms represent the local Coulomb repulsion between f electrons (U_f) and between f and conduction electrons (U_{fc}). Since $U_f \gg U_{fc}$, we assume that U_f is infinite, so that the f sites can either be empty or singly occupied. Due to the strong correlation between f-electrons, it is suitable to introduce Hubbard operators

$$\hat{f}^\dagger_{im} = f^\dagger_{im} \prod_{\tilde{m}(\neq m)} (1 - n^f_{i\tilde{m}}), \tag{2.3}$$

with $n^f_{im} = f^\dagger_{im} f_{im}$. The Hubbard operators do not obey the usual fermionic anticommutation relations, instead one has

$$[\hat{f}^\dagger_{im}, \hat{f}_{im}]_+ \;=\; \mathcal{D}_{im}, \tag{2.4}$$

where

$$\mathcal{D}_{im} \;=\; \prod_{\tilde{m}(\neq m)} (1 - f^\dagger_{i\tilde{m}} f_{i\tilde{m}}).$$

The quantity $\mathcal{D}_{im}$ is a local projection operator on f states at site i which are either empty or singly occupied with an electron with index m.

It is useful to separate this quantity into two parts, a projection operator $\mathcal{P}_0(i)$ on the empty f state at site i and the projection operator $\hat{n}^f_{im}$ on the singly occupied f-state, where one electron with index m is present. That means, $\mathcal{D}_{im}$ can be rewritten as

$$\mathcal{D}_{im} \;=\; \mathcal{P}_0(i) + \hat{n}^f_{im} \;=\; 1 - \sum_{\tilde{m}(\neq m)} \hat{n}^f_{i\tilde{m}}, \tag{2.5}$$

where we have defined

$$\mathcal{P}_0(i) \;=\; \prod_{\tilde{m}} (1 - f^\dagger_{i\tilde{m}} f_{i\tilde{m}}), \tag{2.6}$$

$$\hat{n}^f_{im} \;=\; \hat{f}^\dagger_{im} \hat{f}_{im} \;=\; f^\dagger_{im} f_{im} \prod_{\tilde{m}(\neq m)} (1 - f^\dagger_{i\tilde{m}} f_{i\tilde{m}}). \tag{2.7}$$

With $U_f \to \infty$ we rewrite the Hamiltonian (2.1) as

$$\begin{aligned}\mathcal{H} = (\varepsilon_f - \mu) \sum_{i,m} \hat{f}^\dagger_{im} \hat{f}_{im} + \sum_{\mathbf{k},m} (\varepsilon_{\mathbf{k}} - \mu) c^\dagger_{\mathbf{k}m} c_{\mathbf{k}m} \\ + \frac{1}{\sqrt{N}} \sum_{\mathbf{k},i,m} V \left(\hat{f}^\dagger_{im} c_{\mathbf{k}m}\, e^{\mathrm{i}\mathbf{k}\mathbf{R}_i} + \text{h.c.} \right) + U_{fc} \sum_{i,mm'} n^c_{im} \hat{n}^f_{im'}.\end{aligned} \tag{2.8}$$

For simplifying our further calculation, we use the identity

$$n^c_{im} \hat{n}^f_{im'} = n^c_{im} \langle \hat{n}^f_{im'} \rangle + \hat{n}^f_{im'} \langle n^c_{im} \rangle + \delta(n^c_{im}) \delta(\hat{n}^f_{im'}), \tag{2.9}$$

so that

$$\begin{aligned}\mathcal{H} = (\varepsilon_f + U_{fc} \langle n^c \rangle - \mu) \sum_{i,m} \hat{f}^\dagger_{im} \hat{f}_{im} + \sum_{\mathbf{k},m} \left(\varepsilon_{\mathbf{k}} + U_{fc} \langle \hat{n}^f \rangle - \mu \right)\ c^\dagger_{\mathbf{k}m} c_{\mathbf{k}m} \\ + \frac{1}{\sqrt{N}} \sum_{\mathbf{k},i,m} V \left(\hat{f}^\dagger_{im} c_{\mathbf{k}m}\, e^{\mathrm{i}\mathbf{k}\mathbf{R}_i} + \text{h.c.} \right) + U_{fc} \sum_{i,mm'} \delta(n^c_{im}) \delta(\hat{n}^f_{im'}) - U_{fc} N \langle n^c \rangle \langle \hat{n}^f \rangle.\end{aligned} \tag{2.10}$$

The influence of U_{fc} on the valence transition was first discussed in the impurity Anderson model [36]. In a mean field approximation, a discontinuous valence transition was obtained for some large values of U_{fc}. For the periodic Anderson model, there exist some studies of the effect of U_{fc} on valence fluctuations within Hartree-Fock like approximations [37, 38], slave boson, and large-N expansions [21]. In all these approaches, U_{fc} could explain a rapid change of the number of f-electrons as the f-level, ϵ_f, increases.

Without U_{fc}, (2.10) was successfully solved by the PRM in order to investigate the valence transition in the case of fixed chemical potential [31, 32]. In the case of small values of ν_f, the f occupation drastically changes which shows a breakdown of a mixed-valence state. On the other hand, without the hybridization term, the Hamiltonian (2.10) describes the Falicov-Kimball model, which has also been discussed in the framework of the PRM [39] in one dimension. The remarkable results show that there appears a gap, which is of the order of the Coulomb repulsion, U_{fc}, in the quasiparticle excitation energy of the conduction electrons. In the present work, the PRM is applied to (2.10) for the case that a Coulomb repulsion U_{fc} and a hybridization V terms between localized and conduction electrons are simultaneously present. Therefore, gaps in the quasiparticle spectrum of the conduction electrons can appear not only due to the Coulomb repulsion

but also due to the hybridization. The influence of the hybridization on valence transition as well as on superconductivity in the presence of the Coulomb interaction will also be discussed.

Chapter 3

Projector-based renormalization method

In this chapter, we present the concepts of the projector-based renormalization method (PRM). The PRM was firstly introduced for solving many particle systems [30] based on perturbation theory. The approach resembles Wegner's flow equation method [40] and the similarity renormalization by Wilson [41, 42] in some aspects. The PRM was successful in investigating superconductivity based on the electron-phonon interaction [43] as well as in the metal-insulator transition in the Holstein model [44]. Moreover, the PRM can be expanded by applying it to many-particle Hamiltonians such as the periodic Anderson model (PAM) in a non-perturbation way [45]. As a result, the PRM describes very well the behavior of heavy-fermion systems. The famous slave-boson mean field theory [46], solving for PAM, leads to an effectively free system consisting of two non-interacting fermionic quasi-particles. Here in contrast, in the PRM the periodic Anderson model is mapped onto an effective model that still takes into account electronic correlations. Thus, in principle both the mixed valence and the integral valence solution can be found [31]. A slight modification of this PRM version is found by choosing suitable generators of the unitary transformation. This modification is more adequate to investigate the periodic Anderson model. Here, the discrete unitary transformation in the former version is replaced by

a continuous one [32, 33]. This has the advantage that one can use available computer subroutines to solve the renormalized equations in differential form. The exact solution of the continuous approach in the framework of the PRM for the Fano-Anderson model is shown in Appendix A.

The PRM starts from the separation of a given many-particle Hamiltonian, $\mathcal{H} = \mathcal{H}_0 + \mathcal{H}_1$. It is assumed that the eigenvalues $E_n^{(0)}$ and the eigenvectors $|n\rangle$ of the unperturbed part $\mathcal{H}_0$

$$\mathcal{H}_0|n\rangle = E_n^{(0)}|n\rangle, \tag{3.1}$$

are known. They are used to investigate the corrections due to the presence of $\mathcal{H}_1$ in perturbation theory. The interaction Hamiltonian $\mathcal{H}_1$, which does not commute with $\mathcal{H}_0$, has off-diagonal matrix elements, $\langle n|\mathcal{H}_1|m\rangle \neq 0$ but no diagonal elements. The presence of the interaction Hamiltonian usually prevents an exact solution of the full Hamiltonian $\mathcal{H}$, so that approximations are necessary.

The goal of the PRM is to transform the initial Hamiltonian into an effective Hamiltonian $\mathcal{H}_\lambda$ which has no transition matrix elements with energy differences larger than a chosen cutoff $\lambda < \Lambda$. Here Λ is the largest energy difference between any two eigenstates of $\mathcal{H}_0$, which are connected by $\mathcal{H}_1$. The Hamiltonian $\mathcal{H}_\lambda$ is determined by a unitary transformation as

$$\mathcal{H}_\lambda = e^{X_\lambda}\,\mathcal{H}\,e^{-X_\lambda}, \tag{3.2}$$

which can also be written as a sum of two terms

$$\mathcal{H}_\lambda = \mathcal{H}_{0,\lambda} + \mathcal{H}_{1,\lambda}. \tag{3.3}$$

Here for $\mathcal{H}_{1,\lambda}$ all matrix elements $\langle n|\mathcal{H}_{1,\lambda}|m\rangle$ with energy differences $|E_n^\lambda - E_m^\lambda| > \lambda$ vanish, $\langle n|\mathcal{H}_{1,\lambda}|m\rangle = 0$, where E_n^λ and $|n\rangle$ are the new eigenvalues and eigenstates of $\mathcal{H}_{0,\lambda}$. Note that in this framework, neither $|n\rangle$ nor $|m\rangle$ have to be low-energy eigenstates of $\mathcal{H}_{0,\lambda}$. The unitary transformation (3.2) guarantees that the new Hamiltonian has the same eigenspectrum as the original one. To ensure the hermiticity of $\mathcal{H}_\lambda$, the generator X_λ of the unitary transformation satisfies $X_\lambda^\dagger = -X_\lambda$.

In the PRM, a crucial idea of the elimination of the transition matrix elements is carried out by defining projection operators

$$\mathbf{P}_\lambda \mathcal{A} = \sum_{\substack{m,n \\ |E_n^\lambda - E_m^\lambda| \leq \lambda}} |n\rangle\langle m| \, \langle n|\mathcal{A}|m\rangle. \tag{3.4}$$

Note that $\mathbf{P}_\lambda$ is a superoperator acting on ordinary operators $\mathcal{A}$ of the Hilbert space of the system. Therefore, $\mathbf{P}_\lambda$ can be interpreted as a projection operator in the Liouville space that is built up by all operators of the Hilbert space. In the expression (3.4), only states $|n\rangle$ and $|m\rangle$ satisfying $\left|E_n^\lambda - E_m^\lambda\right| \leq \lambda$ contribute to the transition matrix. The orthogonal complement of $\mathbf{P}_\lambda$, $\mathbf{Q}_\lambda = \mathbf{1} - \mathbf{P}_\lambda$, projects on the high-energy transitions of $\mathcal{A}$. To find an appropriate generator X_λ of the unitary transformation, we employ the condition that the matrix elements for transitions of $\mathcal{H}_\lambda$ with energy differences larger than λ vanish, *i.e.*,

$$\mathbf{Q}_\lambda \mathcal{H}_\lambda \;\; = \;\; 0, \tag{3.5}$$

has to be fulfilled.

With the chosen generator X_λ, the Hamiltonian $\mathcal{H}_\lambda$ can be evaluated by Eq. (3.2). It is convenient to perform the elimination procedure step-wise. In this procedure, each step reduces the cutoff energy λ by a small amount $\Delta\lambda$. Starting at the initial cutoff Λ, after the first step, all transitions with energy transfers between Λ and $\Lambda - \Delta\lambda$ are removed. The subsequent steps remove all transitions larger than $\Lambda - \Delta\lambda$, $\Lambda - 2\Delta\lambda$, and so on. The unitary transformation for the step from an intermediate cutoff λ to the new cutoff $\lambda - \Delta\lambda$ can be evaluated as follows

$$\mathcal{H}_{\lambda-\Delta\lambda} \;\; = \;\; e^{X_{\lambda,\Delta\lambda}} \, \mathcal{H}_\lambda \, e^{-X_{\lambda,\Delta\lambda}}, \tag{3.6}$$

where the generator $X_{\lambda,\Delta\lambda}$ is fixed by

$$\mathbf{Q}_{\lambda-\Delta\lambda} \mathcal{H}_{\lambda-\Delta\lambda} \;\; = \;\; 0, \tag{3.7}$$

in analogy to (3.2). This condition specifies that $\mathcal{H}_{\lambda-\Delta\lambda}$ contains no matrix elements which connect eigenstates of $\mathcal{H}_{0,\lambda-\Delta\lambda}$ with energy differences larger than $\lambda - \Delta\lambda$.

It turns out that the generator $X_{\lambda,\Delta\lambda}$ of the unitary transformation is not yet completely determined by Eqs. (3.6) and (3.7). Indeed, the low-energetic excitations included in $X_{\lambda,\Delta\lambda}$, namely the part $\mathbf{P}_{\lambda-\Delta\lambda}X_{\lambda,\Delta\lambda}$, can be chosen arbitrarily. In principle, the result of the renormalization scheme does not depend on the particular choice of the part $\mathbf{P}_{\lambda-\Delta\lambda}X_{\lambda,\Delta\lambda}$. However, in practice the particular choice of $\mathbf{P}_{\lambda-\Delta\lambda}X_{\lambda,\Delta\lambda}$ is important. If $\mathbf{P}_{\lambda-\Delta\lambda}X_{\lambda,\Delta\lambda} = 0$ is chosen, the minimal transformation is performed to match requirement (3.7). This choice has been used in [30] and also in the discrete version of the PRM [31]. However, in particular cases a non-zero choice for $\mathbf{P}_{\lambda-\Delta\lambda}X_{\lambda,\Delta\lambda}$ might help to circumvent problems in the evaluation of the renormalization equations. In the continuous version of the PRM [33], a non-zero $\mathbf{P}_{\lambda-\Delta\lambda}X_{\lambda,\Delta\lambda}$ is allowed and the generator $X_{\lambda,\Delta\lambda}$ can be written as follows

$$X_{\lambda,\Delta\lambda} = \mathbf{P}_{\lambda-\Delta\lambda}X_{\lambda,\Delta\lambda} + \mathbf{Q}_{\lambda-\Delta\lambda}X_{\lambda,\Delta\lambda}. \tag{3.8}$$

Here the part $\mathbf{Q}_{\lambda-\Delta\lambda}X_{\lambda,\Delta\lambda}$ ensures that Eq. (3.7) is fulfilled. An appropriate choice of the remaining part $\mathbf{P}_{\lambda-\Delta\lambda}X_{\lambda,\Delta\lambda}$ can be found in such a way that it almost completely eliminates all interaction parameters before the cutoff energy λ is reached. Therefore, the former part ($\mathbf{Q}_{\lambda-\Delta\lambda}X_{\lambda,\Delta\lambda}$) can be neglected.

Note that in general, new interaction terms can be generated in each renormalization step. This might allow the investigation of competing interactions which naturally emerge in the renormalization procedure. However, actual calculations require a closed set of renormalization equations. Thus it is assumed that the originally chosen operator structure of $\mathcal{H}_\lambda$ is invariant with respect to further unitary transformations. Therefore a factorization approximation has to be performed in order to trace back newly arising complicated operators to terms already appearing in the renormalization ansatz. Consequently, derived effective Hamiltonians might be limited in their possible applications to certain parameter regions, if important operators have not been included in the renormalization scheme for parameter values outside these regions.

Due to the mentioned procedure, the renormalization equations contain expectation values that must be calculated separately. In principle, these expectation values are

defined with respect to $\mathcal{H}_\lambda$ because the factorization approximation was employed for the renormalization step that transformed $\mathcal{H}_\lambda$ to $\mathcal{H}_{\lambda-\Delta\lambda}$. However, $\mathcal{H}_\lambda$ still contains interactions that prevent a straight evaluation of the expectation values. The easiest way to circumvent this difficulty is to neglect the interactions and to use the diagonal unperturbed part $\mathcal{H}_{0,\lambda}$ instead of $\mathcal{H}_\lambda$. This approach has been successfully applied to the Holstein model to investigate single particle excitations and phonon softening [47]. However, it turns out that often the interaction terms in $\mathcal{H}_\lambda$ are crucial for a proper calculation of the required expectation values. Therefore, we include interaction effects by calculating the expectation values with respect to the full Hamiltonian $\mathcal{H}$ instead of $\mathcal{H}_\lambda$. In this case, the renormalization equations need to be solved in a self-consistent manner because they depend on expectation values defined with the full Hamiltonian $\mathcal{H}$. They are not known from the very beginning but can be determined from the fully renormalized Hamiltonian $\tilde{\mathcal{H}} = \lim_{\lambda\to 0} \mathcal{H}_\lambda$ as follows:

The first way to evaluate the expectation values is based on the free energy that can be calculated either from the original $\mathcal{H}$ or the renormalized $\tilde{\mathcal{H}}$ Hamiltonian,

$$F = -\frac{1}{\beta} \ln \mathrm{Tr} e^{-\beta\mathcal{H}} = -\frac{1}{\beta} \ln \mathrm{Tr} e^{-\beta\tilde{\mathcal{H}}}, \tag{3.9}$$

since $\tilde{\mathcal{H}}$ is obtained from $\mathcal{H}$ by a unitary transformation. The desired expectation values can then be determined from the free energy by functional derivatives [43, 45].

The second one employs an additional unitary transformation for the operator variable $\mathcal{A}$

$$\langle \mathcal{A} \rangle = \frac{\mathrm{Tr}\left(\mathcal{A} e^{-\beta\mathcal{H}}\right)}{\mathrm{Tr} e^{-\beta\mathcal{H}}} = \frac{\mathrm{Tr}\left(\tilde{\mathcal{A}} e^{-\beta\tilde{\mathcal{H}}}\right)}{\mathrm{Tr} e^{-\beta\tilde{\mathcal{H}}}}. \tag{3.10}$$

Here we defined $\tilde{\mathcal{A}} = \lim_{\lambda\to 0} \mathcal{A}_\lambda$, where $\mathcal{A}_\lambda = e^{X_\lambda}\, \mathcal{A}\, e^{-X_\lambda}$. Therefore, additional renormalization equations need to be derived for the required operator variables $\mathcal{A}_\lambda$.

In order to derive renormalization equations for the λ-dependence of $\mathcal{H}_\lambda$ (and similar for $\mathcal{A}_\lambda$) one compares the λ-dependent coefficients of the respective operator terms in the renormalization ansatz (3.3) for $\mathcal{H}_\lambda$ at cut-off $\lambda - \Delta\lambda$ with those of the explicitly evaluated expression Eq. (3.6). In the case of $\Delta\lambda \to 0$, the difference equations reduce to

differential equations. The final step $\lambda \to 0$ determines the fully renormalized Hamiltonian $\mathcal{H}_{\lambda\to 0} = \mathcal{H}_{0,\lambda\to 0}$. The coefficients in the fully renormalized Hamiltonian depend on the initial parameter values of the original model at cutoff Λ. At $\lambda \to 0$ the interaction Hamiltonian $\mathcal{H}_1$ is completely vanished, $\mathcal{H}_{1,\lambda\to 0} = 0$.

The PRM is based on the general idea that the interaction terms of a many particle system $\mathcal{H}$ are eliminated by unitary transformations. This approach removes high energy transitions but does not reduce the Hilbert space. This is different to the poor man's scaling [48] which removes high energy states, and then the Hilbert space is changed. The similarity transformation of Wilson [41, 42] and the Wegner's flow equation method [40] start from *continuous* transformations in differential form. The present PRM is based on *discrete* transformations which lead to coupled difference equations. Moreover, the step-wise renormalization of the PRM allows a unified treatment on both sides of a quantum phase transition [44] which seems not to be possible in the flow equation method. The continuous transformation of Ref. [48] as discussed above also can be understood in the framework of the PRM [33].

Chapter 4

Renormalization of the EPAM

4.1 Generator of the unitary transformation

In order to derive the renormalization equations, at first we have to find an approximate expression for the generator of the unitary transformation (3.6). In this section, the generator is found for the EPAM based on the continuous transformation idea in (3.8). Let us start by formally writing down the Hamiltonian of the EPAM (Eq. (2.10)) as

$$\begin{aligned}\mathcal{H}_0 &= (\varepsilon_f + U_{fc}\langle n^c\rangle - \mu)\sum_{i,m}\hat{f}^\dagger_{im}\hat{f}_{im} + \sum_{\mathbf{k},m}(\varepsilon_{\mathbf{k}} + U_{fc}\langle\hat{n}^f\rangle - \mu)\; c^\dagger_{\mathbf{k}m}c_{\mathbf{k}m} \\ &- U_{fc}N\langle n^c\rangle\langle\hat{n}^f\rangle \end{aligned} \tag{4.1}$$

and

$$\mathcal{H}_1 = \frac{1}{\sqrt{N}}\sum_{\mathbf{k},i,m} V\left(\hat{f}^\dagger_{im}c_{\mathbf{k}m}\, e^{\mathrm{i}\mathbf{k}\mathbf{R}_i} + \text{h.c.}\right) + U_{fc}\sum_{\mathbf{kq},m} a_{\mathbf{k},\mathbf{k}+\mathbf{q},m}, \tag{4.2}$$

with

$$a_{\mathbf{k},\mathbf{k}+\mathbf{q},m} = \frac{1}{N}\delta(c^\dagger_{\mathbf{k}m}c_{\mathbf{k}+\mathbf{q},m})\sum_{i,m}\delta(\hat{f}^\dagger_{im'}\hat{f}_{im'})e^{-i\mathbf{q}\mathbf{R}_i}. \tag{4.3}$$

Here, the perturbation $\mathcal{H}_1$ only contains the fluctuation part of the Coulomb repulsion U_{fc}. In order to find an ansatz for $\mathcal{H}_\lambda$ we consider the following ansatz for the generator X_λ

$$X_\lambda \sim \frac{1}{\mathcal{L}_0}\mathcal{H}_1, \tag{4.4}$$

which is motivated by perturbation theory [30]. Here $\mathcal{L}_0$ is the unperturbed Liouville operator which is defined by $\mathcal{L}_0 A = [\mathcal{H}_0, A]$ for any operator variable A. For the operators in (4.2), we obtain

$$\begin{aligned} \mathcal{L}_0 a_{\mathbf{k},\mathbf{k}+\mathbf{q},m} &= (\varepsilon_{\mathbf{k}} - \varepsilon_{\mathbf{k}+\mathbf{q}}) a_{\mathbf{k},\mathbf{k}+\mathbf{q},m}, \\ \mathcal{L}_0 \hat{f}^\dagger_{\mathbf{k}m} c_{\mathbf{k}m} &= (\varepsilon_f - \varepsilon_{\mathbf{k}}) \hat{f}^\dagger_{\mathbf{k}m} c_{\mathbf{k}m}. \end{aligned} \tag{4.5}$$

As one can see from these equations, the operators $a_{\mathbf{k},\mathbf{k}+\mathbf{q},m}$ and $\hat{f}^\dagger_{\mathbf{k}m} c_{\mathbf{k}m}$ can be interpreted as eigenoperators of the Liouville operator $\mathcal{L}_0$. That means, the generator X_λ to first order would have the form

$$X_\lambda = \sum_{\mathbf{k}\mathbf{q},m} \mathcal{U}_{\mathbf{k},\mathbf{k}+\mathbf{q},\lambda} a_{\mathbf{k},\mathbf{k}+\mathbf{q},m} + \sum_{\mathbf{k},m} \mathcal{V}_{\mathbf{k},\lambda} (\hat{f}^\dagger_{\mathbf{k}m} c_{\mathbf{k}m} - \text{h.c.}), \tag{4.6}$$

where $\mathcal{U}_{\mathbf{k},\mathbf{k}+\mathbf{q},\lambda}$ and $\mathcal{V}_{\mathbf{k},\lambda}$ are prefactors. Thus, according to (4.6) and (3.2), an ansatz for $\mathcal{H}_\lambda$ should read

$$\mathcal{H}_\lambda \;=\; \mathcal{H}_{0,\lambda} + \mathcal{H}_{1,\lambda}, \tag{4.7}$$

with

$$\begin{aligned} \mathcal{H}_{0,\lambda} &= N\mu_{f,\lambda} \sum_m \left(\hat{f}^\dagger_m \hat{f}_m\right)_L + \sum_{\mathbf{k},m} \gamma_{\mathbf{k},\lambda} \left(\hat{f}^\dagger_{\mathbf{k}m} \hat{f}_{\mathbf{k}m}\right)_{\text{NL}} \\ &\quad + \sum_{\mathbf{k},m} \varepsilon_{\mathbf{k},\lambda}\; c^\dagger_{\mathbf{k}m} c_{\mathbf{k}m} + \sum_{\substack{i,j\neq i \\ mm'}} g_{ij,\lambda} \delta\hat{n}^f_{im} \delta\hat{n}^f_{jm'} + E_\lambda, \\ \mathcal{H}_{1,\lambda} &= \mathbf{P}_\lambda \mathcal{H}_1 \;=\; \mathbf{P}_\lambda \sum_{\mathbf{k},m} V_{\mathbf{k},\lambda} \;\left(\hat{f}^\dagger_{\mathbf{k}m} c_{\mathbf{k}m} + \text{h.c.}\right) + \mathbf{P}_\lambda \sum_{\mathbf{k}\mathbf{q},m} U_{\mathbf{k},\mathbf{k}+\mathbf{q},\lambda} a_{\mathbf{k},\mathbf{k}+\mathbf{q},m}, \end{aligned} \tag{4.8}$$

after all excitations with energies larger than cutoff λ have been eliminated. Here, $\mathbf{P}_\lambda$ is the projector in the Liouville space, which projects on the low-energy transitions smaller than λ with respect to the $\mathcal{H}_{0,\lambda}$. Note that due to the renormalization, an energy shift E_λ, an additional hopping term between different f sites

$$\left(\hat{f}^\dagger_{\mathbf{k}m} \hat{f}_{\mathbf{k}m}\right)_{\text{NL}} = \frac{1}{N} \sum_{i,j(\neq i)} \hat{f}^\dagger_{im} \hat{f}_{jm} e^{i\mathbf{k}(\mathbf{R}_i - \mathbf{R}_j)}, \tag{4.9}$$

as well as a new density-density interaction between localized electrons have been generated in $\mathcal{H}_{0,\lambda}$. The hopping term between different f sites can also be called nonlocal (NL) f particle-hole excitations in contrast to the local (L) one. They obey a simple relation

$$\left(\hat{f}^\dagger_{\mathbf{k}m}\hat{f}_{\mathbf{k}m}\right)_{\mathrm{NL}} + \left(\hat{f}^\dagger_{m}\hat{f}_{m}\right)_{L} = \hat{f}^\dagger_{\mathbf{k}m}\hat{f}_{\mathbf{k}m}, \tag{4.10}$$

with

$$\left(\hat{f}^\dagger_{m}\hat{f}_{m}\right)_{L} := \frac{1}{N}\sum_{\mathbf{k}} \hat{f}^\dagger_{\mathbf{k}m}\hat{f}_{\mathbf{k}m} = \frac{1}{N}\sum_{i} \hat{f}^\dagger_{im}\hat{f}_{im}. \tag{4.11}$$

Here, the Fourier transformation of f electrons has been introduced

$$\hat{f}^\dagger_{\mathbf{k}m} = \frac{1}{\sqrt{N}}\sum_{i} \hat{f}^\dagger_{im} e^{i\mathbf{k}\mathbf{R}_i}. \tag{4.12}$$

The initial parameter values of the original model (denoted by $\lambda = \Lambda$) are

$$\begin{aligned} &\mu_{f,\Lambda} = \epsilon_f + U_{fc}\langle n^c\rangle - \mu, \quad g_{ij,\Lambda} = 0, \quad \gamma_{\mathbf{k},\Lambda} = 0, \quad V_{\mathbf{k},\Lambda} = V, \\ &\varepsilon_{\mathbf{k},\Lambda} = \varepsilon_{\mathbf{k}} + U_{fc}\langle \hat{n}^f\rangle - \mu, \quad U_{\mathbf{k},\mathbf{k}+\mathbf{q},\Lambda} = U_{fc}, \quad E_\lambda = -NU_{fc}\langle n^c\rangle\langle \hat{n}^f\rangle. \end{aligned} \tag{4.13}$$

Next, we have to evaluate the action of the superoperator $\mathbf{P}_\lambda$ on the interaction operators, so that the requirement $\mathbf{Q}_\lambda\mathcal{H}_\lambda = 0$ is fulfilled. In order to find the excitation energies of $\mathcal{H}_{1,\lambda}$, we have to apply the unperturbed Liouville operator $\mathcal{L}_{0,\lambda}$ on $\left(\hat{f}^\dagger_{\mathbf{k}m}c_{\mathbf{k}m} + \mathrm{h.c.}\right)$ and $a_{\mathbf{k},\mathbf{k}+\mathbf{q},m}$. The resulting eigenvalues of $\mathcal{L}_{0,\lambda}$ can be understood as excitation energies due to the hybridization and the Coulomb interaction, respectively.

Considering the contribution of the hybridization term, we have

$$\begin{aligned} \mathcal{L}_{0,\lambda}\hat{f}^\dagger_{\mathbf{k}m}c_{\mathbf{k}m} &= [\mathcal{H}_{0,\lambda}, \hat{f}^\dagger_{\mathbf{k}m}c_{\mathbf{k}m}] \\ &= (\varepsilon_{f,\lambda} - \varepsilon_{\mathbf{k},\lambda})\,\hat{f}^\dagger_{\mathbf{k}m}c_{\mathbf{k}m} + \frac{1}{N^{3/2}}\sum_{\mathbf{p},ij}(1-\delta_{ij})\gamma_{\mathbf{p},\lambda}\hat{f}^\dagger_{im}D_{jm}c_{\mathbf{k}m}e^{i(\mathbf{k}-\mathbf{p})\mathbf{R}_j}e^{i\mathbf{p}\mathbf{R}_i} \\ &+ \frac{1}{N^{3/2}}\sum_{\mathbf{p},ij,m'}(1-\delta_{mm'})\gamma_{\mathbf{p},\lambda}\hat{f}^\dagger_{im}\hat{f}^\dagger_{jm}\hat{f}_{jm'}c_{\mathbf{k}m}e^{i(\mathbf{k}-\mathbf{p})\mathbf{R}_j}e^{i\mathbf{p}\mathbf{R}_i}, \end{aligned} \tag{4.14}$$

where additional contributions which lead to double occupied f sites cancel. The second and third term on the right hand side of Eq. (4.14) come from the special form of the anticommutator relations (2.4). From the second term of (4.14) we see that only f electron

operators, belonging to different sites $i \neq j$, contribute. Therefore we can replace the operator D_{jm} by its expectation value

$$D = \langle D_{jm} \rangle = 1 - \frac{\nu_f - 1}{\nu_f} \langle \hat{n}_j^f \rangle, \tag{4.15}$$

where the averaged occupation number of f electrons at site j, $\langle \hat{n}_j^f \rangle = \sum_m \langle \hat{f}_{jm}^\dagger \hat{f}_{jm}^\dagger \rangle$, enters. Note that the factor D is independent on j and m. By neglecting the spin-flip processes in (4.14), we obtain

$$\mathcal{L}_{0,\lambda} \hat{f}_{\mathbf{k}m}^\dagger c_{\mathbf{k}m} \;\; = \;\; (\varepsilon_{f,\lambda} + D\gamma_{\mathbf{k},\lambda} - \varepsilon_{\mathbf{k},\lambda})\, \hat{f}_{\mathbf{k}m}^\dagger c_{\mathbf{k}m}, \tag{4.16}$$

where

$$\varepsilon_{f,\lambda} = \mu_{f,\lambda} - D\bar{\gamma}_\lambda, \tag{4.17}$$

and $\bar{\gamma}_\lambda = \sum_{\mathbf{k}} \gamma_{\mathbf{k},\lambda}/N$ is the averaged f dispersion.

Similarly, we also obtain the excitation energies of the Coulomb repulsion between the f- and conduction electrons

$$\begin{aligned} \mathcal{L}_{0,\lambda} a_{\mathbf{k},\mathbf{k+q},m} &= (\varepsilon_{\mathbf{k},\lambda} - \varepsilon_{\mathbf{k+q},\lambda}) a_{\mathbf{k},\mathbf{k+q},m} \\ &\quad + \sum_{\mathbf{p}} (\gamma_{\mathbf{p},\lambda} - \gamma_{\mathbf{p-q},\lambda}) b_{\mathbf{k},\mathbf{k+q},\mathbf{p},m}, \end{aligned} \tag{4.18}$$

where

$$b_{\mathbf{k},\mathbf{k+q},\mathbf{p},m} = \frac{1}{N} \delta(c_{\mathbf{k}m}^\dagger c_{\mathbf{k+q},m}) \sum_{i,j(\neq i),m'} \delta(\hat{f}_{im'}^\dagger \hat{f}_{jm'}) e^{i\mathbf{q}\mathbf{R}_j + i\mathbf{p}(\mathbf{R}_i - \mathbf{R}_j)}. \tag{4.19}$$

The dispersion relation between f electrons in lowest order, $\gamma_{\mathbf{k},\lambda} \sim V^2/(\varepsilon_{\mathbf{k}} - \varepsilon_f)$, is small in the case of small hybridization V. So we can neglect the last term in Eq. (4.18), which simplifies our further calculation. Thus, to ensure that $\mathbf{Q}_\lambda \mathcal{H}_\lambda = 0$ is fulfilled, the hybridization as well as the Coulomb repulsion matrix elements should include additional θ-functions. Thus we can write

$$\begin{aligned} \mathcal{H}_{1,\lambda} = \mathbf{P}_\lambda \mathcal{H}_1 &= \sum_{\mathbf{k},m} \theta(\lambda - |\varepsilon_{f,\lambda} + D\gamma_{\mathbf{k},\lambda} - \varepsilon_{\mathbf{k},\lambda}|) V_{\mathbf{k},\lambda} \Big(\hat{f}_{\mathbf{k}m}^\dagger c_{\mathbf{k}m} + \text{h.c} \Big) \\ &\quad + \sum_{\mathbf{kq},m} \theta(\lambda - |\varepsilon_{\mathbf{k},\lambda} - \varepsilon_{\mathbf{k+q},\lambda}|) U_{\mathbf{k},\mathbf{k+q},\lambda} a_{\mathbf{k},\mathbf{k+q},m}. \end{aligned} \tag{4.20}$$

The included θ functions restrict the excitations to transition energies smaller than λ. With this expression of $\mathcal{H}_{1,\lambda}$, we can form the generator $X_{\lambda,\Delta\lambda}$ as it was done before in X_λ

$$X_{\lambda,\Delta\lambda} = \sum_{\mathbf{k},m} \alpha_{\mathbf{k}}(\lambda,\Delta\lambda)(\hat{f}^\dagger_{\mathbf{k}m} c_{\mathbf{k}m} - \text{h.c.}) + \sum_{\mathbf{kq},m} \beta_{\mathbf{k},\mathbf{k+q}}(\lambda,\Delta\lambda) a_{\mathbf{k},\mathbf{k+q},m}, \tag{4.21}$$

with new parameters $\alpha_{\mathbf{k}}(\lambda,\Delta\lambda)$ and $\beta_{\mathbf{k},\mathbf{k+q}}(\lambda,\Delta\lambda)$. Note that $\alpha_{\mathbf{k}}(\lambda,\Delta\lambda)$ and $\beta_{\mathbf{k},\mathbf{k+q}}(\lambda,\Delta\lambda)$ have to be chosen in such a way that the condition (3.7), $\mathbf{Q}_{\lambda-\Delta\lambda}\mathcal{H}_{\lambda-\Delta\lambda} = 0$, is satisfied. As discussed in the previous section, in the continuous version of the PRM, we choose $\mathbf{P}_{\lambda-\Delta\lambda} X_{\lambda,\Delta\lambda} \neq 0$. We make the following ansatz

$$\begin{aligned} \alpha_{\mathbf{k}}(\lambda,\Delta\lambda) &= \frac{A_{\mathbf{k},\lambda}\theta(\lambda - |A_{\mathbf{k},\lambda}|)}{\kappa(\lambda - |A_{\mathbf{k},\lambda}|)^2} V_{\mathbf{k},\lambda}\Delta\lambda, \\ \beta_{\mathbf{k},\mathbf{k+q}}(\lambda,\Delta\lambda) &= \frac{B_{\mathbf{k},\mathbf{k+q},\lambda}\theta(\lambda - |B_{\mathbf{k},\mathbf{k+q},\lambda}|)}{\kappa(\lambda - |B_{\mathbf{k},\mathbf{k+q},\lambda}|)^2} U_{\mathbf{k},\mathbf{k+q},\lambda}\Delta\lambda, \end{aligned} \tag{4.22}$$

where

$$A_{\mathbf{k},\lambda} = \varepsilon_{f,\lambda} + D\gamma_{\mathbf{k},\lambda} - \varepsilon_{\mathbf{k},\lambda}, \quad B_{\mathbf{k},\mathbf{k+q},\lambda} = \varepsilon_{\mathbf{k},\lambda} - \varepsilon_{\mathbf{k+q},\lambda}. \tag{4.23}$$

The constant κ in (4.22) denotes an energy constant to ensure that the parameters $\alpha_{\mathbf{k}}(\lambda,\Delta\lambda)$ and $\beta_{\mathbf{k},\mathbf{k+q}}(\lambda,\Delta\lambda)$ are dimensionless. In the limit of small $\Delta\lambda$, we expect an exponential decay for the interaction contributions in the renormalizing procedure due to the choice (4.22).

4.2 Renormalization equations

This section is devoted to derive the renormalization equations for the parameters of the Hamiltonian (4.8). For that purpose, we compare two different expressions of $\mathcal{H}_{\lambda-\Delta\lambda}$ in order to obtain a relation of the renormalized parameters between the cutoffs λ and $\lambda-\Delta\lambda$. The first expression of $\mathcal{H}_{\lambda-\Delta\lambda}$ is obtained by rewriting the renormalization ansatz (4.7)

at cutoff $\lambda - \Delta\lambda$

$$\begin{aligned}\mathcal{H}_{\lambda-\Delta\lambda} = &\sum_{\mathbf{k},m} \varepsilon_{\mathbf{k},\lambda-\Delta\lambda}\; c^\dagger_{\mathbf{k}m} c_{\mathbf{k}m} + N\mu_{f,\lambda-\Delta\lambda} \sum_m \left(\hat{f}^\dagger_m \hat{f}_m\right)_{\mathrm{L}} \\ &+ \sum_{\mathbf{k},m} \gamma_{\mathbf{k},\lambda-\Delta\lambda} \left(\hat{f}^\dagger_{\mathbf{k}m} \hat{f}_{\mathbf{k}m}\right)_{\mathrm{NL}} + \sum_{\substack{i,j\neq i\\ mm'}} g_{ij,\lambda-\Delta\lambda} \delta\hat{n}^f_{im} \delta\hat{n}^f_{jm'} + E_{\lambda-\Delta\lambda} \\ &+ \mathbf{P}_{\lambda-\Delta\lambda} \sum_{\mathbf{k},m} V_{\mathbf{k},\lambda-\Delta\lambda} \left(\hat{f}^\dagger_{\mathbf{k}m} c_{\mathbf{k}m} + \mathrm{h.c.}\right) + \mathbf{P}_{\lambda-\Delta\lambda} \sum_{\mathbf{k}\mathbf{q},m} U_{\mathbf{k},\mathbf{k}+\mathbf{q},\lambda-\Delta\lambda} a_{\mathbf{k},\mathbf{k}+\mathbf{q},m}.\end{aligned} \tag{4.24}$$

In Eq. (4.24), $\mathbf{P}_{\lambda-\Delta\lambda}$ is the projection operator in the Liouville space which projects on the lower energy transition smaller than $\lambda-\Delta\lambda$ with respect to the $\mathcal{H}_{0,\lambda-\Delta\lambda}$. That means, all excitations with energies larger than cutoff $\lambda - \Delta\lambda$ have been eliminated.

The second expression for $\mathcal{H}_{\lambda-\Delta\lambda}$ is obtained from the unitary transformation applied to $\mathcal{H}_\lambda$. From Eqs. (3.6) and (4.7) we have

$$\begin{aligned}\mathcal{H}_{\lambda-\Delta\lambda} = &\sum_{\mathbf{k},m} \varepsilon_{\mathbf{k},\lambda} e^{X_{\lambda,\Delta\lambda}}\; c^\dagger_{\mathbf{k}m} c_{\mathbf{k}m} e^{-X_{\lambda,\Delta\lambda}} + \sum_{\mathbf{k},m} \gamma_{\mathbf{k},\lambda} e^{X_{\lambda,\Delta\lambda}} \left(\hat{f}^\dagger_{\mathbf{k}m} \hat{f}_{\mathbf{k}m}\right)_{\mathrm{NL}} e^{-X_{\lambda,\Delta\lambda}} \\ &+ N\mu_{f,\lambda} \sum_m e^{X_{\lambda,\Delta\lambda}} \left(\hat{f}^\dagger_m \hat{f}_m\right)_{\mathrm{L}} e^{-X_{\lambda,\Delta\lambda}} + \sum_{\substack{i,j\neq i\\ mm'}} g_{ij,\lambda} e^{X_{\lambda,\Delta\lambda}} \delta\hat{n}^f_{im} \delta\hat{n}^f_{jm'} e^{-X_{\lambda,\Delta\lambda}} + E_\lambda \\ &+ \mathbf{P}_\lambda \sum_{\mathbf{k},m} V_{\mathbf{k},\lambda}\; e^{X_{\lambda,\Delta\lambda}} \left(\hat{f}^\dagger_{\mathbf{k}m} c_{\mathbf{k}m} + \mathrm{h.c.}\right) e^{-X_{\lambda,\Delta\lambda}} \\ &+ \mathbf{P}_\lambda \sum_{\mathbf{k}\mathbf{q},m} U_{\mathbf{k},\mathbf{k}+\mathbf{q},\lambda} e^{X_{\lambda,\Delta\lambda}} a_{\mathbf{k},\mathbf{k}+\mathbf{q},m} e^{-X_{\lambda,\Delta\lambda}}.\end{aligned} \tag{4.25}$$

Since $\alpha_{\mathbf{k}}(\lambda, \Delta\lambda)$ and $\beta_{\mathbf{k},\mathbf{k}+\mathbf{p}}(\lambda, \Delta\lambda)$ are proportional to $\Delta\lambda$, only the first order contributions in $X_{\lambda,\Delta\lambda}$ have to be considered in the elimination procedure. That means, for any operator A, we have

$$e^{X_{\lambda,\Delta\lambda}} A e^{-X_{\lambda,\Delta\lambda}} - A \approx \mathbf{X}_{\lambda,\Delta\lambda} A, \tag{4.26}$$

where $\mathbf{X}_{\lambda,\Delta\lambda}$ is a new superoperator, defined by $\mathbf{X}_{\lambda,\Delta\lambda} A = [X_{\lambda,\Delta\lambda}, A]$.

Applying (4.26) to all operators in the Hamiltonian (4.25), we obtain

$$
\begin{aligned}
e^{X_{\lambda,\Delta\lambda}}\, c^\dagger_{\mathbf{k}m}c_{\mathbf{k}m}e^{-X_{\lambda,\Delta\lambda}} &= c^\dagger_{\mathbf{k}m}c_{\mathbf{k}m} + \alpha_{\mathbf{k}}(\lambda,\Delta\lambda)(\hat{f}^\dagger_{\mathbf{k}m}c_{\mathbf{k}m} + \text{h.c.}) \\
&\quad + \sum_{\mathbf{q}} \beta_{\mathbf{k},\mathbf{k}+\mathbf{q}}(\lambda,\Delta\lambda)a_{\mathbf{k},\mathbf{k}+\mathbf{q},m} - \sum_{\mathbf{q}} \beta_{\mathbf{k}+\mathbf{q},\mathbf{k}}(\lambda,\Delta\lambda)a_{\mathbf{k}+\mathbf{q},\mathbf{k},m}, \\
e^{X_{\lambda,\Delta\lambda}} \left(\hat{f}^\dagger_m\hat{f}_m\right)_{\text{L}} e^{-X_{\lambda,\Delta\lambda}} &= \left(\hat{f}^\dagger_m\hat{f}_m\right)_{\text{L}} - \frac{1}{N}\sum_{\mathbf{p}} \alpha_{\mathbf{p}}(\lambda,\Delta\lambda)(\hat{f}^\dagger_{\mathbf{p}m}c_{\mathbf{p}m} + \text{h.c.}), \\
e^{X_{\lambda,\Delta\lambda}} \left(\hat{f}^\dagger_{\mathbf{k}m}\hat{f}_{\mathbf{k}m}\right)_{\text{NL}} e^{-X_{\lambda,\Delta\lambda}} &= \left(\hat{f}^\dagger_{\mathbf{k}m}\hat{f}_{\mathbf{k}m}\right)_{\text{NL}} - \alpha_{\mathbf{k}}(\lambda,\Delta\lambda)\Bigg[D\left(\hat{f}^\dagger_{\mathbf{k}m}c_{\mathbf{k}m} + \text{h.c.}\right) \\
&\quad + \left\langle \hat{f}^\dagger_{\mathbf{k}m}c_{\mathbf{k}m} + \text{h.c.}\right\rangle \Big[1 - D - \sum_{\tilde{m}(\neq m)} \left(\hat{f}^\dagger_{\tilde{m}}\hat{f}_{\tilde{m}}\right)_{\text{L}}\Big]\Bigg] \\
&\quad + \frac{1}{N}\sum_{\mathbf{p}} \alpha_{\mathbf{p}}(\lambda,\Delta\lambda)\Bigg[D(\hat{f}^\dagger_{\mathbf{p}m}c_{\mathbf{p}m} + \text{h.c.}) + \langle \hat{f}^\dagger_{\mathbf{p}m}c_{\mathbf{p}m} + \text{h.c.}\rangle \\
&\quad \times \Big[1 - D - \sum_{\tilde{m}(\neq m)} \left(\hat{f}^\dagger_{\tilde{m}}\hat{f}_{\tilde{m}}\right)_{\text{L}}\Big]\Bigg], \qquad (4.27) \\
e^{X_{\lambda,\Delta\lambda}}\delta\hat{n}^f_{im}\delta\hat{n}^f_{jm'}e^{-X_{\lambda,\Delta\lambda}} &= \delta\hat{n}^f_{im}\delta\hat{n}^f_{jm'}, \\
e^{X_{\lambda,\Delta\lambda}} \left(\hat{f}^\dagger_{\mathbf{k}m}c_{\mathbf{k}m} + \text{h.c.}\right) e^{-X_{\lambda,\Delta\lambda}} &= \left(\hat{f}^\dagger_{\mathbf{k}m}c_{\mathbf{k}m} + \text{h.c.}\right) + 2\alpha_{\mathbf{k}}(\lambda,\Delta\lambda)\Bigg[\left(\hat{f}^\dagger_{\mathbf{k}m}\hat{f}_{\mathbf{k}m}\right)_{\text{NL}} \\
&\quad + \left(\hat{f}^\dagger_m\hat{f}_m\right)_{\text{L}} - Dc^\dagger_{\mathbf{k}m}c_{\mathbf{k}m} - \left\langle c^\dagger_{\mathbf{k}m}c_{\mathbf{k}m}\right\rangle \Big[1 - D - \sum_{\tilde{m}(\neq m)} \left(\hat{f}^\dagger_{\tilde{m}}\hat{f}_{\tilde{m}}\right)_{\text{L}}\Big]\Bigg], \\
e^{X_{\lambda,\Delta\lambda}}a_{\mathbf{k},\mathbf{k}+\mathbf{q},m}e^{-X_{\lambda,\Delta\lambda}} &= a_{\mathbf{k},\mathbf{k}+\mathbf{q},m} + \frac{1}{N}\beta_{\mathbf{k}+\mathbf{q},\mathbf{k}}(\lambda,\Delta\lambda)\Bigg[C^{ff}_\rho(\mathbf{q})\left(c^\dagger_{\mathbf{k}+\mathbf{q},m}c_{\mathbf{k}+\mathbf{q},m} - c^\dagger_{\mathbf{k}m}c_{\mathbf{k}m}\right) \\
&\quad + \left(1 - 2\langle n^f\rangle\right)\left(\langle c^\dagger_{\mathbf{k}+\mathbf{q},m}c_{\mathbf{k}+\mathbf{q},m}\rangle - \langle c^\dagger_{\mathbf{k}m}c_{\mathbf{k}m}\rangle\right)\frac{1}{N}\sum_{i\sigma'} \hat{f}^\dagger_{i\sigma'}\hat{f}_{i\sigma'} \\
&\quad - \left(\langle c^\dagger_{\mathbf{k}m}c_{\mathbf{k}m}\rangle - \langle c^\dagger_{\mathbf{k}+\mathbf{q},m}c_{\mathbf{k}+\mathbf{q},m}\rangle\right)\left(\langle n^f\rangle - 2\langle n^f\rangle^2\right)\Bigg].
\end{aligned}
$$

Here

$$
C^{ff}_\rho(\mathbf{q}) = \frac{1}{N}\sum_{\substack{ij\\mm'}} \langle \delta\hat{n}^f_{im}\delta\hat{n}^f_{jm'}\rangle e^{i\mathbf{q}(\mathbf{R}_i - \mathbf{R}_j)}. \qquad (4.28)
$$

In deriving the above expressions, additional factorization approximations were used in order to keep only operators, which are also present in the renormalization ansatz (4.24).

The spin-flip contributions have also been neglected. Substituting these results into the second expression of $\mathcal{H}_{\lambda-\Delta\lambda}$ and comparing it with the first one, we obtain the following difference equations

$$
\begin{aligned}
\varepsilon_{\mathbf{k},\lambda-\Delta\lambda} &= \varepsilon_{\mathbf{k},\lambda} - 2\Big[DV_{\mathbf{k},\lambda}\alpha_{\mathbf{k}}(\lambda,\Delta\lambda) + \frac{1}{N}\sum_{\mathbf{q}m'} C_{\rho}^{ff}(\mathbf{q})U_{\mathbf{k},\mathbf{k}+\mathbf{q},\lambda}\beta_{\mathbf{k}+\mathbf{q},\mathbf{k}}(\lambda,\Delta\lambda)\Big],\\
\mu_{f,\lambda-\Delta\lambda} &= \mu_{f,\lambda} + \frac{\nu_f - 1}{N}\sum_{\mathbf{k}}(\gamma_{\mathbf{k},\lambda} - \bar{\gamma}_{\lambda})\alpha_{\mathbf{k}}(\lambda,\Delta\lambda)\langle \hat{f}^{\dagger}_{\mathbf{k}m}c_{\mathbf{k}m} + \text{h.c.}\rangle\\
&\quad + \frac{2}{N}\sum_{\mathbf{k}} V_{\mathbf{k},\lambda}\alpha_{\mathbf{k}}(\lambda,\Delta\lambda)[1 + (\nu_f - 1)\langle c^{\dagger}_{\mathbf{k}m}c_{\mathbf{k}m}\rangle]\\
&\quad + (1 - 2\langle n^f\rangle)\frac{2}{N^2}\sum_{\mathbf{q}\mathbf{k}m'} U_{\mathbf{k},\mathbf{k}+\mathbf{q},\lambda}\beta_{\mathbf{k}+\mathbf{q},\mathbf{k}}(\lambda,\Delta\lambda)\langle c^{\dagger}_{\mathbf{k}+\mathbf{q},m'}c_{\mathbf{k}+\mathbf{q},m'}\rangle,\\
\gamma_{\mathbf{k},\lambda-\Delta\lambda} &= \gamma_{\mathbf{k},\lambda} + 2DV_{\mathbf{k},\lambda}\alpha_{\mathbf{k}}(\lambda,\Delta\lambda),\\
g_{\mathbf{k},\lambda-\Delta\lambda} &= g_{\mathbf{k},\lambda} + \frac{1}{N}\sum_{\mathbf{q},m} U_{\mathbf{q},\mathbf{q}+\mathbf{k},\lambda}\beta_{\mathbf{q}+\mathbf{k},\mathbf{q}}(\lambda,\Delta\lambda)\left(\langle c^{\dagger}_{\mathbf{q}+\mathbf{k},m}c_{\mathbf{q}+\mathbf{k},m}\rangle - \langle c^{\dagger}_{\mathbf{q}m}c_{\mathbf{q}m}\rangle\right)\\
&\quad - \frac{1}{N^2}\sum_{\mathbf{q}\mathbf{k}',m} U_{\mathbf{q},\mathbf{q}+\mathbf{k}',\lambda}\beta_{\mathbf{q}+\mathbf{k}',\mathbf{q}}(\lambda,\Delta\lambda)\left(\langle c^{\dagger}_{\mathbf{q}+\mathbf{k}',m}c_{\mathbf{q}+\mathbf{k}',m}\rangle - \langle c^{\dagger}_{\mathbf{q}m}c_{\mathbf{q}m}\rangle\right),\\
V_{\mathbf{k},\lambda-\Delta\lambda} &= V_{\mathbf{k},\lambda} - A_{\mathbf{k},\lambda}\alpha_{\mathbf{k}}(\lambda,\Delta\lambda),\\
U_{\mathbf{k},\mathbf{k}+\mathbf{q},\lambda-\Delta\lambda} &= U_{\mathbf{k},\mathbf{k}+\mathbf{q},\lambda} - B_{\mathbf{k},\mathbf{k}+\mathbf{q},\lambda}\beta_{\mathbf{k}+\mathbf{q},\mathbf{k}}(\lambda,\Delta\lambda),\\
E_{\lambda-\Delta\lambda} &= E_{\lambda} - \sum_{\mathbf{k}m}(1-D)\Big[(\gamma_{\mathbf{k},\lambda} - \bar{\gamma}_{\lambda})\langle \hat{f}^{\dagger}_{\mathbf{k}m}c_{\mathbf{k}m} + \text{h.c.}\rangle + 2V_{\mathbf{k}\lambda}\langle c^{\dagger}_{\mathbf{k}m}c_{\mathbf{k}m}\rangle\Big]\alpha_{\mathbf{k}}(\lambda,\Delta\lambda)\\
&\quad - \frac{2}{N}\sum_{\mathbf{q}\mathbf{k},m} U_{\mathbf{k},\mathbf{k}+\mathbf{q},\lambda}\beta_{\mathbf{k}+\mathbf{q},\mathbf{k}}(\lambda,\Delta\lambda)\langle c^{\dagger}_{\mathbf{k}+\mathbf{q},m}c_{\mathbf{k}+\mathbf{q},m}\rangle\left(C_{\rho}^{ff}(\mathbf{q}) - \langle\hat{n}^f\rangle^2\right).
\end{aligned}
\tag{4.29}
$$

Here, the action of the projection operator has been included in $\alpha_{\mathbf{k}}(\lambda,\Delta\lambda)$ as well as in $\beta_{\mathbf{k},\mathbf{k}+\mathbf{q}}(\lambda,\Delta\lambda)$. These equations can be integrated step by step from $\lambda = \Lambda$ to $\lambda = 0$, in order to find the fully renormalized parameters. Nevertheless, $\alpha_{\mathbf{k}}(\lambda,\Delta\lambda)$ and $\beta_{\mathbf{k},\mathbf{k}+\mathbf{q}}(\lambda,\Delta\lambda)$ are proportional to $\Delta\lambda$. For this purpose, we consider the limit of very small steps $\Delta\lambda$ and define

$$\tilde{\alpha}_{\mathbf{k},\lambda} = \lim_{\Delta\lambda\to 0}\frac{\alpha_{\mathbf{k}}(\lambda,\Delta\lambda)}{\Delta\lambda}, \tag{4.30}$$

$$\tilde{\beta}_{\mathbf{k},\mathbf{k}+\mathbf{q},\lambda} = \lim_{\Delta\lambda\to 0}\frac{\beta_{\mathbf{k},\mathbf{k}+\mathbf{q}}(\lambda,\Delta\lambda)}{\Delta\lambda}. \tag{4.31}$$

So, in the limit of $\Delta\lambda \to 0$, the above difference equations become differential equations, which simplify the further evaluation

$$
\begin{aligned}
\frac{d\varepsilon_{\mathbf{k},\lambda}}{d\lambda} &= 2\Big[DV_{\mathbf{k},\lambda}\tilde{\alpha}_{\mathbf{k},\lambda} + \frac{1}{N}\sum_{\mathbf{q}} C_\rho^{ff}(\mathbf{q}) U_{\mathbf{k},\mathbf{k}+\mathbf{q},\lambda}\tilde{\beta}_{\mathbf{k}+\mathbf{q},\mathbf{k},\lambda}\Big], \\
\frac{d\mu_{f,\lambda}}{d\lambda} &= -\frac{1}{N}\sum_{\mathbf{k}}(\gamma_{\mathbf{k},\lambda} - \bar{\gamma}_\lambda)(\nu_f - 1)\tilde{\alpha}_{\mathbf{k},\lambda}\langle \hat{f}^\dagger_{\mathbf{k}m} c_{\mathbf{k}m} + \text{h.c.}\rangle \\
&\quad -\frac{2}{N}\sum_{\mathbf{k}} V_{\mathbf{k},\lambda}\tilde{\alpha}_{\mathbf{k},\lambda}[1 + (\nu_f - 1)\langle c^\dagger_{\mathbf{k}m} c_{\mathbf{k}m}\rangle] \\
&\quad -(1 - 2\langle n^f\rangle)\frac{2}{N^2}\sum_{\mathbf{q}\mathbf{k}m'} U_{\mathbf{k},\mathbf{k}+\mathbf{q},\lambda}\tilde{\beta}_{\mathbf{k}+\mathbf{q},\mathbf{k},\lambda}\langle c^\dagger_{\mathbf{k}+\mathbf{q},m'} c_{\mathbf{k}+\mathbf{q},m'}\rangle, \\
\frac{d\gamma_{\mathbf{k},\lambda}}{d\lambda} &= -2V_{\mathbf{k},\lambda}\tilde{\alpha}_{\mathbf{k},\lambda}, \qquad (4.32) \\
\frac{dg_{\mathbf{k},\lambda}}{d\lambda} &= -\frac{1}{N}\sum_{\mathbf{q},m} U_{\mathbf{q},\mathbf{q}+\mathbf{k},\lambda}\tilde{\beta}_{\mathbf{q}+\mathbf{k},\mathbf{q},\lambda}\left(\langle c^\dagger_{\mathbf{q}+\mathbf{k},m} c_{\mathbf{q}+\mathbf{k},m}\rangle - \langle c^\dagger_{\mathbf{q}m} c_{\mathbf{q}m}\rangle\right) \\
&\quad -\frac{1}{N^2}\sum_{\mathbf{q}\mathbf{k}',m} U_{\mathbf{q},\mathbf{q}+\mathbf{k}',\lambda}\tilde{\beta}_{\mathbf{q}+\mathbf{k}',\mathbf{q},\lambda}\left(\langle c^\dagger_{\mathbf{q}+\mathbf{k}',m} c_{\mathbf{q}+\mathbf{k}',m}\rangle - \langle c^\dagger_{\mathbf{q}m} c_{\mathbf{q}m}\rangle\right), \\
\frac{dV_{\mathbf{k},\lambda}}{d\lambda} &= A_{\mathbf{k},\lambda}\tilde{\alpha}_{\mathbf{k},\lambda}, \\
\frac{dU_{\mathbf{k},\mathbf{k}+\mathbf{q},\lambda}}{d\lambda} &= B_{\mathbf{k},\mathbf{k}+\mathbf{q},\lambda}\tilde{\beta}_{\mathbf{k},\mathbf{k}+\mathbf{q},\lambda}, \\
\frac{dE_\lambda}{d\lambda} &= \sum_{\mathbf{k}m}(1 - D)\Big[(\gamma_{\mathbf{k},\lambda} - \bar{\gamma}_\lambda)\langle \hat{f}^\dagger_{\mathbf{k}m} c_{\mathbf{k}m} + \text{h.c.}\rangle + 2V_{\mathbf{k}\lambda}\langle c^\dagger_{\mathbf{k}m} c_{\mathbf{k}m}\rangle\Big]\tilde{\alpha}_{\mathbf{k}\lambda} \\
&\quad + \frac{2}{N}\sum_{\mathbf{q}\mathbf{k},m} U_{\mathbf{k},\mathbf{k}+\mathbf{q},\lambda}\tilde{\beta}_{\mathbf{k}+\mathbf{q},\mathbf{k},\lambda}\langle c^\dagger_{\mathbf{k}+\mathbf{q},m} c_{\mathbf{k}+\mathbf{q},m}\rangle\left(C_\rho^{ff}(\mathbf{q}) - \langle \hat{n}^f\rangle^2\right).
\end{aligned}
$$

Note that the last equation for the energy shift E_λ follows from the comparison of the remaining c numbers in (4.24) and (4.25). The differential renormalization equations (4.32) still depend on expectation values $\langle c^\dagger_{\mathbf{k}m} c_{\mathbf{k}m}\rangle$, $\langle \hat{f}^\dagger_{\mathbf{k}m} c_{\mathbf{k}m} + \text{h.c.}\rangle$, $\langle \hat{n}^f\rangle$, and D, as well as on the correlation function $C_\rho^{ff}(\mathbf{k})$, which have to be determined simultaneously. In the following, all the expectation values are assumed to be independent on λ. They will be evaluated in the way, as was discussed in the previous section, Eq. (3.10). Solving the differential equations (4.32) for cut-off $\lambda \to 0$, all contributions from the hybridization and

the Coulomb repulsion between localized and conduction electrons have completely been included in the parameters of a renormalized Hamiltonian. The effective Hamiltonian is written as follows

$$\begin{aligned}\tilde{\mathcal{H}} := \mathcal{H}_{\lambda\to 0} = &\sum_{\mathbf{k},m} \tilde{\varepsilon}_{\mathbf{k}}\ c^{\dagger}_{\mathbf{k}m} c_{\mathbf{k}m} + \tilde{\mu}_f \sum_{i,m} \hat{f}^{\dagger}_{im}\hat{f}_{im} + \tilde{E} \\ &+ \sum_{\substack{i,j\neq i\\ mm'}} \tilde{g}_{ij}\delta\hat{n}^f_{im}\delta\hat{n}^f_{jm'} + \sum_{\mathbf{k},m} \tilde{\gamma}_{\mathbf{k}} \left(\hat{f}^{\dagger}_{\mathbf{k}m}\hat{f}_{\mathbf{k}m}\right)_{NL}.\end{aligned} \tag{4.33}$$

Note that the operator part $\mathcal{H}_{1,\lambda}$ has completely disappeared due to the renormalization procedure.

4.3 Renormalization of $\tilde{\mathcal{H}}$

Using the formalism from (3.10) with the effective Hamiltonian (4.33), we still can not evaluate the expectation values, because there exist simultaneously interaction term $\tilde{g}_{ij}$ and dispersion relation $\tilde{\gamma}_{\mathbf{k}}$ between different f-sites. This prevents us from straightforwardly determining the density of the f-electrons as well as their density-density correlation. Therefore, a further elimination is required. Moreover, if we are concerned in a mixed valence regime with $\langle\hat{n}^f\rangle$ arround 1/2 and U_{fc} larger than V, in principle, $\tilde{\gamma}_{\mathbf{k}}$ should be small in comparison to $\tilde{g}_{ij}$. So we can consider the former part as perturbation in the effective Hamiltonian (4.33) and continue to apply the PRM a second time in order to solve the model. In the Hamiltonian (4.33), only the first term describes conduction electrons and completely commutes with the other parts. Therefore, in order to simplify the calculation, we can consider only the f-part in the Hamiltonian (4.33). The starting point for the renormalization reads as follows

$$\tilde{\mathcal{H}}^f_{\lambda} = \tilde{\mathcal{H}}^f_{0,\lambda} + \tilde{\mathcal{H}}^f_{1,\lambda}, \tag{4.34}$$

with

$$\tilde{\mathcal{H}}^f_{0,\lambda} = \tilde{\mu}^f_\lambda \sum_{i,m} \hat{f}^\dagger_{im}\hat{f}_{im} + \sum_{\substack{i,j\neq i\\ mm'}} \tilde{g}_{ij,\lambda}\delta\hat{n}^f_{im}\delta\hat{n}^f_{jm'} + \tilde{E}_\lambda, \tag{4.35}$$

$$\tilde{\mathcal{H}}^f_{1,\lambda} = \sum_{\substack{i,j\neq i\\ m}} \tilde{\gamma}_{ij,\lambda}\hat{f}^\dagger_{im}\hat{f}_{jm}. \tag{4.36}$$

Here we have rewritten the hopping term between the f-electrons on different sites in the real space

$$\tilde{\gamma}_{ij,\lambda} = \frac{1}{N}\sum_{\mathbf{k}} \tilde{\gamma}_{\mathbf{k},\lambda} e^{-i\mathbf{k}(\mathbf{R}_i-\mathbf{R}_j)}. \tag{4.37}$$

The initial conditions for the second PRM, according to (4.33), are

$$\tilde{\mu}^f_\Lambda = \tilde{\mu}_f, \quad \tilde{g}_{ij,\Lambda} = \tilde{g}_{ij}, \quad \tilde{\gamma}_{ij,\Lambda} = \tilde{\gamma}_{ij}, \quad \tilde{E}_\Lambda = \tilde{E}. \tag{4.38}$$

In order to derive the renormalization equations for the parameters of the Hamiltonian (4.34), we first apply the unitary transformation

$$\tilde{\mathcal{H}}^f_{\lambda-\Delta\lambda} = e^{X^f_{\lambda,\Delta\lambda}}\tilde{\mathcal{H}}^f_\lambda e^{-X^f_{\lambda,\Delta\lambda}}, \tag{4.39}$$

where $X^f_{\lambda,\Delta\lambda}$ is the new generator.

Similar to the renormalization before, the generator $X^f_{\lambda,\Delta\lambda}$ can be found

$$X^f_{\lambda,\Delta\lambda} = \sum_{\substack{i,j\neq i\\ m}} \alpha^f_{ij}(\lambda,\Delta\lambda)\mathcal{A}^f_{m,ij}. \tag{4.40}$$

Here

$$\mathcal{A}^f_{m,ij} = \frac{2}{\omega_{ij,\lambda}}\left(\sum_{\substack{i,r\neq i\\ n}} \tilde{g}_{ri,\lambda}\delta\hat{n}^f_{rn}\hat{f}^\dagger_{im}\hat{f}_{jm} - \sum_{\substack{i,r\neq j\\ n}} \tilde{g}_{rj,\lambda}\hat{f}^\dagger_{im}\hat{f}_{jm}\delta\hat{n}^f_{rn}\right), \tag{4.41}$$

with the prefactor

$$\alpha^f_{ij}(\lambda,\Delta\lambda) = \frac{\omega_{ij,\lambda}\gamma_{ij,\lambda}\theta(\lambda-|\omega_{ij,\lambda}|)}{(\lambda-|\omega_{ij,\lambda}|)^2}\Delta\lambda, \tag{4.42}$$

where

$$\omega_{ij,\lambda} = \pm 2 \left(\sum_{\substack{r,s\neq\{i,j\} \\ nn'}} (\tilde{g}_{ri,\lambda}\tilde{g}_{si,\lambda} - 2\tilde{g}_{ri,\lambda}\tilde{g}_{sj,\lambda} + \tilde{g}_{rj,\lambda}\tilde{g}_{sj,\lambda}) \langle \delta\hat{n}^f_{rn}\delta\hat{n}^f_{sn'}\rangle \right)^{1/2}. \tag{4.43}$$

Similarly as before, we find the renormalization equations for the parameters of the Hamiltonian by comparing $\tilde{\mathcal{H}}^f_\lambda$ in Eq. (4.34) at cutoff $\lambda - \Delta\lambda$ and $\tilde{\mathcal{H}}^f_{\lambda-\Delta\lambda}$ by the unitary transformation (4.39)

$$\begin{aligned}
\frac{d\tilde{\mu}^f_\lambda}{d\lambda} &= -\frac{2D}{N^3} \sum_{\substack{\{jlr\}\neq i \\ m}} \left[\tilde{\gamma}_{lj,\lambda}(\tilde{g}_{ir,\lambda} - \tilde{g}_{il,\lambda}) \frac{\tilde{\alpha}^f_{rl,\lambda}}{\omega_{rl,\lambda}} - \tilde{\gamma}_{rl,\lambda}(\tilde{g}_{il,\lambda} - \tilde{g}_{ij,\lambda}) \frac{\tilde{\alpha}^f_{lj,\lambda}}{\omega_{lj,\lambda}} \right] \langle \hat{f}^\dagger_{rm}\hat{f}_{jm}\rangle, \\
\frac{d\tilde{g}_{ij,\lambda}}{d\lambda} &= -\frac{4}{N^2} \sum_{\substack{r,s\neq r \\ m}} (\tilde{g}_{sj,\lambda} - \tilde{g}_{rj,\lambda})(\tilde{g}_{ir,\lambda} - \tilde{g}_{is,\lambda}) \frac{\tilde{\alpha}^f_{rs,\lambda}}{\omega_{rs,\lambda}} \langle \hat{f}^\dagger_{rm}\hat{f}_{sm}\rangle, \\
\frac{d\tilde{\gamma}_{ij,\lambda}}{d\lambda} &= \omega_{ij,\lambda}\tilde{\alpha}^f_{ij,\lambda},
\end{aligned} \tag{4.44}$$

where

$$\tilde{\alpha}^f_{ij,\lambda} = \lim_{\Delta\lambda\to 0} \frac{\alpha^f_{ij}(\lambda, \Delta\lambda)}{\Delta\lambda}. \tag{4.45}$$

Solving the set of differential equations (4.44) with initial conditions (4.38), we can find the renormalized parameters for $\lambda \to 0$. Thus, the renormalized Hamiltonian for the f-electrons reads

$$\tilde{\tilde{\mathcal{H}}}^f = \tilde{\tilde{\mu}}^f \sum_{i,m} \hat{f}^\dagger_{im}\hat{f}_{im} + \sum_{\substack{i,j\neq i \\ mm'}} \tilde{\tilde{g}}_{ij}\delta\hat{n}^f_{im}\delta\hat{n}^f_{jm'} + \tilde{\tilde{E}}. \tag{4.46}$$

This effective Hamiltonian describes the lattice-gas model of ions, which interact via a possibly long-range interaction $\tilde{\tilde{g}}_{ij}$. Therefore, we can use an additional Monte-Carlo simulation or also a simple exact-diagonalization approach to evaluate the expectation values $\langle \hat{n}^f \rangle_{\tilde{\tilde{\mathcal{H}}}^f}$ and $C^{ff}_{\rho,ij} \approx \sum_{mm'} \langle \delta\hat{n}^f_{im}\delta\hat{n}^f_{jm'}\rangle_{\tilde{\tilde{\mathcal{H}}}^f}$.

Together with the conduction electron part of (4.33), the final fully renormalized Hamiltonian becomes

$$\tilde{\tilde{\mathcal{H}}} = \sum_{\mathbf{k},m} \tilde{\epsilon}_{\mathbf{k}} c^\dagger_{\mathbf{k}m} c_{\mathbf{k}m} + \tilde{\tilde{\mu}}^f \sum_{i,m} \hat{f}^\dagger_{im}\hat{f}_{im} + \sum_{\substack{i,j\neq i \\ mm'}} \tilde{\tilde{g}}_{ij}\delta\hat{n}^f_{im}\delta\hat{n}^f_{im'} + \tilde{\tilde{E}}. \tag{4.47}$$

This result is similar to the one obtained by employing the PRM to the Falicov-Kimball model [39].

4.4 Expectation values

To evaluate $\langle c^\dagger_{\mathbf{k}m} c_{\mathbf{k}m}\rangle$, $\langle \hat{n}^f\rangle$ as well as $\langle \hat{f}^\dagger_{\mathbf{k}m} c_{\mathbf{k}m} + \text{h.c.}\rangle$ with the fully renormalized Hamiltonian (4.47), we use the formulism (3.10). For instance, in order to evaluate $\langle c^\dagger_{\mathbf{k}m} c_{\mathbf{k}m}\rangle$, one can use the renormalization equations for the operators $(c^\dagger_{\mathbf{k}m} c_{\mathbf{k}m})_\lambda$, which can be evaluated as it was done for the Hamiltonian by choosing the same ansatz as in (4.24). The obtained renormalization equations would have the same form as (4.32). However, they have to be solved with different initial values. Similar to $\langle c^\dagger_{\mathbf{k}m} c_{\mathbf{k}m}\rangle$, the other expectation values $\langle \hat{n}^f\rangle$ and $\langle \hat{f}^\dagger_{\mathbf{k}m} c_{\mathbf{k}m} + \text{h.c.}\rangle$ could also be evaluated. However, to restrict the numeric effort, we are going to evaluate the expectation values by using separate renormalization equations for the single creation and annihilation operators. For $(c^\dagger_{\mathbf{k}m} c_{\mathbf{k}m})_\lambda = c^\dagger_{\mathbf{k}m}(\lambda) c_{\mathbf{k}m}(\lambda)$ for instance, we make the following ansatz

$$c^\dagger_{\mathbf{k}m}(\lambda) = x_{\mathbf{k},\lambda} c^\dagger_{\mathbf{k}m} + y_{\mathbf{k},\lambda} \hat{f}^\dagger_{\mathbf{k}m}, \tag{4.48}$$

where $x_{\mathbf{k},\lambda}$ and $y_{\mathbf{k},\lambda}$ are λ dependent coefficients with the initial values at $\lambda = \Lambda$

$$x_{\mathbf{k},\Lambda} = 1,\ y_{\mathbf{k},\Lambda} = 0. \tag{4.49}$$

The operator structure of $c^\dagger_{\mathbf{k}m}(\lambda)$ in (4.48) is determined by the first order expression in the interaction. We employ that the λ-dependent operators also fulfill the fermionic anticommutator relations and find that

$$|x_{\mathbf{k},\lambda}|^2 + D|y_{\mathbf{k},\lambda}|^2 = 1 \tag{4.50}$$

has to hold for all $\mathbf{k}$ and λ values.

In order to derive the renormalization equations for the prefactors $x_{\mathbf{k},\lambda}$ and $y_{\mathbf{k},\lambda}$ we again consider the transformation step of $c^\dagger_{\mathbf{k}m}(\lambda)$ from λ to $\lambda - \Delta\lambda$. Similarly to the

procedure for the full Hamiltonian, we obtain the differential equations

$$\begin{aligned}\frac{dx_{\mathbf{k},\lambda}}{d\lambda} &= Dy_{\mathbf{k},\lambda}\tilde{\alpha}_{\mathbf{k},\lambda},\\ \frac{dy_{\mathbf{k},\lambda}}{d\lambda} &= -x_{\mathbf{k},\lambda}\tilde{\alpha}_{\mathbf{k},\lambda}.\end{aligned} \tag{4.51}$$

Analogously, we employ

$$\hat{f}^{\dagger}_{\mathbf{k}m}(\lambda) = -Dy_{\mathbf{k},\lambda}c^{\dagger}_{\mathbf{k}m} + x_{\mathbf{k},\lambda}\hat{f}^{\dagger}_{\mathbf{k}m} \tag{4.52}$$

to evaluate the other expectation values, $\langle\hat{n}^f\rangle$ and $\langle\hat{f}^{\dagger}_{\mathbf{k}m}c_{\mathbf{k}m}+\text{h.c.}\rangle$. Solving the differential equations (4.51) with the initial conditions (4.49) and taking the limit $\lambda\to 0$, we obtain renormalized prefactors $\tilde{x}_{\mathbf{k}}$ and $\tilde{y}_{\mathbf{k}}$. Now we can evaluate the expectation values

$$\begin{aligned}\langle c^{\dagger}_{\mathbf{k}m}c_{\mathbf{k}m}\rangle &= |\tilde{x}_{\mathbf{k}}|^2 f(\tilde{\varepsilon}_{\mathbf{k}}) + |\tilde{y}_{\mathbf{k}}|^2\langle\hat{n}^f_m\rangle_{\tilde{\mathcal{H}}},\\ \langle\hat{f}^{\dagger}_{\mathbf{k}m}\hat{f}_{\mathbf{k}m}\rangle &= D^2|\tilde{y}_{\mathbf{k}}|^2 f(\tilde{\varepsilon}_{\mathbf{k}}) + |\tilde{x}_{\mathbf{k}}|^2\langle\hat{n}^f_m\rangle_{\tilde{\mathcal{H}}},\\ \langle\hat{f}^{\dagger}_{\mathbf{k}m}c_{\mathbf{k}m}+\text{h.c.}\rangle &= -2\tilde{x}_{\mathbf{k}}\tilde{y}_{\mathbf{k}}\left[Df(\tilde{\varepsilon}_{\mathbf{k}}) - \langle\hat{n}^f_m\rangle_{\tilde{\mathcal{H}}}\right],\end{aligned} \tag{4.53}$$

where

$$\langle\hat{n}^f_m\rangle_{\tilde{\mathcal{H}}} = \frac{1}{N}\sum_i\langle\hat{n}^f_{im}\rangle_{\tilde{\mathcal{H}}}, \quad f(\tilde{\varepsilon}_{\mathbf{k}}) := \langle c^{\dagger}_{\mathbf{k}m}c_{\mathbf{k}m}\rangle_{\tilde{\mathcal{H}}} = \frac{1}{e^{\beta\tilde{\varepsilon}_{\mathbf{k}}}+1}, \tag{4.54}$$

with $\beta = 1/T$ is inverse temperature.

Previous numerical results for the density-density correlation function of the f-electrons, $\langle\delta\hat{n}^f_i\delta\hat{n}^f_j\rangle$, obtained by employing classical Monte-Carlo to the renormalized Hamiltonian of the Falicov-Kimball model (FKM) [39], shows that at non-zero temperature, this correlation function has a maximum at $\mathbf{R}_i = \mathbf{R}_j$ and decreases exponentially with increasing distance $|\mathbf{R}_i - \mathbf{R}_j|$. As discussed above, the correlation function $\mathcal{C}^{ff}_{\rho,ij} = \langle\delta\hat{n}^f_{im}\delta\hat{n}^f_{jm'}\rangle_{\tilde{\mathcal{H}}}$ of the present model should behave similarly. At $i = j$ we have

$$\begin{aligned}\sum_{mm'}\langle\delta\hat{n}^f_{im}\delta\hat{n}^f_{jm'}\rangle_{\tilde{\mathcal{H}}} \approx \sum_{mm'}\langle\delta\hat{n}^f_{im}\delta\hat{n}^f_{jm'}\rangle &= \sum_{mm'}\delta_{ij}\langle(\hat{n}^f_{im} - \langle\hat{n}^f_{im}\rangle)(\hat{n}^f_{jm'} - \langle\hat{n}^f_{jm'}\rangle)\rangle\\ &= \langle\hat{n}^f\rangle(1 - \langle\hat{n}^f\rangle).\end{aligned} \tag{4.55}$$

This maximum value depends on the average occupation number $\langle\hat{n}^f\rangle$ of the f-electrons. In the regimes in which $\langle\hat{n}^f\rangle$ is either small or large, the contribution due to correlations

between localized f-electrons becomes small. Furthermore, in the situation in which $\langle \hat{n}^f \rangle$ changes abruptly from large values $\langle \hat{n}^f_m \rangle \approx 1$ to small values $\langle \hat{n}^f_m \rangle \approx 0$, when $\tilde{\epsilon}_f$ reaches the Fermi level, we can neglect the contributions from correlations between f-electrons. In the weak coupling limit (small values of U_{fc}) the g-term, which was created due to the density-density correlation between the localized electrons, can also be left out. Within these approximations, the finally renormalized Hamiltonian becomes simple and reads

$$\tilde{\mathcal{H}} \;=\; \sum_{\mathbf{k},m} \tilde{\varepsilon}_{\mathbf{k}}\; c^{\dagger}_{\mathbf{k}m} c_{\mathbf{k}m} + \tilde{\mu}_f \sum_{i,m} \hat{f}^{\dagger}_{im} \hat{f}_{im} + \sum_{\mathbf{k},m} \tilde{\gamma}_{\mathbf{k}} \left(\hat{f}^{\dagger}_{\mathbf{k}m} \hat{f}_{\mathbf{k}m} \right)_{NL} + \tilde{E}. \tag{4.56}$$

This result looks the same as the one which was obtained by renormalizing the periodic Anderson model [31, 32]. Nevertheless, it is different because the Coulomb interaction strength U_{fc} not only changes the initial values of the differential equations but also changes itself during the renormalization procedure. Thus, all renormalized parameters depend on U_{fc}. With the modified Hamiltonian (4.56), we now continue using the ansatzs (4.48) and (4.52). We evaluate the expectation values

$$\begin{aligned} \langle c^{\dagger}_{\mathbf{k}m} c_{\mathbf{k}m} \rangle &= |\tilde{x}_{\mathbf{k}}|^2 f(\tilde{\varepsilon}_{\mathbf{k}}) + D|\tilde{y}_{\mathbf{k}}|^2 \bar{f}(\tilde{\omega}_{\mathbf{k}}), \\ \langle \hat{f}^{\dagger}_{\mathbf{k}m} \hat{f}_{\mathbf{k}m} \rangle &= D^2|\tilde{y}_{\mathbf{k}}|^2 f(\tilde{\varepsilon}_{\mathbf{k}}) + D|\tilde{x}_{\mathbf{k}}|^2 \bar{f}(\tilde{\omega}_{\mathbf{k}}), \end{aligned} \tag{4.57}$$

and

$$\langle \hat{f}^{\dagger}_{\mathbf{k}m} c_{\mathbf{k}m} + \text{h.c.} \rangle \;=\; -2D\tilde{x}_{\mathbf{k}}\tilde{y}_{\mathbf{k}} \left[f(\tilde{\varepsilon}_{\mathbf{k}}) - \bar{f}(\tilde{\omega}_{\mathbf{k}}) \right]. \tag{4.58}$$

Here, the *tilde* symbols denote the renormalized parameters in the limit $\lambda \to 0$ and $\tilde{\omega}_{\mathbf{k}} = \tilde{\mu}_f + D(\tilde{\gamma}_{\mathbf{k}} - \tilde{\bar{\gamma}})$. Besides the conventional Fermi function for the conduction electrons from (4.54), we also have introduced

$$\bar{f}(\tilde{\omega}_{\mathbf{k}}) := \frac{1}{D} \langle \hat{f}^{\dagger}_{\mathbf{k}m} \hat{f}_{\mathbf{k}m} \rangle_{\tilde{\mathcal{H}}}, \tag{4.59}$$

where the factor D has been defined in (4.15).

Note, due to the unusual properties of the Hubbard operators in the Hamiltonian, there is no straightforward way to evaluate (4.59) and further approximations are necessary. As discussed in reference [31], when the renormalized f level is located above the chemical

potential, one finds $\bar{f}(\tilde{\omega}_{\mathbf{k}}) \approx f(\tilde{\omega}_{\mathbf{k}})$. In this case, the mean-field treatment of the electronic correlations, contained in $\mathcal{H}$, is sufficient. Nevertheless, we are also concerned with different position of the f level. So (4.59), is evaluated as follows

$$\langle \hat{f}^{\dagger}_{\mathbf{k}m} \hat{f}_{\mathbf{k}m} \rangle_{\tilde{\mathcal{H}}} = \frac{1}{\mathrm{Tr} e^{-\beta\tilde{\mathcal{H}}}} \mathrm{Tr} \left(\hat{f}^{\dagger}_{\mathbf{k}m} \hat{f}_{\mathbf{k}m} e^{-\beta\tilde{\mathcal{H}}} \right) = \frac{1}{\mathrm{Tr} e^{-\beta\tilde{\mathcal{H}}}} \mathrm{Tr} \left(e^{\beta\tilde{\mathcal{H}}} \hat{f}_{\mathbf{k}m} e^{-\beta\tilde{\mathcal{H}}} \hat{f}^{\dagger}_{\mathbf{k}m} e^{-\beta\tilde{\mathcal{H}}} \right), \quad (4.60)$$

where we have introduced the identity $e^{-\beta\tilde{\mathcal{H}}} e^{\beta\tilde{\mathcal{H}}} = 1$ and have used the property of cyclic invariance of operators under the trace, $\mathrm{Tr}(abc) = \mathrm{Tr}(bca)$. From the renormalized Hamiltonian (4.56) and the anticommutator relation (2.4), we obtain

$$\langle \hat{f}^{\dagger}_{\mathbf{k}m} \hat{f}_{\mathbf{k}m} \rangle_{\tilde{\mathcal{H}}} \approx \frac{e^{-\beta\tilde{\omega}_{\mathbf{k}}}}{1 + e^{-\beta\tilde{\omega}_{\mathbf{k}}}} \left\langle \left\{ \hat{f}^{\dagger}_{\mathbf{k}m}, \hat{f}_{\mathbf{k}m} \right\} \right\rangle_{\tilde{\mathcal{H}}} = f(\tilde{\omega}_{\mathbf{k}}) \langle D \rangle_{\tilde{\mathcal{H}}}. \quad (4.61)$$

Thus (4.59), can be written as

$$\bar{f}(\tilde{\omega}_{\mathbf{k}}) = \frac{f(\tilde{\omega}_{\mathbf{k}})}{D \left[1 + \frac{\nu_f - 1}{N} \sum_{\mathbf{p}} f(\tilde{\omega}_{\mathbf{p}}) \right]}. \quad (4.62)$$

At this point, all physical quantities can be calculated. Their dependence on the model parameters such as temperature T, hybridization V, Coulomb repulsion U_{fc} etc. can be found by solving the renormalization equations self-consistently. This procedure is processed as follows: (i) Using guessed initial values for the expectation values $\langle c^{\dagger}_{\mathbf{k}m} c_{\mathbf{k}m} \rangle$, $\langle \hat{n}^f \rangle$, $\langle \hat{f}^{\dagger}_{\mathbf{k}m} c_{\mathbf{k}m} + \mathrm{h.c.} \rangle$, we can solve the differential equations (4.32) and (4.51) and obtain renormalized parameters and prefactors. (ii) Next, we calculate a new approximation for the set of expectation values. (iii) Finally, we perform the renormalization again by using the new set of expectation values and repeat steps (ii) and (iii), until the iteration is converged. The convergence is reached, if the difference of two consecutive approximations to the expectation values is smaller than a chosen limit. Using the final expectation values, we can calculate the physical quantities for describing the systems.

Chapter 5

Numerical results for the one-dimensional EPAM

In this chapter we present our numerical results which are obtained by solving self-consistently the renormalization equations for the EPAM. In the case of the impurity Anderson model [49], the conduction band plays a role of the electron bath and hence the chemical potential μ is essentially fixed. However, in the case of the EPAM, μ is considerably affected by U_{fc} itself, so that we have to treat the problem for fixed total number of electrons. In particular, this treatment is indispensable in the valence fluctuation regime [21]. In our thesis, only the results for fixed total occupation number $n = \langle n^c \rangle + \langle \hat{n}^f \rangle = 1.75$ will be discussed. Moreover, we are interested in describing the superconducting state, that means only two spin directions, up and down, of the electrons are possible, thus the degeneracy $\nu_f = 2$ case is concerned.

In the following, numerical results for the one-dimensional EPAM are shown. We choose $\epsilon_k = -2t \cos k$ for a non-interacting dispersion relation of the conduction electrons. Here, $t = 1$ is chosen as a unit of energy. In this content, we discuss the renormalized dispersion relation of conduction electrons. Next, the localized occupation number as function of the bare f-energy ϵ_f is considered, when the valence state of Ce goes over from the Kondo regime to the mixed valence regime by applying external pressure.

5.1 Dispersion relation

At first, let us discuss the fully renormalized dispersion relation of the conduction electrons due to the influence of the interaction terms in the one-dimensional system. As shown in the previous chapter, we can solve the Eqs. (4.32) to obtain the renormalized Hamiltonian (4.33) when the expectation values are known. With this Hamiltonian one can not easily evaluate the expectation values because of the presence of the non-diagonal terms in (4.33). Therefore, the next renormalization process is necessary. Here, we have renormalized the other parameters due to the contributions of $\tilde{\gamma}_k$. So the final Hamiltonian for the f-electrons has a simple form. Combining with the conduction electrons, the final Hamiltonian has the form of a renormalized Falicov-Kimball model (FKM) [39], in which the expectation values $\langle \hat{n}^f \rangle$ and correlation function $C^{ff}_{\rho,ij}$ are easily evaluated either by the classical Monte-Carlo method or by exact-diagonalization (ED). At small temperature, the f-electron states in the FKM favor several almost homogeneous configurations [39, 50]. This result had been rigorously proven in [50] for large Coulomb repulsion between localized and conduction electrons. For arbitrary repulsion, it had been conjectured by [51]. In the one-dimensional case, these configurations are listed in table 5.1 [50].

As a typical case, we consider a f-electron filling of $\langle \hat{n}^f \rangle = 1/3$. There are three equivalent degenerate ground states of period 3 with corresponding arrays $\{100100\dots\}$, $\{010010\dots\}$, and $\{001001\dots\}$. Therefore, we can use the following ansatz for the system at very low temperatures

$$|\Phi_g^{(3)}\rangle = \frac{1}{\sqrt{3}} \left(|100100\dots\rangle + |010010\dots\rangle + |001001\dots\rangle \right). \tag{5.1}$$

Within the state (5.1), we can evaluate the correlation function $\langle \hat{n}_i^f \hat{n}_j^f \rangle$ as

$$\langle \hat{n}_i^f \hat{n}_j^f \rangle = \begin{cases} 1/3 & |R_j - R_i| = 0, 3, 6, 9, \dots \\ 0 & |R_j - R_i| = 1, 2, 4, 5, \dots \end{cases} \tag{5.2}$$

$\langle \hat{n}^f \rangle$	configurations
1	1111111111111111111...
2/3	1101101101101101101...
1/2	1010101010101010101...
1/3	1001001001001001001...
1/4	1000100010001000100...
1/5	1000010000100001000...
...	...
0	0000000000000000000...

Table 5.1: Typical examples of ground state configurations for different fillings.

For $\langle \hat{n}^f \rangle = 1/3$, one obtains the correlation function of the fluctuation operators

$$\langle \delta\hat{n}_i^f \delta\hat{n}_j^f \rangle = \begin{cases} 2/9 & |R_j - R_i| = 0, 3, 6, 9, \ldots \\ -1/9 & |R_j - R_i| = 1, 2, 4, 5, \ldots \end{cases} \tag{5.3}$$

Here we have denoted the lattice constant by $a = 1$. Result of the correlation function $\langle \delta\hat{n}_i^f \delta\hat{n}_j^f \rangle$ in (5.3) is also valid in the case of $\langle \hat{n}^f \rangle = 2/3$.

Similarly, the correlation functions $\langle \delta\hat{n}_i^f \delta\hat{n}_j^f \rangle$ for the other cases of $\langle \hat{n}^f \rangle$ are easily evaluated. Using the Fourier transformation as in Eq. (4.28), we obtain the correlation function $C_\rho^{ff}(k)$ in the momentum-space. Fig. 5.1 shows the dependence of $C_\rho^{ff}(k)$ on momentum k for some different values of $\langle \hat{n}^f \rangle$ with a number of lattice sites $N = 200$. In the case $\langle \hat{n}^f \rangle = 1/2$, there are two Kronecker delta functions located at $k^* = \pm\pi$. For $\langle \hat{n}^f \rangle = 1/3$, the Kronecker delta functions are present at $k^* = \pm 2\pi/3$ with smaller amplitudes. In general, increasing a natural number m with $\langle \hat{n}^f \rangle = 1/m$ leads to smaller amplitudes of the Kronecker delta functions in the correlation functions $C_\rho^{ff}(k)$. It turns out that the results of $C_\rho^{ff}(k)$ for $\langle \hat{n}^f \rangle = 1/m$ and $\langle \hat{n}^f \rangle = 1 - 1/m$ are identical.

On the other hand, at large temperature, the correlation function decreases exponentially with increasing distance $|R_i - R_j|$. That means, approximately only the site $R_i = R_j$

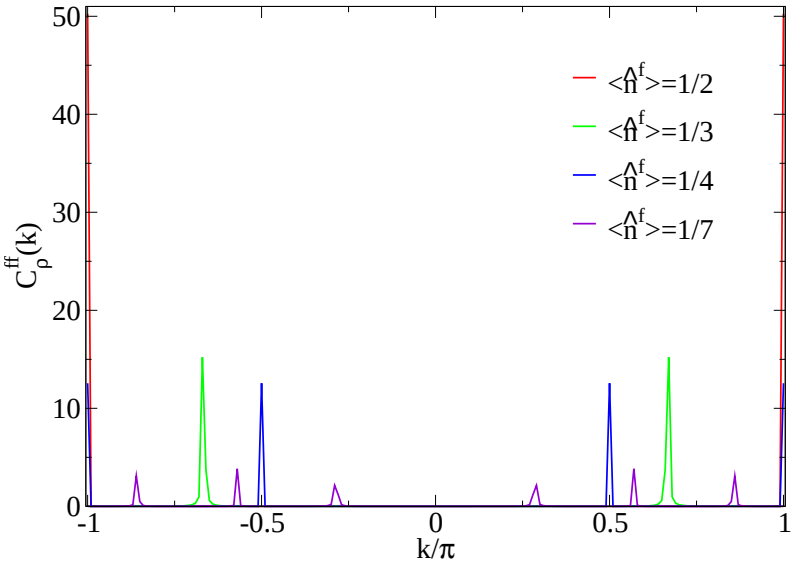

Figure 5.1: Fourier transformation $C_\rho^{ff}(k)$ of $\langle \delta\hat{n}_i^f \delta\hat{n}_j^f \rangle$ for different values of f-electron occupations $\langle \hat{n}^f \rangle$. The correlation functions $\langle \delta\hat{n}_i^f \delta\hat{n}_j^f \rangle$ are evaluated as discussed in Eq. (5.3) for the typical case $\langle \hat{n}^f \rangle = 1/3$. The number of lattice sites is chosen as $N = 200$.

contributes to the correlation function, and its value is $\langle \hat{n}^f \rangle (1 - \langle \hat{n}^f \rangle)$. Therefore, we have $C_\rho^{ff}(k) \approx \langle \hat{n}^f \rangle (1 - \langle \hat{n}^f \rangle)$, which is independent of k.

In the low temperature regime, the density-density correlation function of the localized electrons is, for instance, approximately given by (5.3). Its value in the momentum space is substituted into the differential equations (4.32) with some guessed initial expectation values for $\langle \hat{n}^f \rangle$, $\langle c_{km}^\dagger c_{km} \rangle$ and $\langle \hat{f}_{km}^\dagger c_{km} + \text{h.c.} \rangle$. Solving the set of differential equations with the initial condition (4.13), we can find the renormalized Hamiltonian (4.33). Since the Hamiltonian (4.33) is not diagonal, we have to proceed as discussed in section 3 of chapter 4, in order to remove the hopping part (4.36) of $\tilde{\mathcal{H}}_1^f$. With the fully renormalized Hamiltonian $\tilde{\tilde{\mathcal{H}}}$ according to (4.47), we are able to recalculate the expectation values $\langle \hat{n}^f \rangle$, $\langle c_{km}^\dagger c_{km} \rangle$ and $\langle \hat{f}_{km}^\dagger c_{km} + \text{h.c.} \rangle$ according to (4.53), by using the renormalization equations (4.51). The new expectation values are now used to repeat the self-consistent calculation until convergency is reached. In our work, we have to adjust the chemical potential μ as well as ϵ_f to fulfill the condition $n = \langle n^c \rangle + \langle \hat{n}^f \rangle = 1.75$ for a given value

of $\langle \hat{n}^f \rangle$.

To illustrate the renormalization process, we show in Fig. 5.2 the λ-behavior of the hybridization $V_{k,\lambda}$ and Coulomb repulsion $U_{k,\pi/8,\lambda}$ during the first renormalization step for an one-dimensional lattice with $N = 80$ sites. In the figure, $V_{k,\lambda}$ (left) and $U_{k,\pi/8,\lambda}$ (right), is plotted as functions of λ, for several values of k with $U_{fc} = 1, V = 0.1, \epsilon_f = -1$ and $T = 0.05$. As expected, $V_{k,\lambda}$ and $U_{k,\pi/8,\lambda}$ decrease exponentially by lowering λ for all k-values. Hence, there are no contributions of the hybridization and of the Coulomb interaction in the Hamiltonian for $\lambda \to 0$. Next, it turns out that the hopping term

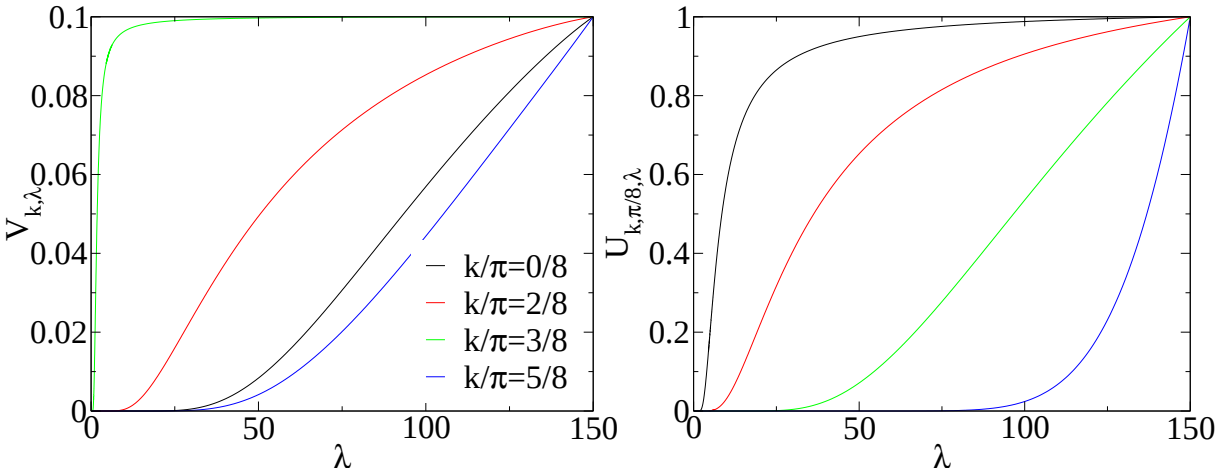

Figure 5.2: The dependence of $V_{k,\lambda}$ (left) and $U_{k,\pi/8,\lambda}$ (right) on λ for several values of momentum k at $T = 0.05$, $V = 0.1$, $U_{fc} = 1$, and $\epsilon_f = -1.0$.

between the localized electrons $\tilde{\gamma}_{ij,\lambda}$, which was introduced in Eq. (4.37), depends only on the distance between lattice sites $\kappa = |R_j - R_i|$. Fig. 5.3 shows the renormalization behavior of $\tilde{\gamma}_{\kappa,\lambda}$ (denoting $\tilde{\gamma}_{ij,\lambda}$) for different fixed values of κ in the second renormalization step. Similarly as before, also the hopping term decreases exponentially to zero, when λ approaches the excitation energies. This observation is valid for all other distances κ in the whole lattice. Therefore, after this step, we can conclude that the original Hamiltonian (4.7) has been completely renormalized to (4.47).

In order to find a reliable result for the renormalized dispersion relation of the con-

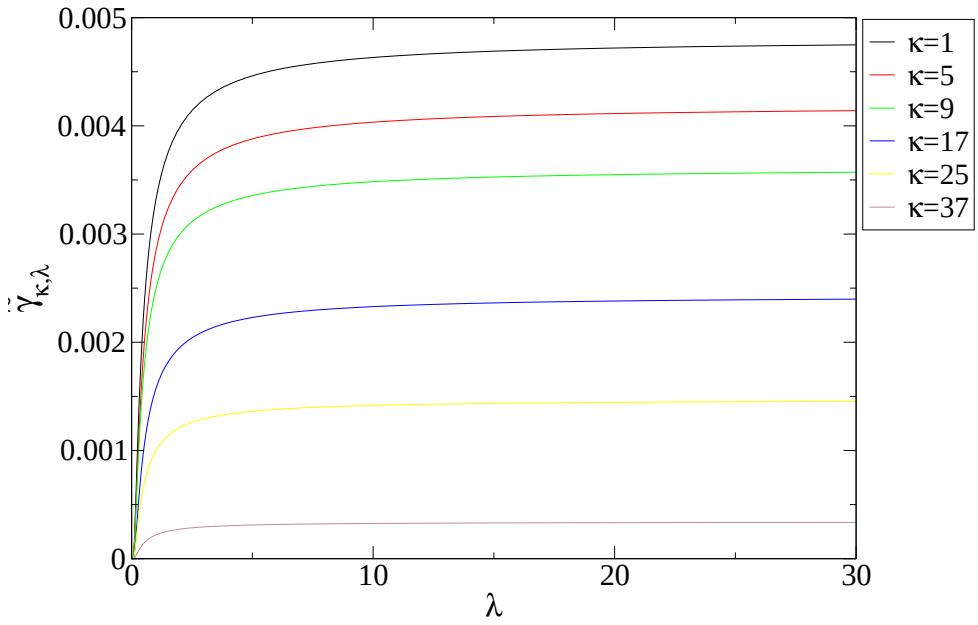

Figure 5.3: The dependence of $\tilde{\gamma}_{\kappa,\lambda}$ on λ for some lattice distances, κ, at $T = 0.05$, $V = 0.1$, $U_{fc} = 1$, and $\epsilon_f = -1.0$.

duction electrons, $\tilde{\epsilon}_k$, a lattice with a larger number of lattice sites $N = 200$ is considered. Fig. 5.4 shows the results for $\tilde{\epsilon}_k$ (opened black circle) with $U_{fc} = 1$, $V = 0.1$ at small temperature, $T = 0.05$ for different values of $\langle \hat{n}^f \rangle$. Because of $\epsilon_k = \epsilon_{-k}$, we can restrict ourselves to the half-plane in momentum space, $k > 0$. In the case of quarter-filling for the localized electrons, $\langle \hat{n}^f \rangle = 1/2$, there are two gaps present. For the lower values of $\langle \hat{n}^f \rangle$, in Fig. 5.4(b,c,d), the number of gaps becomes larger. There is always one gap, which is caused by the hybridization and opens at the Fermi momentum k_F. It enters due to the crossing of the one-particle dispersion relation for the conduction and the localized electrons. The other gaps are caused by the U_{fc}-term. The number of these gaps depends on the number of Kronecker delta functions as well as on how they enter the density-density correlation function $C_\rho^{ff}(k)$. For instance, in the case $\langle \hat{n}^f \rangle = 1/3$, there is one Kronecker delta function in $C_\rho^{ff}(k)$, located at $k^* = 2\pi/3$, for $k > 0$, as discussed in the Fig. (5.1). It follows that the contribution of the second term in the first equation of (4.32) is mainly

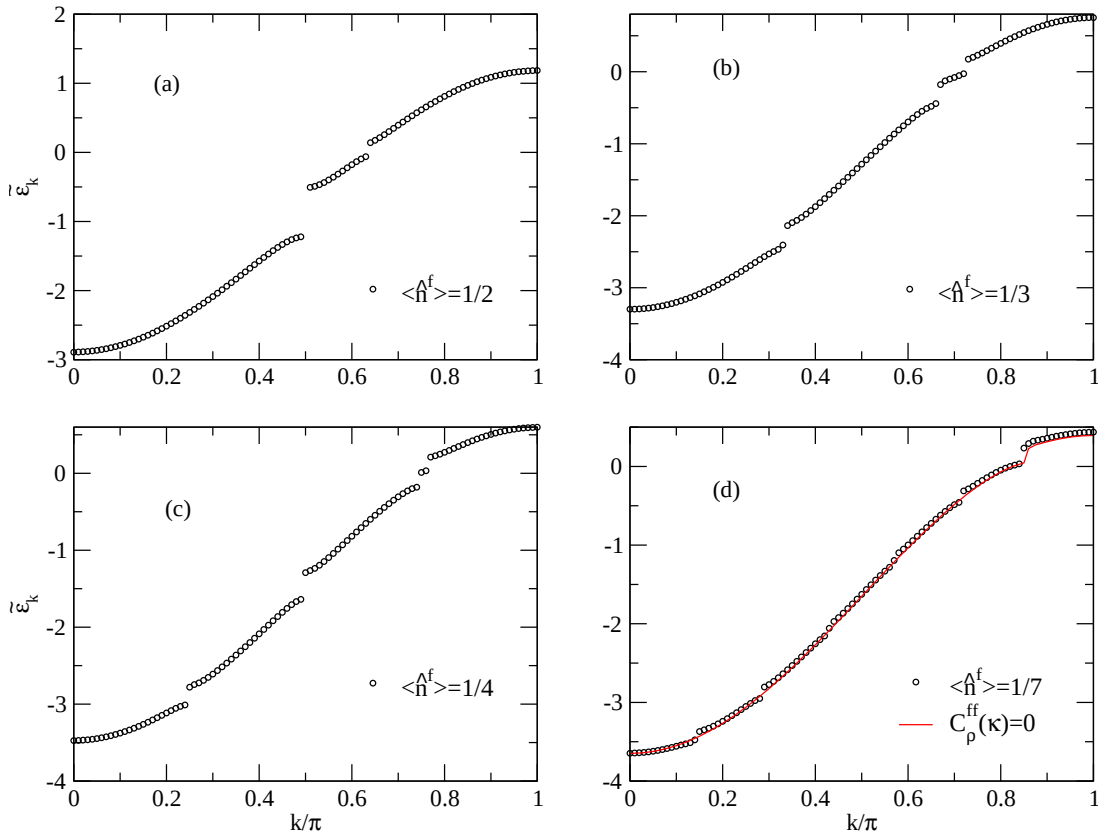

Figure 5.4: Renormalized quasiparticle energies $\tilde{\epsilon}_k$ of c-electrons for several values of the localized electron density $\langle \hat{n}^f \rangle$ with $U_{fc} = 1$, $V = 0.1$, $T = 0.05$ and $N = 200$.

caused by k values close to $p = k^*/2$ and $p = \pi - k^*/2$. That means, only $\epsilon_{k,\lambda}$ values with k close to p change much more than the other k-values. On the other hand, the sign of $\epsilon_{k,\lambda} - \epsilon_{k-q,\lambda}$ in $\beta_{k+q,k,\lambda}$ changes, when k passes through p, which leads to the opening of a gap at these points. Therefore, in the renormalized dispersion relation of conduction electrons for $\langle \hat{n}^f \rangle = 1/3$, there are two gaps at $k = \pi/3$ and $k = 2\pi/3$ caused, by the U_{fc}-term. This result can be understood by noting that the bandgap is created due to a weak periodic potential [52]. For the lattice with periodicity a (a is lattice constant), the gap is present at $k = K/2$ with K is a reciprocal lattice vector, $K = 2n\pi/a$. In the case of $\langle \hat{n}^f \rangle = 1/3$, as discussed above, the periodicity of the system is now $3a$, or the reciprocal lattice vector is $K' = 2n\pi/(3a)$. Thus, the gaps are present at $k = \pi/3$ and $k = 2\pi/3$ in

the range $0 < k < \pi$. This explanation is also valid for the other periodic fillings in the system.

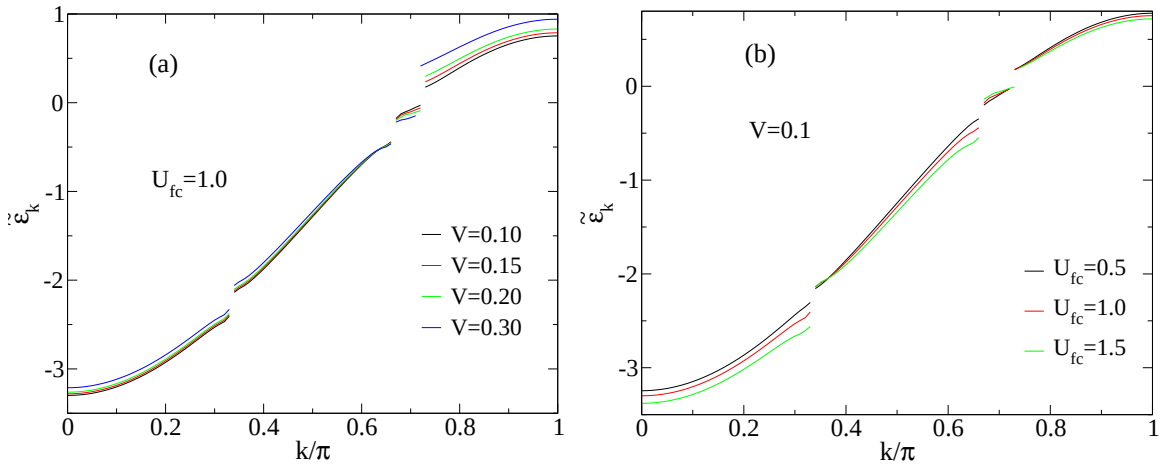

Figure 5.5: Renormalized quasiparticle energies $\tilde{\epsilon}_k$ of c-electrons (a) for several values of V and $U_{fc} = 1$ (b) for several values of U_{fc} and $V = 0.1$ at $T = 0.05$, $N = 200$, and $\langle \hat{n}^f \rangle = 1/3$.

As mentioned before, the number of the Kronecker delta function-like contributions to $C_\rho^{ff}(k)$ depends on $\langle \hat{n}^f \rangle$. However, their weights decrease with increasing number of the Kronecker delta functions, as shown in the Fig. 5.1. According to the renormalization in equation (4.32) for $\epsilon_{k,\lambda}$, this leads to a decrease of the weight of the gaps, which are caused by U_{fc}. For example, in the case of $\langle \hat{n}^f \rangle = 1/7$ (Fig. 5.4(d)), the renormalized energy $\tilde{\epsilon}_k$ has six small gaps which are the same in the case of $\langle \hat{n}^f \rangle = 6/7$. Comparing with $\tilde{\epsilon}_k$ in the case of vanishing U_{fc}-term (first differential equation in (4.32)), we realize that they are almost identical (the red line on the same Fig. 5.4(d)). That means, density-density correlations between the localized electrons due to the U_{fc}-term can be neglected in this case. We conclude that we can neglect the correlations between the localized electrons for $\langle \hat{n}^f \rangle \approx 1$ and $\langle \hat{n}^f \rangle \approx 0$. As a consequence, correlations should also be neglected in the case of a sharp valence transition of the localized electrons, in which the $\langle \hat{n}^f \rangle$ change abruptly from 1 to 0, when $\tilde{\epsilon}_f$ passes through the Fermi level.

In order to investigate the influence of the other parameters on the conduction band gaps, the typical case of a localized electron density $\langle \hat{n}^f \rangle = 1/3$ at small temperature

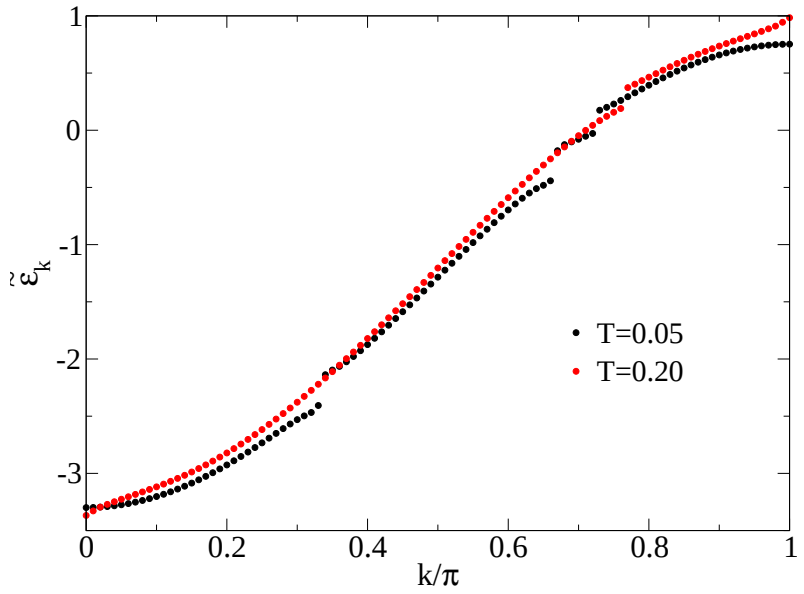

Figure 5.6: Renormalized quasiparticle energies $\tilde{\epsilon}_k$ of the c-electrons for two values of T and $U_{fc} = 1$, $V = 0.1$, $N = 200$, and $\langle \hat{n}^f \rangle = 1/3$.

$T = 0.05$ is considered. Fig. 5.5(a) shows the renormalized energy $\tilde{\epsilon}_k$ for a Coulomb repulsion $U_{fc} = 1$, for different values of the hybridization V. As discussed above, there are two reasons for the gaps. The gaps, caused by U_{fc}, are unchanged with respect to their position in k-space and their amplitudes. In contrast, the gap, caused by the hybridization, becomes larger with increasing V. The latter behavior of $\tilde{\epsilon}_k$ agrees with that for the usual PAM [33, 45]. Fig. 5.5(b) shows $\tilde{\epsilon}_k$ as function of U_{fc} for fixed hybridization $V = 0.1$. In contrast to Fig. 5.5(a), the gaps due to U_{fc} become larger with increasing Coulomb repulsion, although their positions in the k-space are unchanged. This result corresponds to the discussion in [39].

Next, we discuss the influence of the temperature on $\tilde{\epsilon}_k$. In Fig. 5.6, $\tilde{\epsilon}_k$ is plotted for $U_{fc} = 1$, $V = 0.1$, $\langle \hat{n}^f \rangle = 1/3$ for two different values of temperature, $T = 0.05$ and $T = 0.2$. In the case of large temperature, $T = 0.2$, the density-density correlation function of the localized electrons decreases exponentially as function of the distance between the lattice sites [39]. As discussed in the previous chapter, in this case only the

on-site correlation is important, i.e., $C_\rho^{ff}(k) \approx \langle \hat{n}^f \rangle (1 - \langle \hat{n}^f \rangle)$, which does not depend on momentum k. Therefore, the total bandwidth is increased and the gaps due to the Coulomb repulsion vanish.

5.2 Valence transition

This section is devoted to the discussion of the valence transition of the EPAM. Under applied pressure, the f-energy level of the localized electrons is shifted to a position close to the Fermi level. Therefore, the localized electrons can jump to the conduction band, and the f-energy level becomes more and more depopulated. We say, there exists a valence transition. This phenomenon can be described by increasing the f-energy ϵ_f in the EPAM. By exploring the dependence of the localized electron number (as function of ϵ_f) on the other parameters, we can achieve a full picture about the valence transition of the EPAM. In the following, numerical results are given, which were found from the fully renormalized Hamiltonian (4.56). We discuss $\langle \hat{n}^f \rangle$ for the whole range of ϵ_f, with a fixed total number of electrons. A system with $N = 80$ lattice sites is considered.

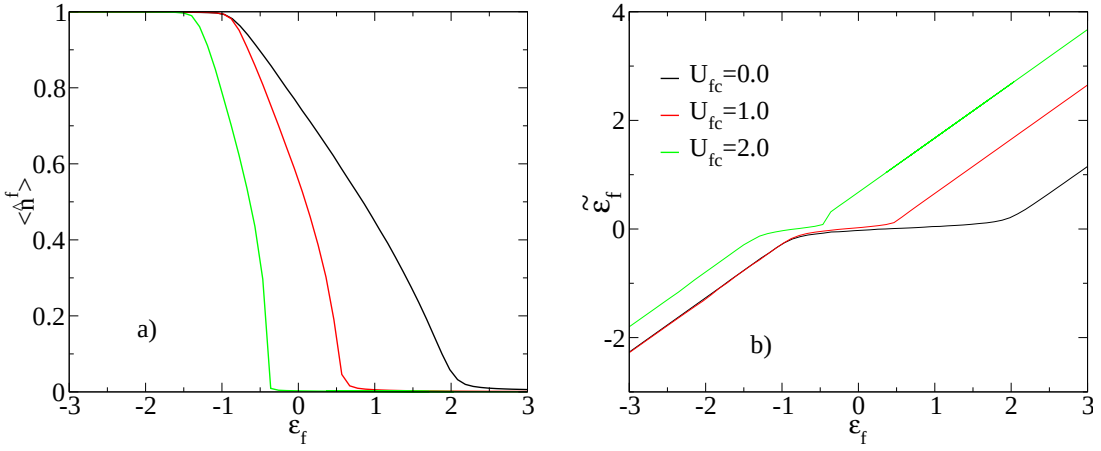

Figure 5.7: (a) Averaged f occupation number $\langle \hat{n}^f \rangle$ and (b) renormalized f level $\tilde{\epsilon}_f$ as a function of the unrenormalized f energy ϵ_f for several values of U_{fc} in the case of $V = 0.1$ and $T = 0.05$.

In Fig. 5.7(a), we present the valence transition as function of the bare f-level ϵ_f

for different values of U_{fc}. It can be seen that increasing U_{fc} leads to a sharper valence transition. Fig. 5.7(b) shows the dependence of the renormalized f electron energy $\tilde{\epsilon}_f$ as function of unrenormalized quantity, ϵ_f. In the regimes with $\langle \hat{n}^f \rangle \approx 1$ and $\langle \hat{n}^f \rangle \approx 0$, $\tilde{\epsilon}_f$ shows a linear dependence on ϵ_f with a slope $\alpha = 1$, i.e, close to these regimes, the f electron level is not renormalized but only shifted due to the chemical potential and MF contribution of U_{fc} (see Eq. (4.13)). Close to these regimes, the MF calculation must be adequate and the assumption that ϵ_f is constant during the renormalization process can be justified [31, 45]. In the mixed valence transition regime, $\tilde{\epsilon}_f$ changes with a smaller slope as function of ϵ_f. The width of this regime is reduced, when U_{fc} is increased, which corresponds to a sharper valence transition. In the case of $U_{fc} = 2$, there is a kink in $\tilde{\epsilon}_f$, which results from the sudden jump of $\langle \hat{n}^f \rangle$, shown in the left figure. Moreover, the transition regime in Fig. 5.7(a) is shifted to the left for an increased value of U_{fc}. Thus, with U_{fc} large enough, ϵ_f has to be small in order to satisfy $\epsilon_f + U_{fc}\langle n^c \rangle \approx E_F$, where E_F is the Fermi level.

In the PRM, the MF contributions of U_{fc} to ϵ_k and to ϵ_f are included in the initial values (4.13). The fluctuation contributions of U_{fc} are responsible for the shift of $\langle \hat{n}^f \rangle$ to the left also before the jump of $\langle \hat{n}^f \rangle$ is visible, see Fig. 5.7(a). If we define a valence susceptibility, $\chi_f := -\partial \langle \hat{n}^f \rangle / \partial \epsilon_f$, our result implies that the maximum position of χ_f is shifted to the left for increasing U_{fc}. This is in contrast to the slave-boson MF calculation [21], in which the maximum of χ_f almost remains at its position, when U_{fc} is varied before the jump of $\langle \hat{n}^f \rangle$ appears. Nevertheless, our result fits with the DMRG calculation of Ref. [22].

To investigate the effect of the other parameters on the valence transition, the dependence of $\langle \hat{n}^f \rangle$ on ϵ_f is shown in Fig. 5.8(a) and Fig. 5.8(b), for different temperatures T and hybridization strengths V. Fig. 5.8(a) shows that the lower temperatures T leads to a sharper $\langle \hat{n}^f \rangle$ as function of ϵ_f. At low temperatures the f-electrons mainly occupy levels with energies smaller than the Fermi energy, E_F. Under these conditions, the f electrons in Ce-systems are in the $4f^1$ state. With increasing temperature, the f-electrons can be excited to higher level which have a $4f^0$+[5d6s] configuration. Correspondingly, at larger

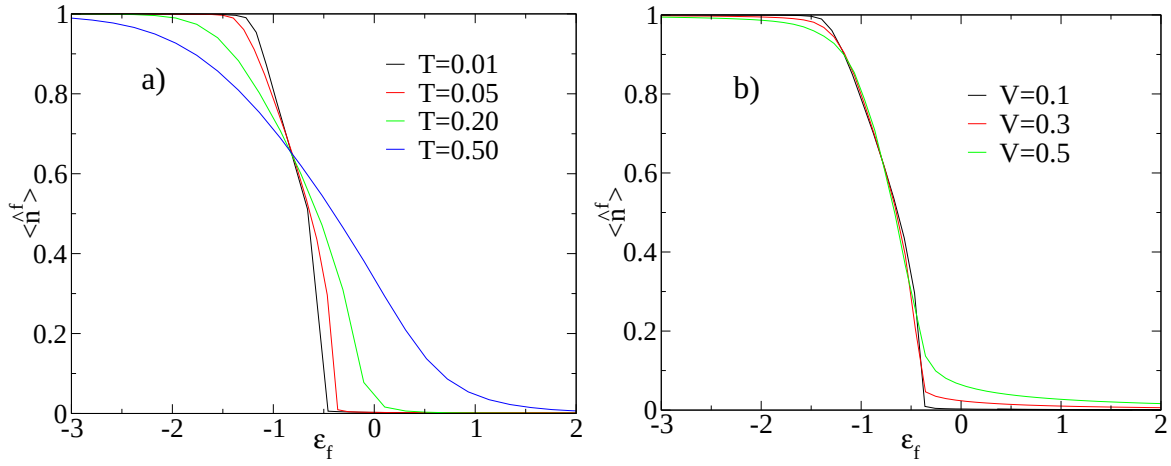

Figure 5.8: Averaged f occupation number $\langle \hat{n}^f \rangle$ as a function of the unrenormalized f energy ϵ_f (a) for some values of temperature T with $U_{fc} = 2$, $V = 0.1$ and (b) for several values of the hybridization V with $U_{fc} = 2$, $T = 0.05$ (b).

temperatures, the valence fluctuation regime is broadened.

For fixed temperature T and Coulomb repulsion U_{fc}, the valence transition behaves similarly when the hybridization energy V is varied. In Fig. 5.8(b), we plot the dependence of $\langle \hat{n}^f \rangle$ on the f energy ϵ_f for several values of V in the case of $T = 0.05$, $U_{fc} = 2$. It shows that the valence transition gets smoother if the hybridization energy is increased. On the other hand, by enhancing the hybridization between localized and conduction electrons, the localized electrons easily convert to conduction electrons, and the two configurations of Ce ions, $4f^1(Ce^{3+})$ and $4f^0(Ce^{4+})$, have the tendency to become degenerate.

Chapter 6

Superconductivity in the EPAM

One of the most advantages of the PRM is the possibility to investigate quantum phase transitions. Already with the simplest version of the PRM with respect to perturbation theory, a BCS-like equation was derived for the coupled electron-phonon system [43]. In contrast to the Fröhlich interaction [53], the deduced effective electron-electron interaction for Cooper pairs did not contain singularities. Recently, also the competition between the formation of charge-density waves and superconductivity for the two-dimensional half-filled Holstein model was studied by the PRM [54]. In order to describe quantum phase transitions on both sides of the transition, one often includes infinitesimally small symmetry breaking fields in the Hamiltonian. During the renormalization processes, the symmetry breaking fields gain weight. Thus, from the fully renormalized Hamiltonian the order parameters can be found. In this chapter, we present an application of the PRM to possible superconductivity in the two-dimensional EPAM. Self-consistent equations for determining the superconducting order parameters are obtained. Our numerical results for the superconducting energy gaps with d-wave symmetry in the two dimensional system will be discussed in chapter 7.

6.1 Renormalized Hamiltonian for superconductivity

The EPAM is gauge symmetry invariant. In order to describe the superconducting state of this model, a BCS-like Hamiltonian will be derived, which breaks the gauge symmetry. That means, the renormalized Hamiltonian includes gauge symmetry breaking fields. Therefore, our ansatz for the Hamiltonian reads

$$\mathcal{H}_\lambda = \mathcal{H}_{0,\lambda} + \mathcal{H}_{0,\lambda}^{BF} + \mathcal{H}_{1,\lambda}, \tag{6.1}$$

after all excitations with energies larger than λ have been eliminated. Here $\mathcal{H}_{0,\lambda}$, $\mathcal{H}_{1,\lambda}$ were introduced in the previous chapter in Eq. (4.8), where the usual EPAM was renormalized. The part $\mathcal{H}_{0,\lambda}^{BF}$ in (6.1) breaks the gauge symmetry. It has the form

$$\begin{aligned}\mathcal{H}_{0,\lambda}^{BF} = &-\sum_{\mathbf{k}} \left(\Delta_{\mathbf{k},\lambda}^{cc} c_{\mathbf{k}\uparrow}^\dagger c_{-\mathbf{k}\downarrow}^\dagger + \Delta_{\mathbf{k},\lambda}^{cc,*} c_{-\mathbf{k}\downarrow} c_{\mathbf{k}\uparrow} \right) - \sum_{\mathbf{k}} \left(\Delta_{\mathbf{k},\lambda}^{ff} \hat{f}_{\mathbf{k}\uparrow}^\dagger \hat{f}_{-\mathbf{k}\downarrow}^\dagger + \Delta_{\mathbf{k},\lambda}^{ff,*} \hat{f}_{-\mathbf{k}\downarrow} \hat{f}_{\mathbf{k}\uparrow} \right) \\ &- \sum_{\mathbf{k}} \left(\Delta_{\mathbf{k},\lambda}^{cf} c_{\mathbf{k}\uparrow}^\dagger \hat{f}_{-\mathbf{k}\downarrow}^\dagger + \Delta_{\mathbf{k},\lambda}^{cf,*} \hat{f}_{-\mathbf{k}\downarrow} c_{\mathbf{k}\uparrow} \right) - \sum_{\mathbf{k}} \left(\Delta_{\mathbf{k},\lambda}^{fc} \hat{f}_{\mathbf{k}\uparrow}^\dagger c_{-\mathbf{k}\downarrow}^\dagger + \Delta_{\mathbf{k},\lambda}^{fc,*} c_{-\mathbf{k}\downarrow} \hat{f}_{\mathbf{k}\uparrow} \right).\end{aligned} \tag{6.2}$$

The four fields $\Delta_{\mathbf{k},\lambda}^{\alpha\beta}$ (α, β denote c or f) in $\mathcal{H}_{0,\lambda}^{BF}$ couple to all possible operators of the electrons which break the gauge invariance. They will play the role of the superconducting energy gaps and depend on λ. The initial values are chosen to be infinitesimally small

$$\Delta_{\mathbf{k},\Lambda}^{\alpha\beta} = \xi^{\alpha\beta} \to 0. \tag{6.3}$$

In order to derive a set of renormalization equations for the Hamiltonian (6.1), one can first use the Bogoliubov transformation [55] in order to diagonalize the Hamiltonian $\mathcal{H}_{0,\lambda} + \mathcal{H}_{0,\lambda}^{BF}$, as was done in Ref. [43]. By this way, the interaction part $\mathcal{H}_{1,\lambda}$ of the Hamiltonian (6.1) has to be expressed by the new quasiparticle operators, which also would depend on the cutoff λ. Moreover, during the renormalization, some additional interactions can appear which are difficult to control. After the renormalization step from λ to $\lambda - \Delta\lambda$, the quasi-particle operators have to be transformed back to the original operators in (6.1). However, there exists an alternative way which can be applied to the renormalization procedure, and which was already used before. In the ansatz (6.1),

$\mathcal{H}_{0,\lambda} + \mathcal{H}_{0,\lambda}^{BF}$ and $\mathcal{H}_{1,\lambda}$ are considered as the dominant part and as perturbation, respectively. To perform the renormalization step by reducing the cutoff from λ to $\lambda - \Delta\lambda$, we use the unitary transformation (3.6), which satisfies (3.7). Note that in this way we have neglected the small influence of $\mathcal{H}_{0,\lambda}^{BF}$ in defining the generator $X_{\lambda,\Delta\lambda}$. By applying the unitary transformation to (6.1), the renormalization contributions up to second order in the interaction are not changed as compared to the normal state. This means, we can use the generator $X_{\lambda,\Delta\lambda}$ from (4.21) to perform the renormalization of the Hamiltonian (6.1). Note that we are considering the superconducting state. Therefore, in the factorization approximation, we have also to consider the possibility that the superconducting order parameters should be non-zero, i.e., $\langle \alpha^\dagger_{\mathbf{k}\uparrow} \beta^\dagger_{-\mathbf{k}\downarrow} \rangle \neq 0$ (α, β denote the c or f-electron operators). In principle, also some other results from (4.27) could change. Nevertheless, here we restrict ourselves in evaluating the unitary transformation to first order. So only the last expression in (4.27) is slightly modified. Thus, the unitary transformation of the operator $a_{\mathbf{k},\mathbf{k+q},m}$ (4.3) reads

$$e^{X_{\lambda,\Delta\lambda}} a_{\mathbf{k},\mathbf{k+q},m} e^{-X_{\lambda,\Delta\lambda}} \approx a_{\mathbf{k},\mathbf{k+q},m} + [X_{\lambda,\Delta\lambda}, a_{\mathbf{k},\mathbf{k+q},m}], \tag{6.4}$$

where

$$\begin{aligned}
[X_{\lambda,\Delta\lambda}, a_{\mathbf{k},\mathbf{k+q},m}] = & \left(\alpha_{\mathbf{k}}(\lambda,\Delta\lambda) \hat{f}^\dagger_{\mathbf{k}m} c_{\mathbf{k+q},m} + \alpha_{\mathbf{k+q}}(\lambda,\Delta\lambda) c^\dagger_{\mathbf{k}m} \hat{f}_{\mathbf{k+q},m} \right) \\
& \times \frac{1}{N} \sum_{i,m'} \delta(\hat{f}^\dagger_{im'} \hat{f}_{im'}) e^{-i\mathbf{q}\mathbf{R}_i} \\
& - \frac{1}{N} \delta(c^\dagger_{\mathbf{k}m} c_{\mathbf{k+q},m}) \sum_{\mathbf{p},\sigma} \alpha_{\mathbf{p}}(\lambda,\Delta\lambda) (\hat{f}^\dagger_{\mathbf{p+q},\sigma} c_{\mathbf{p}\sigma} + c^\dagger_{\mathbf{p}\sigma} \hat{f}_{\mathbf{p-q},\sigma}) \\
& + \frac{1}{N} \beta_{\mathbf{k+q},\mathbf{k}}(\lambda,\Delta\lambda) \Bigg[C^{ff}_\rho(\mathbf{q}) \left(c^\dagger_{\mathbf{k+q},m} c_{\mathbf{k+q},m} - c^\dagger_{\mathbf{k}m} c_{\mathbf{k}m} \right) \\
& \qquad + \left(1 - 2\langle n^f \rangle\right) \left(\langle c^\dagger_{\mathbf{k+q},m} c_{\mathbf{k+q},m} \rangle - \langle c^\dagger_{\mathbf{k}m} c_{\mathbf{k}m} \rangle \right) \frac{1}{N} \sum_{i,\sigma'} \hat{f}^\dagger_{i\sigma'} \hat{f}_{i\sigma'} \\
& \qquad - \left(\langle c^\dagger_{\mathbf{k+q},m} c_{\mathbf{k+q},m} \rangle - \langle c^\dagger_{\mathbf{k}m} c_{\mathbf{k}m} \rangle \right) \left(\langle n^f \rangle - 2\langle n^f \rangle^2 \right) \Bigg],
\end{aligned} \tag{6.5}$$

where $\alpha_{\mathbf{k}}(\lambda,\Delta\lambda)$ and $\beta_{\mathbf{k+q},\mathbf{k}}(\lambda,\Delta\lambda)$ are given by (4.22).

In the non-superconducting state, the contributions proportional to $\alpha_{\mathbf{k}}(\lambda, \Delta\lambda)$ disappear, as already obtained in the previous chapter. In the superconducting state, new contributions from the factorization have to be considered. The factorization of the first term in (6.5) can be performed as follows. First we have

$$\hat{f}^{\dagger}_{\mathbf{k}m} c_{\mathbf{k}+\mathbf{q},m} \frac{1}{N} \sum_{i,m'} \delta(\hat{f}^{\dagger}_{im'} \hat{f}_{im'}) e^{i\mathbf{q}\mathbf{R}_i} = \frac{1}{N} \sum_{i,m'} \left(\hat{f}^{\dagger}_{\mathbf{k}m} c_{\mathbf{k}+\mathbf{q},m} \hat{f}^{\dagger}_{im'} \hat{f}_{im'} \right) e^{i\mathbf{q}\mathbf{R}_i}. \tag{6.6}$$

This equivalence is correct because we are interested only in contributions with $\mathbf{k} \neq \mathbf{k}+\mathbf{q}$. Using the Fourier transformation to the momentum-space for the f-operators, we obtain

$$\begin{aligned}
&\frac{1}{N} \sum_{i,m'} \left(\hat{f}^{\dagger}_{\mathbf{k}m} c_{\mathbf{k}+\mathbf{q},m} \hat{f}^{\dagger}_{im'} \hat{f}_{im'} \right) e^{i\mathbf{q}\mathbf{R}_i} = \frac{1}{N^2} \sum_{\substack{\mathbf{p}_1\mathbf{p}_2 \\ im'}} \hat{f}^{\dagger}_{\mathbf{k}m} c_{\mathbf{k}+\mathbf{q},m} \hat{f}^{\dagger}_{\mathbf{p}_1 m'} \hat{f}_{\mathbf{p}_2 m'} e^{i(\mathbf{q}-\mathbf{p}_1+\mathbf{p}_2)\mathbf{R}_i} \\
&= \frac{1}{N} \sum_{\substack{\mathbf{p}_1\mathbf{p}_2 \\ m'}} \delta_{\mathbf{q},\mathbf{p}_1-\mathbf{p}_2} \hat{f}^{\dagger}_{\mathbf{k}m} c_{\mathbf{k}+\mathbf{q},m} \hat{f}^{\dagger}_{\mathbf{p}_1 m'} \hat{f}_{\mathbf{p}_2 m'} = -\frac{1}{N} \sum_{\substack{\mathbf{p}_1\mathbf{p}_2 \\ m'}} \delta_{\mathbf{q},\mathbf{p}_1-\mathbf{p}_2} \hat{f}^{\dagger}_{\mathbf{k}m} \hat{f}^{\dagger}_{\mathbf{p}_1 m'} c_{\mathbf{k}+\mathbf{q},m} \hat{f}_{\mathbf{p}_2 m'} \\
&= -\frac{1}{N} \sum_{\substack{\mathbf{p}_1\mathbf{p}_2 \\ m'}} \delta_{\mathbf{q},\mathbf{p}_1-\mathbf{p}_2} (1-\delta_{mm'}) \delta_{\mathbf{k},-\mathbf{p}_1} \delta_{\mathbf{k}+\mathbf{q},-\mathbf{p}_2} \hat{f}^{\dagger}_{\mathbf{k}m} \hat{f}^{\dagger}_{-\mathbf{k}m'} c_{\mathbf{k}+\mathbf{q},m} \hat{f}_{-(\mathbf{k}+\mathbf{q}),m'} \\
&= -\frac{1}{N} \sum_{m'} (1-\delta_{mm'}) \hat{f}^{\dagger}_{\mathbf{k}m} \hat{f}^{\dagger}_{-\mathbf{k}m'} c_{\mathbf{k}+\mathbf{q},m} \hat{f}_{-(\mathbf{k}+\mathbf{q}),m'} \\
&\quad = -\frac{1}{N} \sum_{m'} \left[\delta_{m\uparrow}\delta_{m'\downarrow} \hat{f}^{\dagger}_{\mathbf{k}\uparrow} \hat{f}^{\dagger}_{-\mathbf{k}\downarrow} c_{\mathbf{k}+\mathbf{q},\uparrow} \hat{f}_{-(\mathbf{k}+\mathbf{q}),\downarrow} + \delta_{m\downarrow}\delta_{m'\uparrow} \hat{f}^{\dagger}_{\mathbf{k}\downarrow} \hat{f}^{\dagger}_{-\mathbf{k}\uparrow} c_{\mathbf{k}+\mathbf{q},\downarrow} \hat{f}_{-(\mathbf{k}+\mathbf{q}),\uparrow} \right] \\
&\qquad = \frac{1}{N} \delta_{m\uparrow} \hat{f}^{\dagger}_{\mathbf{k}\uparrow} \hat{f}^{\dagger}_{-\mathbf{k}\downarrow} \hat{f}_{-(\mathbf{k}+\mathbf{q}),\downarrow} c_{\mathbf{k}+\mathbf{q},\uparrow} + \frac{1}{N} \delta_{m\downarrow} \hat{f}^{\dagger}_{-\mathbf{k}\uparrow} \hat{f}^{\dagger}_{\mathbf{k}\downarrow} c_{\mathbf{k}+\mathbf{q},\downarrow} \hat{f}_{-(\mathbf{k}+\mathbf{q}),\uparrow}.
\end{aligned} \tag{6.7}$$

By the same way, we also find

$$\begin{aligned}
&c^{\dagger}_{\mathbf{k}m} \hat{f}_{\mathbf{k}+\mathbf{q},m} \frac{1}{N} \sum_{i,m'} \delta(\hat{f}^{\dagger}_{im'} \hat{f}_{im'}) e^{i\mathbf{q}\mathbf{R}_i} \\
&\qquad = \frac{1}{N} \delta_{m\uparrow} c^{\dagger}_{\mathbf{k}\uparrow} \hat{f}^{\dagger}_{-\mathbf{k}\downarrow} \hat{f}_{-(\mathbf{k}+\mathbf{q}),\downarrow} \hat{f}_{\mathbf{k}+\mathbf{q},\uparrow} - \frac{1}{N} \delta_{m\downarrow} \hat{f}^{\dagger}_{-\mathbf{k}\uparrow} c^{\dagger}_{\mathbf{k}\downarrow} \hat{f}_{\mathbf{k}+\mathbf{q},\downarrow} \hat{f}_{-(\mathbf{k}+\mathbf{q}),\uparrow},
\end{aligned} \tag{6.8}$$

and

$$\begin{aligned}
&\frac{1}{N}\delta(c^\dagger_{\mathbf{k}m}c_{\mathbf{k+q},m})\sum_{\mathbf{p},m'}\alpha_{\mathbf{p}}(\lambda,\Delta\lambda)(\hat{f}^\dagger_{\mathbf{p+q},m'}c_{\mathbf{p}m'}+c^\dagger_{\mathbf{p}m'}\hat{f}_{\mathbf{p-q},m'})\\
&=\frac{1}{N}\delta_{m\uparrow}\left(\alpha_{-(\mathbf{k+q})}(\lambda,\Delta\lambda)c^\dagger_{\mathbf{k}\uparrow}\hat{f}^\dagger_{-\mathbf{k}\downarrow}c_{-(\mathbf{k+q}),\downarrow}c_{\mathbf{k+q},\uparrow}+\alpha_{-\mathbf{k}}(\lambda,\Delta\lambda)c^\dagger_{\mathbf{k}\uparrow}c^\dagger_{-\mathbf{k}\downarrow}\hat{f}_{-(\mathbf{k+q}),\downarrow}c_{\mathbf{k+q},\uparrow}\right)\\
&+\frac{1}{N}\delta_{m\downarrow}\left(\alpha_{-(\mathbf{k+q})}(\lambda,\Delta\lambda)\hat{f}^\dagger_{-\mathbf{k}\uparrow}c^\dagger_{\mathbf{k}\downarrow}c_{\mathbf{k+q},\downarrow}c_{-(\mathbf{k+q}),\uparrow}+\alpha_{-\mathbf{k}}(\lambda,\Delta\lambda)c^\dagger_{-\mathbf{k}\uparrow}c^\dagger_{\mathbf{k}\downarrow}c_{\mathbf{k+q},\downarrow}\hat{f}_{-(\mathbf{k+q}),\uparrow}\right).
\end{aligned}\tag{6.9}$$

Therefore, after factorizing (6.5) becomes

$$\begin{aligned}
[X_{\lambda,\Delta\lambda},\ a_{\mathbf{k},\mathbf{k+p},m}] =\\
&\alpha_{\mathbf{k}}(\lambda,\Delta\lambda)\frac{1}{N}\Big[\delta_{m\uparrow}\left(\langle\hat{f}^\dagger_{\mathbf{k}\uparrow}\hat{f}^\dagger_{-\mathbf{k}\downarrow}\rangle\hat{f}_{-(\mathbf{k+q}),\downarrow}c_{\mathbf{k+q},\uparrow}+\hat{f}^\dagger_{\mathbf{k}\uparrow}\hat{f}^\dagger_{-\mathbf{k}\downarrow}\langle\hat{f}_{-(\mathbf{k+q}),\downarrow}c_{\mathbf{k+q},\uparrow}\rangle\right)\\
&\qquad+\delta_{m\downarrow}\left(\langle\hat{f}^\dagger_{-\mathbf{k}\uparrow}\hat{f}^\dagger_{\mathbf{k}\downarrow}\rangle c_{\mathbf{k+q},\downarrow}\hat{f}_{-(\mathbf{k+q}),\uparrow}+\hat{f}^\dagger_{-\mathbf{k}\uparrow}\hat{f}^\dagger_{\mathbf{k}\downarrow}\langle c_{\mathbf{k+q},\downarrow}\hat{f}_{-(\mathbf{k+q}),\uparrow}\rangle\right)\Big]\\
&+\alpha_{\mathbf{k+q}}(\lambda,\Delta\lambda)\frac{1}{N}\Big[\delta_{m\uparrow}\left(\langle c^\dagger_{\mathbf{k}\uparrow}\hat{f}^\dagger_{-\mathbf{k}\downarrow}\rangle\hat{f}_{-(\mathbf{k+q}),\downarrow}\hat{f}_{\mathbf{k+q},\uparrow}+c^\dagger_{\mathbf{k}\uparrow}\hat{f}^\dagger_{-\mathbf{k}\downarrow}\langle\hat{f}_{-(\mathbf{k+q}),\downarrow}\hat{f}_{\mathbf{k+q},\uparrow}\rangle\right)\\
&\qquad+\delta_{m\downarrow}\left(\langle\hat{f}^\dagger_{-\mathbf{k}\uparrow}c^\dagger_{\mathbf{k}\downarrow}\rangle\hat{f}_{\mathbf{k+q},\downarrow}\hat{f}_{-(\mathbf{k+q}),\uparrow}+\hat{f}^\dagger_{-\mathbf{k}\uparrow}c^\dagger_{\mathbf{k}\downarrow}\langle\hat{f}_{\mathbf{k+q},\downarrow}\hat{f}_{-(\mathbf{k+q}),\uparrow}\rangle\right)\Big]\\
&+\alpha_{-(\mathbf{k+q})}(\lambda,\Delta\lambda)\frac{1}{N}\Big[\delta_{m\uparrow}\left(\langle c^\dagger_{\mathbf{k}\uparrow}\hat{f}^\dagger_{-\mathbf{k}\downarrow}\rangle c_{-(\mathbf{k+q}),\downarrow}c_{\mathbf{k+q},\uparrow}+c^\dagger_{\mathbf{k}\uparrow}\hat{f}^\dagger_{-\mathbf{k}\downarrow}\langle c_{-(\mathbf{k+q}),\downarrow}c_{\mathbf{k+q},\uparrow}\rangle\right)\\
&\qquad+\delta_{m\uparrow}\left(\langle\hat{f}^\dagger_{-\mathbf{k}\uparrow}c^\dagger_{\mathbf{k}\downarrow}\rangle c_{\mathbf{k+q},\downarrow}c_{-(\mathbf{k+q}),\uparrow}+\hat{f}^\dagger_{-\mathbf{k}\uparrow}c^\dagger_{\mathbf{k}\downarrow}\langle c_{\mathbf{k+q},\downarrow}c_{-(\mathbf{k+q}),\uparrow}\rangle\right)\Big]\\
&+\alpha_{-\mathbf{k}}(\lambda,\Delta\lambda)\frac{1}{N}\Big[\delta_{m\downarrow}\left(\langle c^\dagger_{\mathbf{k}\uparrow}c^\dagger_{-\mathbf{k}\downarrow}\rangle\hat{f}_{-(\mathbf{k+q}),\downarrow}c_{\mathbf{k+q},\uparrow}+c^\dagger_{\mathbf{k}\uparrow}c^\dagger_{-\mathbf{k}\downarrow}\langle\hat{f}_{-(\mathbf{k+q}),\downarrow}c_{\mathbf{k+q},\uparrow}\rangle\right)\\
&\qquad+\delta_{m\downarrow}\left(\langle c^\dagger_{-\mathbf{k}\uparrow}c^\dagger_{\mathbf{k}\downarrow}\rangle c_{\mathbf{k+q},\downarrow}\hat{f}_{-(\mathbf{k+q}),\uparrow}+c^\dagger_{-\mathbf{k}\uparrow}c^\dagger_{\mathbf{k}\downarrow}\langle c_{\mathbf{k+q},\downarrow}\hat{f}_{-(\mathbf{k+q}),\uparrow}\rangle\right)\Big]\\
&+\text{constant}.
\end{aligned}\tag{6.10}$$

For the operators in (6.2), the unitary transformation is similar. As an example, the commutator of the generator $X_{\lambda,\Delta\lambda}$ with the operator $c^\dagger_{\mathbf{k}\uparrow}c^\dagger_{-\mathbf{k}\downarrow}$ is evaluated as follows

$$\begin{aligned}
[X_{\lambda,\Delta\lambda},c^\dagger_{\mathbf{k}\uparrow}c^\dagger_{-\mathbf{k}\downarrow}] &= \sum_{\mathbf{p},m}\alpha_{\mathbf{p}}(\lambda,\Delta\lambda)[(\hat{f}^\dagger_{\mathbf{p}m}c_{\mathbf{p}m}-\text{h.c.}),c^\dagger_{\mathbf{k}\uparrow}c^\dagger_{-\mathbf{k}\downarrow}]\\
&+\sum_{\mathbf{pq},m}\beta_{\mathbf{p},\mathbf{p+q}}(\lambda,\Delta\lambda)[a_{\mathbf{p},\mathbf{p+q},m},c^\dagger_{\mathbf{k}\uparrow}c^\dagger_{-\mathbf{k}\downarrow}].
\end{aligned}\tag{6.11}$$

The first commutator is

$$[\hat{f}^\dagger_{\mathbf{p}m}c_{\mathbf{p}m},c^\dagger_{\mathbf{k}\uparrow}c^\dagger_{-\mathbf{k}\downarrow}]-[c^\dagger_{\mathbf{p}m}\hat{f}_{\mathbf{p}m},c^\dagger_{\mathbf{k}\uparrow}c^\dagger_{-\mathbf{k}\downarrow}]=\hat{f}^\dagger_{\mathbf{p}m}\left(\delta_{\mathbf{p},\mathbf{k}}\delta_{m\uparrow}c^\dagger_{-\mathbf{k}\downarrow}-\delta_{\mathbf{p},-\mathbf{k}}\delta_{m\downarrow}c^\dagger_{\mathbf{k}\uparrow}\right),\tag{6.12}$$

and the second becomes

$$c^\dagger_{\mathbf{p}m}\left(\delta_{\mathbf{p}+\mathbf{q},\mathbf{k}}\delta_{m\uparrow}c^\dagger_{-\mathbf{k}\downarrow}-\delta_{\mathbf{p}+\mathbf{q},-\mathbf{k}}\delta_{m\downarrow}c^\dagger_{\mathbf{k}\uparrow}\right)\frac{1}{N}\sum_{i,m'}\delta(\hat{f}^\dagger_{im'}\hat{f}_{im'})e^{i\mathbf{q}\mathbf{R}_i}. \tag{6.13}$$

So

$$\begin{aligned}[X_{\lambda,\Delta\lambda},c^\dagger_{\mathbf{k}\uparrow}c^\dagger_{-\mathbf{k}\downarrow}] &= \alpha_{\mathbf{k}}(\lambda,\Delta\lambda)\hat{f}^\dagger_{\mathbf{k}\uparrow}c^\dagger_{-\mathbf{k}\downarrow}-\alpha_{-\mathbf{k}}(\lambda,\Delta\lambda)\hat{f}^\dagger_{-\mathbf{k}\downarrow}c^\dagger_{\mathbf{k}\uparrow}\\ &+\sum_{\mathbf{p}}\beta_{\mathbf{p}\mathbf{k}}(\lambda,\Delta\lambda)c^\dagger_{\mathbf{p}\uparrow}c^\dagger_{-\mathbf{k}\downarrow}\frac{1}{N}\sum_{i,m'}\delta(\hat{f}^\dagger_{im'}\hat{f}_{im'})e^{i(\mathbf{k}-\mathbf{p})\mathbf{R}_i}\\ &-\sum_{\mathbf{p}}\beta_{\mathbf{p},-\mathbf{k}}(\lambda,\Delta\lambda)c^\dagger_{\mathbf{p}\downarrow}c^\dagger_{\mathbf{k}\uparrow}\frac{1}{N}\sum_{i,m'}\delta(\hat{f}^\dagger_{im'}\hat{f}_{im'})e^{-i(\mathbf{p}+\mathbf{k})\mathbf{R}_i}.\end{aligned} \tag{6.14}$$

We see that, only $\mathbf{p}=\mathbf{k}$ in the third and $\mathbf{p}=-\mathbf{k}$ in the fourth terms will contribute in a factorization approximation. This follows that $\beta_{\mathbf{p},\mathbf{k}}$ and $\beta_{\mathbf{p},-\mathbf{k}}$ reduce to $\beta_{\mathbf{k},\mathbf{k}}$ and $\beta_{-\mathbf{k},-\mathbf{k}}$, which are zero. Therefore,

$$[X_{\lambda,\Delta\lambda},c^\dagger_{\mathbf{k}\uparrow}c^\dagger_{-\mathbf{k}\downarrow}]=\alpha_{\mathbf{k}}(\lambda,\Delta\lambda)\hat{f}^\dagger_{\mathbf{k}\uparrow}c^\dagger_{-\mathbf{k}\downarrow}+\alpha_{-\mathbf{k}}(\lambda,\Delta\lambda)c^\dagger_{\mathbf{k}\uparrow}\hat{f}^\dagger_{-\mathbf{k}\downarrow}. \tag{6.15}$$

Similarly, we obtain

$$\begin{aligned}
[X_{\lambda,\Delta\lambda},c_{-\mathbf{k}\downarrow}c_{\mathbf{k}\uparrow}] &= \alpha_{\mathbf{k}}(\lambda,\Delta\lambda)c_{-\mathbf{k}\downarrow}\hat{f}_{\mathbf{k}\uparrow}+\alpha_{-\mathbf{k}}(\lambda,\Delta\lambda)\hat{f}_{-\mathbf{k}\downarrow}c_{\mathbf{k}\uparrow},\\
[X_{\lambda,\Delta\lambda},\hat{f}^\dagger_{\mathbf{k}\uparrow}\hat{f}^\dagger_{-\mathbf{k}\downarrow}] &= -D\left(\alpha_{-\mathbf{k}}(\lambda,\Delta\lambda)\hat{f}^\dagger_{\mathbf{k}\uparrow}c^\dagger_{-\mathbf{k}\downarrow}+\alpha_{\mathbf{k}}(\lambda,\Delta\lambda)c^\dagger_{\mathbf{k}\uparrow}\hat{f}^\dagger_{-\mathbf{k}\downarrow}\right),\\
[X_{\lambda,\Delta\lambda},\hat{f}_{-\mathbf{k}\downarrow}\hat{f}_{\mathbf{k}\uparrow}] &= -D\left(\alpha_{-\mathbf{k}}(\lambda,\Delta\lambda)c_{-\mathbf{k}\downarrow}\hat{f}_{\mathbf{k}\uparrow}+\alpha_{\mathbf{k}}(\lambda,\Delta\lambda)\hat{f}_{-\mathbf{k}\downarrow}c_{\mathbf{k}\uparrow}\right),\\
[X_{\lambda,\Delta\lambda},\hat{f}^\dagger_{\mathbf{k}\uparrow}c^\dagger_{-\mathbf{k}\downarrow}] &= \alpha_{-\mathbf{k}}(\lambda,\Delta\lambda)\hat{f}^\dagger_{\mathbf{k}\uparrow}\hat{f}^\dagger_{-\mathbf{k}\downarrow}-D\alpha_{\mathbf{k}}(\lambda,\Delta\lambda)c^\dagger_{\mathbf{k}\uparrow}c^\dagger_{-\mathbf{k}\downarrow},\\
[X_{\lambda,\Delta\lambda},\hat{f}_{-\mathbf{k}\downarrow}c_{\mathbf{k}\uparrow}] &= \alpha_{\mathbf{k}}(\lambda,\Delta\lambda)\hat{f}_{-\mathbf{k}\downarrow}\hat{f}_{\mathbf{k}\uparrow}-D\alpha_{-\mathbf{k}}(\lambda,\Delta\lambda)c_{-\mathbf{k}\downarrow}c_{\mathbf{k}\uparrow},\\
[X_{\lambda,\Delta\lambda},c^\dagger_{\mathbf{k}\uparrow}\hat{f}^\dagger_{-\mathbf{k}\downarrow}] &= \alpha_{\mathbf{k}}(\lambda,\Delta\lambda)\hat{f}^\dagger_{\mathbf{k}\uparrow}\hat{f}^\dagger_{-\mathbf{k}\downarrow}-D\alpha_{-\mathbf{k}}(\lambda,\Delta\lambda)c^\dagger_{\mathbf{k}\uparrow}c^\dagger_{-\mathbf{k}\downarrow},\\
[X_{\lambda,\Delta\lambda},c_{-\mathbf{k}\downarrow}\hat{f}_{\mathbf{k}\uparrow}] &= \alpha_{-\mathbf{k}}(\lambda,\Delta\lambda)\hat{f}_{-\mathbf{k}\downarrow}\hat{f}_{\mathbf{k}\uparrow}-D\alpha_{\mathbf{k}}(\lambda,\Delta\lambda)c_{-\mathbf{k}\downarrow}c_{\mathbf{k}\uparrow}.
\end{aligned} \tag{6.16}$$

Comparing the coefficients of the different operator terms in the renormalization ansatz (6.1) at cutoff $\lambda-\Delta\lambda$ with those, which were explicitly evaluated in the unitary transformation, $\mathcal{H}_{\lambda-\Delta\lambda}=e^{X_{\lambda,\Delta\lambda}}\mathcal{H}_\lambda e^{-X_{\lambda,\Delta\lambda}}$, we can obtain difference equations for the renormalized parameters. In the limit $\Delta\lambda\to 0$, this set of difference equations becomes a set of differential equations. Besides the differential equations, obtained in (4.32)

before, we obtain additional equations for the renormalization of the superconducting energy gaps

$$\begin{aligned}
\frac{d\Delta^{cc}_{\mathbf{k},\lambda}}{d\lambda} &= D\left(\Delta^{fc}_{\mathbf{k},\lambda}\tilde{\alpha}_{\mathbf{k},\lambda} + \Delta^{cf}_{\mathbf{k},\lambda}\tilde{\alpha}_{-\mathbf{k},\lambda}\right) \\
&\quad - \frac{1}{N}\sum_{\mathbf{q}} U_{\mathbf{k},\mathbf{k}+\mathbf{q},\lambda}\left(\tilde{\alpha}_{-\mathbf{k},\lambda}\langle\hat{f}_{-(\mathbf{k}+\mathbf{q}),\downarrow}c_{\mathbf{k}+\mathbf{q},\uparrow}\rangle + \tilde{\alpha}_{\mathbf{k},\lambda}\langle c_{-(\mathbf{k}+\mathbf{q}),\downarrow}\hat{f}_{\mathbf{k}+\mathbf{q},\uparrow}\rangle\right), \\
\frac{d\Delta^{ff}_{\mathbf{k},\lambda}}{d\lambda} &= -\left(\Delta^{fc}_{\mathbf{k},\lambda}\tilde{\alpha}_{-\mathbf{k},\lambda} + \Delta^{cf}_{\mathbf{k},\lambda}\tilde{\alpha}_{\mathbf{k},\lambda}\right) \\
&\quad + \frac{1}{N}\sum_{\mathbf{q}} U_{\mathbf{k},\mathbf{k}+\mathbf{q},\lambda}\left(\tilde{\alpha}_{\mathbf{k},\lambda}\langle\hat{f}_{-(\mathbf{k}+\mathbf{q}),\downarrow}c_{\mathbf{k}+\mathbf{q},\uparrow}\rangle + \tilde{\alpha}_{-\mathbf{k},\lambda}\langle c_{-(\mathbf{k}+\mathbf{q}),\downarrow}\hat{f}_{\mathbf{k}+\mathbf{q},\uparrow}\rangle\right), \\
\frac{d\Delta^{fc}_{\mathbf{k},\lambda}}{d\lambda} &= -\Delta^{cc}_{\mathbf{k},\lambda}\tilde{\alpha}_{\mathbf{k},\lambda} + D\Delta^{ff}_{\mathbf{k},\lambda}\tilde{\alpha}_{-\mathbf{k},\lambda} \\
&\quad + \frac{1}{N}\sum_{\mathbf{q}} U_{\mathbf{k},\mathbf{k}+\mathbf{q},\lambda}\left(\tilde{\alpha}_{\mathbf{k}+\mathbf{q},\lambda}\langle\hat{f}_{-(\mathbf{k}+\mathbf{q}),\downarrow}\hat{f}_{\mathbf{k}+\mathbf{q},\uparrow}\rangle - \tilde{\alpha}_{\mathbf{k}+\mathbf{q},\lambda}\langle c_{-(\mathbf{k}+\mathbf{q}),\downarrow}c_{\mathbf{k}+\mathbf{q},\uparrow}\rangle\right), \\
\frac{d\Delta^{cf}_{\mathbf{k},\lambda}}{d\lambda} &= -\Delta^{cc}_{\mathbf{k},\lambda}\tilde{\alpha}_{-\mathbf{k},\lambda} + D\Delta^{ff}_{\mathbf{k},\lambda}\tilde{\alpha}_{\mathbf{k},\lambda} \\
&\quad + \frac{1}{N}\sum_{\mathbf{q}} U_{\mathbf{k},\mathbf{k}+\mathbf{q},\lambda}\left(\tilde{\alpha}_{\mathbf{k}+\mathbf{q},\lambda}\langle\hat{f}_{-(\mathbf{k}+\mathbf{q}),\downarrow}\hat{f}_{\mathbf{k}+\mathbf{q},\uparrow}\rangle - \tilde{\alpha}_{\mathbf{k}+\mathbf{q},\lambda}\langle c_{-(\mathbf{k}+\mathbf{q}),\downarrow}c_{\mathbf{k}+\mathbf{q},\uparrow}\rangle\right).
\end{aligned} \tag{6.17}$$

Combining (6.17) with (4.32), we have obtained a full set of differential equations which determine the renormalization of all parameters of the EPAM in the superconducting state. However, by solving these equations we still can not obtain the fully renormalized Hamiltonian, by which the expectation values can be estimated straightforwardly. This is due to the density-density interaction term in (4.33), which prevents this evaluation. However, in Section 4.4 it was shown that this interaction term is not important in the case of a sharp valence transition regime. On the other hand, we are concerned with the superconducting state which is expected to be found close to the sharp valence transition regimes. Therefore, in the following the density-density interaction will be left out.

6.2 Superconducting pairing functions

Without the density-density correlation between the localized electrons, the set of differential equations for determining the parameters for the renormalized EPAM in the su-

perconducting state becomes quite simple to solve. In order to solve the equations (4.32) and (6.17) for the initial conditions (4.13) and (6.3), the expectation values which include $\langle c^{\dagger}_{\mathbf{k}m} c_{\mathbf{k}m}\rangle$, $\langle \hat{f}^{\dagger}_{\mathbf{k}m} c_{\mathbf{k}m} + \text{h.c.}\rangle$, $\langle \hat{n}^f\rangle$ as well as the superconducting pairing functions have to be first determined. Similar to the previous chapter, these expectation values are assumed to be defined for the original full Hamiltonian. Thus, they have to be evaluated self-consistently. Starting by given expectation values, we can evaluate new values for the renormalization parameters by using the renormalization procedure. After getting a self-consistent solution, we have obtained the final Hamiltonian to describe the superconducting state. In the limit $\lambda \to 0$, this Hamiltonian reads

$$\begin{aligned}\tilde{\mathcal{H}} =& \tilde{\mu}_f \sum_{\mathbf{k},m} \hat{f}^{\dagger}_{\mathbf{k}m}\hat{f}_{\mathbf{k}m} + \sum_{\mathbf{k},m} \tilde{\gamma}_{\mathbf{k}} \left(\hat{f}^{\dagger}_{\mathbf{k}m}\hat{f}_{\mathbf{k}m}\right)_{\text{NL}} + \sum_{\mathbf{k},m} \tilde{\varepsilon}_{\mathbf{k}}\; c^{\dagger}_{\mathbf{k}m} c_{\mathbf{k}m} + \tilde{E} \\ &- \sum_{\mathbf{k}} \left(\tilde{\Delta}^{cc}_{\mathbf{k}} c^{\dagger}_{\mathbf{k}\uparrow} c^{\dagger}_{-\mathbf{k}\downarrow} + \tilde{\Delta}^{cc,*}_{\mathbf{k}} c_{-\mathbf{k}\downarrow} c_{\mathbf{k}\uparrow}\right) - \sum_{\mathbf{k}} \left(\tilde{\Delta}^{cf}_{\mathbf{k}} c^{\dagger}_{\mathbf{k}\uparrow} \hat{f}^{\dagger}_{-\mathbf{k}\downarrow} + \tilde{\Delta}^{cf,*}_{\mathbf{k}} \hat{f}_{-\mathbf{k}\downarrow} c_{\mathbf{k}\uparrow}\right) \\ &- \sum_{\mathbf{k}} \left(\tilde{\Delta}^{ff}_{\mathbf{k}} \hat{f}^{\dagger}_{\mathbf{k}\uparrow} \hat{f}^{\dagger}_{-\mathbf{k}\downarrow} + \tilde{\Delta}^{ff,*}_{\mathbf{k}} \hat{f}_{-\mathbf{k}\downarrow} \hat{f}_{\mathbf{k}\uparrow}\right) - \sum_{\mathbf{k}} \left(\tilde{\Delta}^{fc}_{\mathbf{k}} \hat{f}^{\dagger}_{\mathbf{k}\uparrow} c^{\dagger}_{-\mathbf{k}\downarrow} + \tilde{\Delta}^{fc,*}_{\mathbf{k}} c_{-\mathbf{k}\downarrow} \hat{f}_{\mathbf{k}\uparrow}\right).\end{aligned} \tag{6.18}$$

Here, the *tilde* symbols are used to denote the fully renormalized parameters. Employing the Bogoliubov diagonalization to (6.18) (see Appendix B), we can rewrite this result as follows

$$\begin{aligned}\tilde{\mathcal{H}} =& \sum_{\mathbf{k}} \mathcal{E}^1_{\mathbf{k}} (\mu^{1\dagger}_{\mathbf{k}} \mu^1_{\mathbf{k}} + \mu^{2\dagger}_{\mathbf{k}} \mu^2_{\mathbf{k}}) + \sum_{\mathbf{k}} \mathcal{E}^2_{\mathbf{k}} (\mu^{3\dagger}_{\mathbf{k}} \mu^3_{\mathbf{k}} + \mu^{4\dagger}_{\mathbf{k}} \mu^4_{\mathbf{k}}) \\ &+ \sum_{\mathbf{k}} \left[\tilde{\varepsilon}_{\mathbf{k}} + \tilde{\omega}_{\mathbf{k}} - (\mathcal{E}^1_{\mathbf{k}} + \mathcal{E}^2_{\mathbf{k}})\right] + \sum_{\mathbf{k}} \tilde{E}_{\mathbf{k}}.\end{aligned} \tag{6.19}$$

Here $\mu^i_{\mathbf{k}}$ (linear combinations of the conduction and localized electron operators) are new fermion quasiparticle operators which have excitation energies, $\mathcal{E}^{1,2}_{\mathbf{k}} = \left[(u_{\mathbf{k}} \pm \sqrt{\Phi_{\mathbf{k}}})/2\right]^{1/2}$. The somewhat lengthy expressions for $u_{\mathbf{k}}$ and $\Phi_{\mathbf{k}}$ are given in the Appendix B (Eq. B.9). From the diagonal Hamiltonian (6.19), we can evaluate the free energy

$$\begin{aligned}F =& -\frac{1}{\beta} \ln \text{Tr} e^{-\beta H} = -\frac{1}{\beta} \ln \text{Tr} e^{-\beta \tilde{\mathcal{H}}} \\ =& -\frac{2}{\beta} \left(\sum_{\mathbf{k}} \ln\left[1 + e^{-\beta \mathcal{E}^1_{\mathbf{k}}}\right] + \sum_{\mathbf{k}} \ln\left[1 + e^{-\beta \mathcal{E}^2_{\mathbf{k}}}\right]\right) \\ &+ \sum_{\mathbf{k}} \left[\tilde{\varepsilon}_{\mathbf{k}} + \tilde{\omega}_{\mathbf{k}} - (\mathcal{E}^1_{\mathbf{k}} + \mathcal{E}^2_{\mathbf{k}})\right] + \sum_{\mathbf{k}} \tilde{E}_{\mathbf{k}}\end{aligned} \tag{6.20}$$

which can be used to determine the superconducting pairing functions by functional derivation. An example is

$$\begin{aligned}\langle c_{-\mathbf{k}\downarrow} c_{\mathbf{k}\uparrow}\rangle_{\tilde{\mathcal{H}}} &= -\frac{\partial F}{\partial \tilde{\Delta}^{cc,*}_{\mathbf{k}}} \\ &= \sum_{\mathbf{k}'}\Big[1-2f(\mathcal{E}^1_{\mathbf{k}'})\Big]\frac{\partial \mathcal{E}^1_{\mathbf{k}'}}{\partial \tilde{\Delta}^{cc,*}_{\mathbf{k}}} + \sum_{\mathbf{k}'}\Big[1-2f(\mathcal{E}^2_{\mathbf{k}'})\Big]\frac{\partial \mathcal{E}^2_{\mathbf{k}'}}{\partial \tilde{\Delta}^{cc,*}_{\mathbf{k}}}.\end{aligned} \tag{6.21}$$

Here, $f(\mathcal{E}_{\mathbf{k}})$ denotes the Fermi function with respect to the energy $\mathcal{E}_{\mathbf{k}}$. Using $\partial\tilde{\Delta}^{\alpha\beta,*}_{\mathbf{k}'}/\partial\tilde{\Delta}^{\alpha\beta,*}_{\mathbf{k}} = \delta_{\mathbf{k}'\mathbf{k}}$ and the explicit expression of $\mathcal{E}^{1,2}_{\mathbf{k}}$, Eq. (6.21) can be simplified to

$$\begin{aligned}\langle c_{-\mathbf{k}\downarrow} c_{\mathbf{k}\uparrow}\rangle_{\tilde{\mathcal{H}}} = \frac{1-2f(\mathcal{E}^1_{\mathbf{k}})}{4\mathcal{E}^1_{\mathbf{k}}}\Bigg\{&\left(1+\frac{u_{\mathbf{k}}}{\sqrt{\Phi_{\mathbf{k}}}}\right)\tilde{\Delta}^{cc}_{\mathbf{k}} \\ &-\frac{2}{\sqrt{\Phi_{\mathbf{k}}}}\Big[(\tilde{\omega}^2_{\mathbf{k}}+|D\tilde{\Delta}^f_{\mathbf{k}}|^2)\tilde{\Delta}^{cc}_{\mathbf{k}} - D^2\tilde{\Delta}^{cf}_{\mathbf{k}}\tilde{\Delta}^{fc}_{\mathbf{k}}\tilde{\Delta}^{ff,*}_{\mathbf{k}}\Big]\Bigg\} \\ + \frac{1-2f(\mathcal{E}^2_{\mathbf{k}})}{4\mathcal{E}^2_{\mathbf{k}}}\Bigg\{&\left(1-\frac{u_{\mathbf{k}}}{\sqrt{\Phi_{\mathbf{k}}}}\right)\tilde{\Delta}^{cc}_{\mathbf{k}} \\ &+\frac{2}{\sqrt{\Phi_{\mathbf{k}}}}\Big[(\tilde{\omega}^2_{\mathbf{k}}+|D\tilde{\Delta}^f_{\mathbf{k}}|^2)\tilde{\Delta}^{cc}_{\mathbf{k}} - D^2\tilde{\Delta}^{cf}_{\mathbf{k}}\tilde{\Delta}^{fc}_{\mathbf{k}}\tilde{\Delta}^{ff,*}_{\mathbf{k}}\Big]\Bigg\}.\end{aligned} \tag{6.22}$$

Similarly, we have

$$\begin{aligned}\langle \hat{f}_{-\mathbf{k}\downarrow}\hat{f}_{\mathbf{k}\uparrow}\rangle_{\tilde{\mathcal{H}}} = \frac{D\,[1-2f(\mathcal{E}^1_{\mathbf{k}})]}{4\mathcal{E}^1_{\mathbf{k}}}\Bigg\{&\left(1+\frac{u_{\mathbf{k}}}{\sqrt{\Phi_{\mathbf{k}}}}\right)\tilde{\Delta}^{ff}_{\mathbf{k}} \\ &-\frac{2}{\sqrt{\Phi_{\mathbf{k}}}}\Big[(\tilde{\epsilon}^2_{\mathbf{k}}+|\tilde{\Delta}^c_{\mathbf{k}}|^2)\tilde{\Delta}^{ff}_{\mathbf{k}} - \tilde{\Delta}^{cf}_{\mathbf{k}}\tilde{\Delta}^{fc}_{\mathbf{k}}\tilde{\Delta}^{cc,*}_{\mathbf{k}}\Big]\Bigg\} \\ + \frac{D\,[1-2f(\mathcal{E}^2_{\mathbf{k}})]}{4\mathcal{E}^2_{\mathbf{k}}}\Bigg\{&\left(1-\frac{u_{\mathbf{k}}}{\sqrt{\Phi_{\mathbf{k}}}}\right)\tilde{\Delta}^{ff}_{\mathbf{k}} \\ &+\frac{2}{\sqrt{\Phi_{\mathbf{k}}}}\Big[(\tilde{\epsilon}^2_{\mathbf{k}}+|\tilde{\Delta}^c_{\mathbf{k}}|^2)\tilde{\Delta}^{ff}_{\mathbf{k}} - \tilde{\Delta}^{cf}_{\mathbf{k}}\tilde{\Delta}^{fc}_{\mathbf{k}}\tilde{\Delta}^{cc,*}_{\mathbf{k}}\Big]\Bigg\},\end{aligned} \tag{6.23}$$

and

$$\begin{aligned}\langle c_{-\mathbf{k}\downarrow}\hat{f}_{\mathbf{k}\uparrow}\rangle_{\tilde{\mathcal{H}}} = \frac{D\left[1-2f(\mathcal{E}^1_{\mathbf{k}})\right]}{4\mathcal{E}^1_{\mathbf{k}}}\Bigg\{ & \left(1+\frac{u_{\mathbf{k}}}{\sqrt{\Phi_{\mathbf{k}}}}\right)\tilde{\Delta}^{fc}_{\mathbf{k}} \\ & -\frac{2}{\sqrt{\Phi_{\mathbf{k}}}}\left[\tilde{\epsilon}_{\mathbf{k}}\tilde{\omega}_{\mathbf{k}}\tilde{\Delta}^{fc}_{\mathbf{k}} + D^3|\tilde{\Delta}^{fc}_{\mathbf{k}}|^2\tilde{\Delta}^{fc}_{\mathbf{k}} - D\tilde{\Delta}^{cc}_{\mathbf{k}}\tilde{\Delta}^{ff}_{\mathbf{k}}\tilde{\Delta}^{cf,*}_{\mathbf{k}}\right]\Bigg\} \\ + \frac{D\left[1-2f(\mathcal{E}^2_{\mathbf{k}})\right]}{4\mathcal{E}^2_{\mathbf{k}}}\Bigg\{ & \left(1-\frac{u_{\mathbf{k}}}{\sqrt{\Phi_{\mathbf{k}}}}\right)\tilde{\Delta}^{fc}_{\mathbf{k}} \\ & +\frac{2}{\sqrt{\Phi_{\mathbf{k}}}}\left[\tilde{\epsilon}_{\mathbf{k}}\tilde{\omega}_{\mathbf{k}}\tilde{\Delta}^{fc}_{\mathbf{k}} + D^3|\tilde{\Delta}^{fc}_{\mathbf{k}}|^2\tilde{\Delta}^{fc,*}_{\mathbf{k}} - D\tilde{\Delta}^{cc}_{\mathbf{k}}\tilde{\Delta}^{ff}_{\mathbf{k}}\tilde{\Delta}^{cf,*}_{\mathbf{k}}\right]\Bigg\}.\end{aligned} \tag{6.24}$$

From the two last equations in (6.17) we can see that $\Delta^{fc}_{\mathbf{k},\lambda} = \Delta^{cf}_{\mathbf{k},\lambda}$, because $\tilde{\alpha}_{\mathbf{k},\lambda} = \tilde{\alpha}_{-\mathbf{k},\lambda}$. Therefore, $\tilde{\Delta}^{fc}_{\mathbf{k}} = \tilde{\Delta}^{cf}_{\mathbf{k}}$ and

$$\langle \hat{f}_{-\mathbf{k}\downarrow}c_{\mathbf{k}\uparrow}\rangle_{\tilde{\mathcal{H}}} \;= \langle c_{-\mathbf{k}\downarrow}\hat{f}_{\mathbf{k}\uparrow}\rangle_{\tilde{\mathcal{H}}}. \tag{6.25}$$

To evaluate the superconducting pairing functions with the full Hamiltonian, we can still use the ansatz (4.48) and (4.52) with the renormalized prefactors $\tilde{x}_{\mathbf{k}}$ and $\tilde{y}_{\mathbf{k}}$. Therefore,

$$\begin{aligned}\langle c_{-\mathbf{k}\downarrow}c_{\mathbf{k}\uparrow}\rangle &= \tilde{x}^2_{\mathbf{k}}\langle c_{-\mathbf{k}\downarrow}c_{\mathbf{k}\uparrow}\rangle_{\tilde{\mathcal{H}}} + \tilde{y}^2_{\mathbf{k}}\langle \hat{f}_{-\mathbf{k}\downarrow}\hat{f}_{\mathbf{k}\uparrow}\rangle_{\tilde{\mathcal{H}}} + 2\tilde{x}_{\mathbf{k}}\tilde{y}_{\mathbf{k}}\langle \hat{f}_{-\mathbf{k}\downarrow}c_{\mathbf{k}\uparrow}\rangle_{\tilde{\mathcal{H}}}, \\ \langle \hat{f}_{-\mathbf{k}\downarrow}\hat{f}_{\mathbf{k}\uparrow}\rangle &= D^2\tilde{y}^2_{\mathbf{k}}\langle c_{-\mathbf{k}\downarrow}c_{\mathbf{k}\uparrow}\rangle_{\tilde{\mathcal{H}}} + \tilde{x}^2_{\mathbf{k}}\langle \hat{f}_{-\mathbf{k}\downarrow}\hat{f}_{\mathbf{k}\uparrow}\rangle_{\tilde{\mathcal{H}}} - 2D\tilde{x}_{\mathbf{k}}\tilde{y}_{\mathbf{k}}\langle \hat{f}_{-\mathbf{k}\downarrow}c_{\mathbf{k}\uparrow}\rangle_{\tilde{\mathcal{H}}}, \\ \langle \hat{f}_{-\mathbf{k}\downarrow}c_{\mathbf{k}\uparrow}\rangle &= \left(\tilde{x}^2_{\mathbf{k}} - D\tilde{y}^2_{\mathbf{k}}\right)\langle \hat{f}_{-\mathbf{k}\downarrow}c_{\mathbf{k}\uparrow}\rangle_{\tilde{\mathcal{H}}} - \tilde{x}_{\mathbf{k}}\tilde{y}_{\mathbf{k}}\left(D\langle c_{-\mathbf{k}\downarrow}c_{\mathbf{k}\uparrow}\rangle_{\tilde{\mathcal{H}}} - \langle \hat{f}_{-\mathbf{k}\downarrow}\hat{f}_{\mathbf{k}\uparrow}\rangle_{\tilde{\mathcal{H}}}\right).\end{aligned} \tag{6.26}$$

The other expectation values, such as $\langle c^\dagger_{\mathbf{k}m}c_{\mathbf{k}m}\rangle$, $\langle \hat{f}^\dagger_{\mathbf{k}m}c_{\mathbf{k}m} + \text{h.c.}\rangle$, and $\langle \hat{n}^f\rangle$ are determined similarly to chapter 3, Eqs. (4.57) and (4.58).

From the above analytical calculations, we have obtained a set of self-consistent equations for evaluating the expectation values as well as superconducting pairing functions of the EPAM by employing PRM. In chapter 7, we will discuss in detail its numerical results for the two-dimensional systems. By concerning only on the valence transition regime, a BCS-like self-consistent equation for determining the superconducting energy gap in momentum space is also obtained. A nature of d-wave superconductivity due to the valence fluctuations is profoundly discussed.

6.3 Approximate solution for a large lattice

Another advantage of the analytical projector-based renormalization method (PRM) is the possibility to consider larger systems than in usual numerical methods. Therefore, one is able to investigate two- or three-dimensional systems for reasonably large lattice sizes. The PRM is now applied to the two-dimensional EPAM in order to explore the superconducting state in particular in the valence transition regime.

In the general case, we have to solve self-consistently the renormalization equations in order to obtain analytical results as discussed in the previous section. However, we encounter a large number of differential equations, which need a long time for being numerically integrated, if we consider a large number of lattice sites. Thus, only a small two-dimensional system with $N = 16 \times 16$ lattice sites can be considered without additional approximations. The results for this case will be discussed in the next chapter. Nevertheless, in order to make sure that the small system is enough to mimic the thermodynamic limit, we shall first present a simplified solution which can be used for a larger lattice. By using additional approximations, the solution becomes simple so that we can explore a large system. We shall also obtain a BCS-like equation for the superconducting energy gaps. An effective pairing interaction, which is strongly dependent on momentum, is found in a simple relation with the hybridization V and the Coulomb repulsion U_{fc} between the localized electrons and conduction electrons. It shows that superconductivity can only occur in the case of simultaneous presence of U_{fc} and V. It also clarifies that superconductivity due to the valence fluctuations is of d-wave nature. Therefore in the next chapter, only numerical results for d-wave superconductivity will be considered. Our results affirm that in heavy-fermion systems, d-wave symmetry is favored by valence fluctuation [27, 56]. Note that by solving the Eliashberg equation in the fluctuation-exchange approximation for the EPAM it was also found in Ref. [29] that the d-wave symmetry is dominant as compared to the other symmetries in the valence transition regime.

As explained, this section is devoted to an analytical solution of the renormalization equations for the EPAM in the superconducting state. In chapter 7, we shall give the

corresponding numerical results for large systems. In order to evaluate analytically the renormalization equations (4.32), we assume a λ-independent energy of the f electrons as in [31, 33], $\mu_{f,\lambda} - D\bar{\Delta}_\lambda \approx \tilde{\epsilon}_f$. Also, the density-density correlation part between the localized electrons is neglected. Therefore, from (4.32) we have

$$\frac{d\varepsilon_{\mathbf{k},\lambda}}{d\lambda} = 2DV_{\mathbf{k},\lambda}\tilde{\alpha}_{\mathbf{k},\lambda}, \tag{6.27}$$

$$\frac{d\gamma_{\mathbf{k},\lambda}}{d\lambda} = -\frac{1}{D}\frac{d\varepsilon_{\mathbf{k},\lambda}}{d\lambda}, \tag{6.28}$$

$$\frac{dV_{\mathbf{k},\lambda}}{d\lambda} = A_{\mathbf{k},\lambda}\tilde{\alpha}_{\mathbf{k},\lambda}, \tag{6.29}$$

where $A_{\mathbf{k},\lambda} = \tilde{\varepsilon}_f + D\gamma_{\mathbf{k},\lambda} - \varepsilon_{\mathbf{k},\lambda}$.

Eq. (6.28) leads to the simple result

$$\gamma_{\mathbf{k},\lambda} = \frac{\varepsilon_{\mathbf{k},\Lambda} - \varepsilon_{\mathbf{k},\lambda}}{D}, \tag{6.30}$$

where we have used the initial conditions (4.13). Thus, Eq. (6.29) can be rewritten as

$$\tilde{\alpha}_{\mathbf{k},\lambda} = \frac{1}{\tilde{\varepsilon}_f + \varepsilon_{\mathbf{k},\Lambda} - 2\varepsilon_{\mathbf{k},\lambda}}\frac{dV_{\mathbf{k},\lambda}}{d\lambda}. \tag{6.31}$$

Inserting it into Eq. (6.27), one finds

$$\frac{d}{d\lambda}\left\{\varepsilon_{\mathbf{k},\lambda}^2 - (\tilde{\varepsilon}_f + \varepsilon_{\mathbf{k},\Lambda})\,\varepsilon_{\mathbf{k},\lambda} + DV_{\mathbf{k},\lambda}^2\right\} = 0 \tag{6.32}$$

which can easily be integrated and a quadratic equation for $\tilde{\epsilon}_{\mathbf{k}}$ is obtained. In the PRM, the quasi-particles in the final Hamiltonian $\tilde{\mathcal{H}}$ do not change their characters as function of the wave vector $\mathbf{k}$. Therefore, $\tilde{\epsilon}_{\mathbf{k}}$ jumps between the two solutions of the quadratic equation (6.32) in order to minimize the derivations from the original $\varepsilon_{\mathbf{k},\Lambda}$ (see (4.13))

$$\tilde{\epsilon}_{\mathbf{k}} = \frac{\tilde{\varepsilon}_f + \varepsilon_{\mathbf{k},\Lambda}}{2} - \frac{\mathrm{sgn}(\tilde{\varepsilon}_f - \varepsilon_{\mathbf{k},\Lambda})}{2}W_{\mathbf{k}}, \tag{6.33}$$

$$W_{\mathbf{k}} = \sqrt{(\varepsilon_{\mathbf{k},\Lambda} - \tilde{\varepsilon}_f)^2 + 4DV^2}. \tag{6.34}$$

The second quasi-particle band is given by

$$\tilde{\omega}_{\mathbf{k}} := \tilde{\varepsilon}_f + D\tilde{\gamma}_{\mathbf{k}} = \frac{\tilde{\varepsilon}_f + \varepsilon_{\mathbf{k},\Lambda}}{2} + \frac{\mathrm{sgn}(\tilde{\varepsilon}_f - \varepsilon_{\mathbf{k},\Lambda})}{2}W_{\mathbf{k}}. \tag{6.35}$$

The expectation values, formed with the original Hamiltonian, can be calculated by using the renormalized one-particle operators as discussed in the chapter 4

$$c^{\dagger}_{\mathbf{k}m}(\lambda \to 0) = \tilde{x}_{\mathbf{k}} c^{\dagger}_{\mathbf{k}m} + \tilde{y}_{\mathbf{k}} \hat{f}^{\dagger}_{\mathbf{k}m}, \tag{6.36}$$

$$\hat{f}^{\dagger}_{\mathbf{k}m}(\lambda \to 0) = -D\tilde{y}_{\mathbf{k}} c^{\dagger}_{\mathbf{k}m} + \tilde{x}_{\mathbf{k}} \hat{f}^{\dagger}_{\mathbf{k}m}, \tag{6.37}$$

where we defined

$$|\tilde{x}_{\mathbf{k}}|^2 = \frac{1}{2}\left[1 + \mathrm{sgn}(\tilde{\varepsilon}_f - \varepsilon_{\mathbf{k},\Lambda})\frac{\tilde{\varepsilon}_f - \varepsilon_{\mathbf{k},\Lambda}}{W_{\mathbf{k}}}\right], \tag{6.38}$$

$$|\tilde{y}_{\mathbf{k}}|^2 = \frac{1}{2D}\left[1 - \mathrm{sgn}(\tilde{\varepsilon}_f - \varepsilon_{\mathbf{k},\Lambda})\frac{\tilde{\varepsilon}_f - \varepsilon_{\mathbf{k},\Lambda}}{W_{\mathbf{k}}}\right]. \tag{6.39}$$

Therefore, the expectation values can easily be evaluated

$$\begin{aligned}\langle c^{\dagger}_{\mathbf{k}m} c_{\mathbf{k}m}\rangle = &\frac{1}{2}\left[1 + \mathrm{sgn}(\tilde{\varepsilon}_f - \varepsilon_{\mathbf{k},\Lambda})\frac{\tilde{\varepsilon}_f - \varepsilon_{\mathbf{k},\Lambda}}{W_{\mathbf{k}}}\right] f(\tilde{\varepsilon}_{\mathbf{k}}) \\ &+ \frac{1}{2}\left[1 - \mathrm{sgn}(\tilde{\varepsilon}_f - \varepsilon_{\mathbf{k},\Lambda})\frac{\tilde{\varepsilon}_f - \varepsilon_{\mathbf{k},\Lambda}}{W_{\mathbf{k}}}\right] \bar{f}(\tilde{\omega}_{\mathbf{k}})\end{aligned} \tag{6.40}$$

and

$$\begin{aligned}\langle \hat{n}^f\rangle = &\frac{1}{2}\frac{\nu_f}{N}\sum_{\mathbf{k}}\left[1 - \mathrm{sgn}(\tilde{\varepsilon}_f - \varepsilon_{\mathbf{k},\Lambda})\frac{\tilde{\varepsilon}_f - \varepsilon_{\mathbf{k},\Lambda}}{W_{\mathbf{k}}}\right] f(\tilde{\varepsilon}_{\mathbf{k}}) \\ &+ \frac{1}{2}\frac{\nu_f}{N}\sum_{\mathbf{k}}\left[2D - 1 + \mathrm{sgn}(\tilde{\varepsilon}_f - \varepsilon_{\mathbf{k},\Lambda})\frac{\tilde{\varepsilon}_f - \varepsilon_{\mathbf{k},\Lambda}}{W_{\mathbf{k}}}\right] \bar{f}(\tilde{\omega}_{\mathbf{k}}),\end{aligned} \tag{6.41}$$

where $\bar{f}(\tilde{\omega}_{\mathbf{k}})$ has been defined in (4.59).

In order to solve analytically the renormalization equations (6.17) for the superconducting energy gaps, we note that the superconducting state only occurs at a momentum, in which both f-band and c-band are close to the Fermi level. That means that at momentum $\mathbf{k}$ both quasi-particle bands, $\tilde{\omega}_{\mathbf{k}}$ and $\tilde{\varepsilon}_{\mathbf{k}}$, are located in the vicinity of the Fermi level. This minimizes the factor $|\tilde{A}_{\mathbf{k}}| = |\tilde{\omega}_{\mathbf{k}} - \tilde{\varepsilon}_{\mathbf{k}}|$. Moreover, the most dominant contributions of $\tilde{\alpha}_{\mathbf{k},\lambda}$ during the renormalization is at momenta $\mathbf{k}$ with the smallest values $|A_{\mathbf{k},\lambda}|_{\min}$ of $|A_{\mathbf{k},\lambda}|$. When $\lambda \to |A_{\mathbf{k},\lambda}|_{\min}$, the renormalization procedure is completed. Therefore, we can substitute the λ-dependent parameters in (6.17) by their renormalized

values. For some momenta $\mathbf{k}$ close to the Fermi momentum, $\mathbf{k}_F$, we can approximate the λ dependence of $\tilde{\alpha}_{\mathbf{k},\lambda}$ by

$$\tilde{\alpha}_{\mathbf{k},\lambda} \approx \frac{\tilde{A}_{\mathbf{k}}}{\kappa(\lambda - |\tilde{A}_{\mathbf{k}}|)^2} V \exp\left\{ -\frac{\tilde{A}_{\mathbf{k}}^2}{\kappa(\lambda - |\tilde{A}_{\mathbf{k}}|)} \right\} \theta(\lambda - |\tilde{A}_{\mathbf{k}}|). \tag{6.42}$$

The constant κ ensures that the exponent is dimensionless. Therefore, we obtain

$$\tilde{\alpha}_{\mathbf{k},\lambda} \approx \frac{V}{\tilde{A}_{\mathbf{k}}} \delta(\lambda - |\tilde{A}_{\mathbf{k}}|)\theta(\lambda - |\tilde{A}_{\mathbf{k}}|), \tag{6.43}$$

where the δ function denotes the delta Dirac function.

So, the set of renormalization equations (6.17) is easily evaluated. The result is

$$\begin{aligned}
\tilde{\Delta}_{\mathbf{k}}^{cc} &= -\frac{2DV}{\tilde{A}_{\mathbf{k}}} \tilde{\Delta}_{\mathbf{k}}^{fc} + \frac{2V}{\tilde{A}_{\mathbf{k}}} \frac{1}{N} \sum_{\mathbf{q}} U_{\mathbf{k},\mathbf{k}+\mathbf{q}} \langle \hat{f}_{-(\mathbf{k}+\mathbf{q}),\downarrow} c_{\mathbf{k}+\mathbf{q},\uparrow} \rangle, && (6.44)\\
\tilde{\Delta}_{\mathbf{k}}^{ff} &= \frac{2V}{\tilde{A}_{\mathbf{k}}} \tilde{\Delta}_{\mathbf{k}}^{fc} - \frac{2V}{\tilde{A}_{\mathbf{k}}} \frac{1}{N} \sum_{\mathbf{q}} U_{\mathbf{k},\mathbf{k}+\mathbf{q}} \langle \hat{f}_{-(\mathbf{k}+\mathbf{q}),\downarrow} c_{\mathbf{k}+\mathbf{q},\uparrow} \rangle, && (6.45)\\
\tilde{\Delta}_{\mathbf{k}}^{fc} &= \left(\tilde{\Delta}_{\mathbf{k}}^{cc} - D\tilde{\Delta}_{\mathbf{k}}^{ff} \right) \frac{V}{\tilde{A}_{\mathbf{k}}} \\
&- \frac{V}{N} \sum_{\mathbf{q}} \frac{U'_{\mathbf{k},\mathbf{k}+\mathbf{q}}}{\tilde{A}_{\mathbf{k}+\mathbf{q}}} \left(\langle \hat{f}_{-(\mathbf{k}+\mathbf{q}),\downarrow} \hat{f}_{\mathbf{k}+\mathbf{q},\uparrow} \rangle - \langle c_{-(\mathbf{k}+\mathbf{q}),\downarrow} c_{\mathbf{k}+\mathbf{q},\uparrow} \rangle \right). && (6.46)
\end{aligned}$$

Here we have used $\tilde{\Delta}_{\mathbf{k}}^{fc} = \tilde{\Delta}_{\mathbf{k}}^{cf}$, $\langle \hat{f}_{-(\mathbf{k}+\mathbf{q}),\downarrow} c_{\mathbf{k}+\mathbf{q},\uparrow} \rangle = \langle c_{-(\mathbf{k}+\mathbf{q}),\downarrow} \hat{f}_{\mathbf{k}+\mathbf{q},\uparrow} \rangle$, and the following approximations

$$\begin{aligned}
U_{\mathbf{k},\mathbf{k}+\mathbf{q}} &\approx U_{fc} \exp\left\{ -\frac{|\tilde{B}_{\mathbf{k},\mathbf{k}+\mathbf{q}}|^2}{\kappa(|\tilde{A}_{\mathbf{k}}| - |\tilde{B}_{\mathbf{k},\mathbf{k}+\mathbf{q}}|)} \right\} \theta(|\tilde{A}_{\mathbf{k}}| - |\tilde{B}_{\mathbf{k},\mathbf{k}+\mathbf{q}}|), \\
U'_{\mathbf{k},\mathbf{k}+\mathbf{q}} &\approx U_{fc} \exp\left\{ -\frac{|\tilde{B}_{\mathbf{k},\mathbf{k}+\mathbf{q}}|^2}{\kappa(|\tilde{A}_{\mathbf{k}+\mathbf{q}}| - |\tilde{B}_{\mathbf{k},\mathbf{k}+\mathbf{q}}|)} \right\} \theta(|\tilde{A}_{\mathbf{k}+\mathbf{q}}| - |\tilde{B}_{\mathbf{k},\mathbf{k}+\mathbf{q}}|).
\end{aligned} \tag{6.47}$$

If we assume that in the valence fluctuation regime the f-electrons easily change to conduction electrons at some states $\mathbf{k} \sim \mathbf{k}_F$, we have $\langle \hat{f}_{-\mathbf{k}\downarrow} \hat{f}_{\mathbf{k}\uparrow} \rangle \approx -\langle c_{-\mathbf{k}\downarrow} c_{\mathbf{k}\uparrow} \rangle$ and $D\tilde{\Delta}_{\mathbf{k}}^{ff} \approx -\tilde{\Delta}_{\mathbf{k}}^{cc}$ for a constant total number of electrons. Thus, Eq. (6.46) can be rewritten as

$$\tilde{\Delta}_{\mathbf{k}}^{fc} = \frac{2V}{\tilde{A}_{\mathbf{k}}} \tilde{\Delta}_{\mathbf{k}}^{cc} - \frac{2V}{N} \sum_{\mathbf{q}} \frac{U'_{\mathbf{k},\mathbf{k}+\mathbf{q}}}{\tilde{A}_{\mathbf{k}+\mathbf{q}}} \langle c_{-(\mathbf{k}+\mathbf{q}),\downarrow} c_{\mathbf{k}+\mathbf{q},\uparrow} \rangle. \tag{6.48}$$

By neglecting cubic terms in $\tilde{\Delta}^{\alpha\beta}_{\mathbf{k}}$ in Eqs. (6.22-6.25), we can obtain a simple relation between each superconducting energy gap and its superconducting pairing function

$$\begin{aligned} \langle c_{-\mathbf{k}\downarrow} c_{\mathbf{k}\uparrow} \rangle &= f_{\mathbf{k}} \tilde{\Delta}^{cc}_{\mathbf{k}}, \\ \langle \hat{f}_{-\mathbf{k}\downarrow} c_{\mathbf{k}\uparrow} \rangle &= g_{\mathbf{k}} \tilde{\Delta}^{fc}_{\mathbf{k}}, \end{aligned} \tag{6.49}$$

where, at temperature $T \to 0$

$$\begin{aligned} f_{\mathbf{k}} &\approx \frac{1}{4}\left[\left(\frac{1}{\mathcal{E}^1_{\mathbf{k}}} + \frac{1}{\mathcal{E}^2_{\mathbf{k}}}\right) + \left(\frac{1}{\mathcal{E}^1_{\mathbf{k}}} - \frac{1}{\mathcal{E}^2_{\mathbf{k}}}\right)\frac{\tilde{\varepsilon}^2_{\mathbf{k}} - \tilde{\omega}^2_{\mathbf{k}}}{|\tilde{\varepsilon}^2_{\mathbf{k}} - \tilde{\omega}^2_{\mathbf{k}}|}\right], \\ g_{\mathbf{k}} &\approx \frac{1}{4}\left[\left(\frac{1}{\mathcal{E}^1_{\mathbf{k}}} + \frac{1}{\mathcal{E}^2_{\mathbf{k}}}\right) + \left(\frac{1}{\mathcal{E}^1_{\mathbf{k}}} - \frac{1}{\mathcal{E}^2_{\mathbf{k}}}\right)\frac{(\tilde{\varepsilon}_{\mathbf{k}} - \tilde{\omega}_{\mathbf{k}})^2}{|\tilde{\varepsilon}^2_{\mathbf{k}} - \tilde{\omega}^2_{\mathbf{k}}|}\right]. \end{aligned} \tag{6.50}$$

Substituting (6.50) and (6.48) into (6.44) we have

$$\tilde{\Delta}^{cc}_{\mathbf{k}} = -\frac{1}{N}\sum_{\mathbf{q}} \Gamma_{\mathbf{k},\mathbf{k}+\mathbf{q}} \tilde{\Delta}^{cc}_{\mathbf{k}+\mathbf{q}}, \tag{6.51}$$

where

$$\begin{aligned} \Gamma_{\mathbf{k},\mathbf{k}+\mathbf{q}} = \Bigg\{ &\frac{4V^2}{\tilde{A}_{\mathbf{k}}} \frac{U'_{\mathbf{k},\mathbf{k}+\mathbf{q}} f_{\mathbf{k}+\mathbf{q}} - U_{\mathbf{k},\mathbf{k}+\mathbf{q}} g_{\mathbf{k}+\mathbf{q}}}{\tilde{A}_{\mathbf{k}+\mathbf{q}}} \\ &- \frac{4V^2}{\tilde{A}_{\mathbf{k}}} \frac{1}{N} \sum_{\mathbf{q}'} U_{\mathbf{k},\mathbf{k}+\mathbf{q}'} U'_{\mathbf{k},\mathbf{k}+\mathbf{q}} \frac{f_{\mathbf{k}+\mathbf{q}} g_{\mathbf{k}+\mathbf{q}'}}{\tilde{A}_{\mathbf{k}+\mathbf{q}}} \Bigg\} \left(1 + \frac{4V^2}{|\tilde{A}_{\mathbf{k}}|^2}\right)^{-1}. \end{aligned} \tag{6.52}$$

Note from Eqs. (6.47) that only some values of momentum $\mathbf{q}$ and $\mathbf{k}$, at which $|\tilde{B}_{\mathbf{k},\mathbf{k}+\mathbf{q}}|$ approach to $|\tilde{A}_{\mathbf{k}}|$ or $|\tilde{A}_{\mathbf{k}+\mathbf{q}}|$, contribute to $U_{\mathbf{k},\mathbf{k}+\mathbf{q}}$ or $U'_{\mathbf{k},\mathbf{k}+\mathbf{q}}$. Therefore, the second term in the numerator of (6.52) can be neglected. Moreover, in the valence fluctuation regime, $|\tilde{A}_{\mathbf{k}}|$ becomes small, which means $|\tilde{\varepsilon}_{\mathbf{k}}| \sim |\tilde{\omega}_{\mathbf{k}}|$. Thus $g_{\mathbf{k}}$ is small compared to $f_{\mathbf{k}}$ and

$$\Gamma_{\mathbf{k},\mathbf{k}+\mathbf{q}} = V^{\text{eff}}_{\mathbf{k},\mathbf{k}+\mathbf{q}} f_{\mathbf{k}+\mathbf{q}}, \tag{6.53}$$

where

$$V^{\text{eff}}_{\mathbf{k},\mathbf{k}+\mathbf{q}} \approx \frac{4V^2}{\tilde{A}_{\mathbf{k}}} \frac{U'_{\mathbf{k},\mathbf{k}+\mathbf{q}}}{\tilde{A}_{\mathbf{k}+\mathbf{q}}} \left(1 + \frac{4V^2}{|\tilde{A}_{\mathbf{k}}|^2}\right)^{-1}. \tag{6.54}$$

Thus, Eq. (6.51) becomes a simple BCS-type self-consistent equation for the superconducting energy gap $\tilde{\Delta}^{cc}_{\mathbf{k}}$ in momentum space. $V^{\text{eff}}_{\mathbf{k},\mathbf{k}+\mathbf{q}}$ represents the effective two-particle

pairing interaction. In the BCS theory, $V^{\text{eff}}_{\mathbf{k},\mathbf{k+q}}$ is taken as a negative constant and therefore the energy gap solution of Eq. (6.51) is structureless in momentum space (s-wave superconductivity). However, in the present case $V^{\text{eff}}_{\mathbf{k},\mathbf{k+q}}$ strongly depends on momentum. Therefore we may obtain a d-wave symmetrical solution for the superconducting energy gap in momentum space [57]. Furthermore, from (6.54) we see that $V^{\text{eff}}_{\mathbf{k},\mathbf{k+q}}$ becomes dominant if $U'_{\mathbf{k},\mathbf{k+q}}$ is large and $\tilde{A}_{\mathbf{k}}\tilde{A}_{\mathbf{k+q}}$ is small. This only happens at the momentum at which both quasi-particle bands are located close to the Fermi level and close to each other. Therefore, part of the f-level is empty. This is the picture of a valence fluctuation regime. Furthermore, from Eqs. (6.44-6.46) we see that the stable superconductivity can be only obtained if there has a possibility for forming Cooper pairs between the conduction and localized electrons, $\langle \hat{f}_{-\mathbf{k}\downarrow} c_{\mathbf{k}\uparrow} \rangle$. That means the valence fluctuation is a crucial point for mediating the superconductivity. By this analytical result, we can conclude that the nature of the d-wave superconductivity is mediated by the valence fluctuations in the EPAM.

Chapter 7

Numerical results for superconductivity in the two-dimensional EPAM

7.1 Numerical results for a large system

In this section, we discuss our numerical results for the superconducting energy gaps by solving self-consistently Eqs. (6.44-6.46) with the analytical results in Eqs. (6.33, 6.35) and (6.40, 6.41) for a large system of section 6.3. This problem is done in two steps. In the first step, Eqs. (6.33, 6.35) and (6.40, 6.41) are solved self-consistently by arbitrarily initial choices for the expectation values $\langle n^c \rangle$ (density of the conduction electrons) and $\langle \hat{n}^f \rangle$ (density of the localized electrons). After a self-consistent solution is found, the obtained results are used to continue to solve Eqs. (6.44-6.46) self-consistently to obtain the superconducting energy gaps. In order to find d-wave superconductivity, we choose $\tilde{\Delta}^{\alpha\beta}_{k_x k_y} = A_0^{\alpha\beta}(\cos k_x - \cos k_y)$ (where α, β denote c or f) as initial values of the superconducting energy gaps with amplitudes $2A_0^{\alpha\beta}$. The self-consistent procedure is stopped, when convergence is achieved for the second step. In the present chapter, the total occupation number of electrons is also fixed to $n = \langle n^c \rangle + \langle \hat{n}^f \rangle = 1.75$ and dispersion relation

of non-interacting conduction electrons we have chosen $\epsilon_{\mathbf{k}} = -2t(\cos k_x + \cos k_y)$. We set $2t = 1$ as a unit of energy in order to have the same bandwidth of the conduction electrons as in the one-dimensional case. Therefore, the present results and the one-dimensional results, which have been discussed in the previous chapter, can be compared. A two-dimensional system with $N = 320 \times 320$ sites is investigated. The temperature is set to be very small, $T = 10^{-3}$. The former typical values, $U_{fc} = 1$, $V = 0.1$, and $n = 1.75$ are still kept.

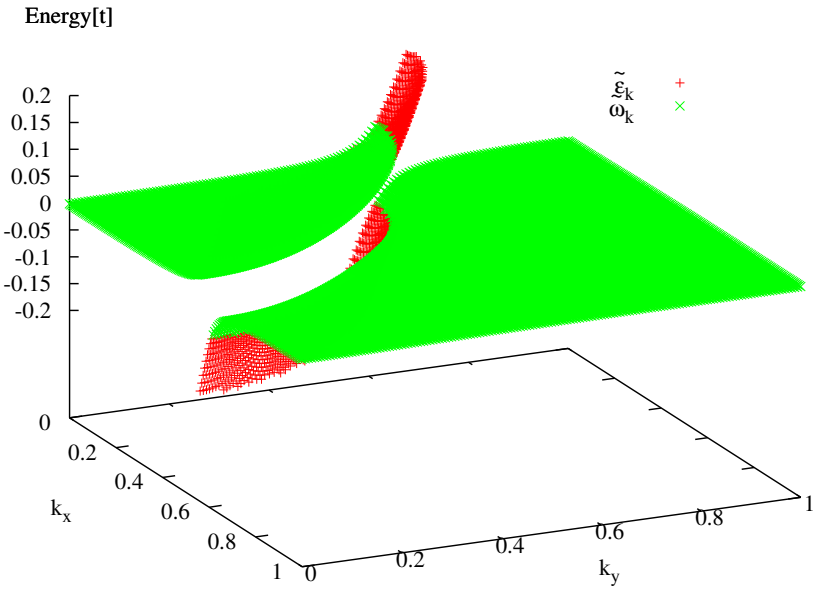

Figure 7.1: Renormalized energies of the conduction electrons, $\tilde{\varepsilon}_{\mathbf{k}}$, and of the localized electrons, $\tilde{\omega}_{\mathbf{k}}$, as functions of momentum $\mathbf{k}$ in the first quarter of the Brillouin zone at $\epsilon_f = -0.53$ for $U_{fc} = 1$, $V = 0.1$ and $T = 10^{-3}$.

At first, in Fig. 7.1 the dispersion relations of the two quasi-particle bands are shown for $\epsilon_f = -0.53$. The red (plus) symbols are for c-electrons and the green (cross) symbols for f-electrons. Because of the hybridization, each quasi-particle band has a jump at the crossover between $\tilde{\epsilon}_f$ and the unrenormalized c-dispersion $\varepsilon_{\mathbf{k},\Lambda}$. For $\epsilon_f = -0.53$, the jump is located close to the Fermi level in which both conduction and localized electrons contribute to the formation of the Fermi surface. This picture describes the situation at

a valence fluctuation regime.

In addition to the result of the dispersion relations in Fig. 7.1, the result for the superconducting energy gap $\tilde{\Delta}^{ff}_{\mathbf{k}}$ is shown in Fig. 7.2 as function of momentum $\mathbf{k}$ in the first quarter of the Brillouin zone for the same parameters as in Fig. 7.1. Note that the nodes

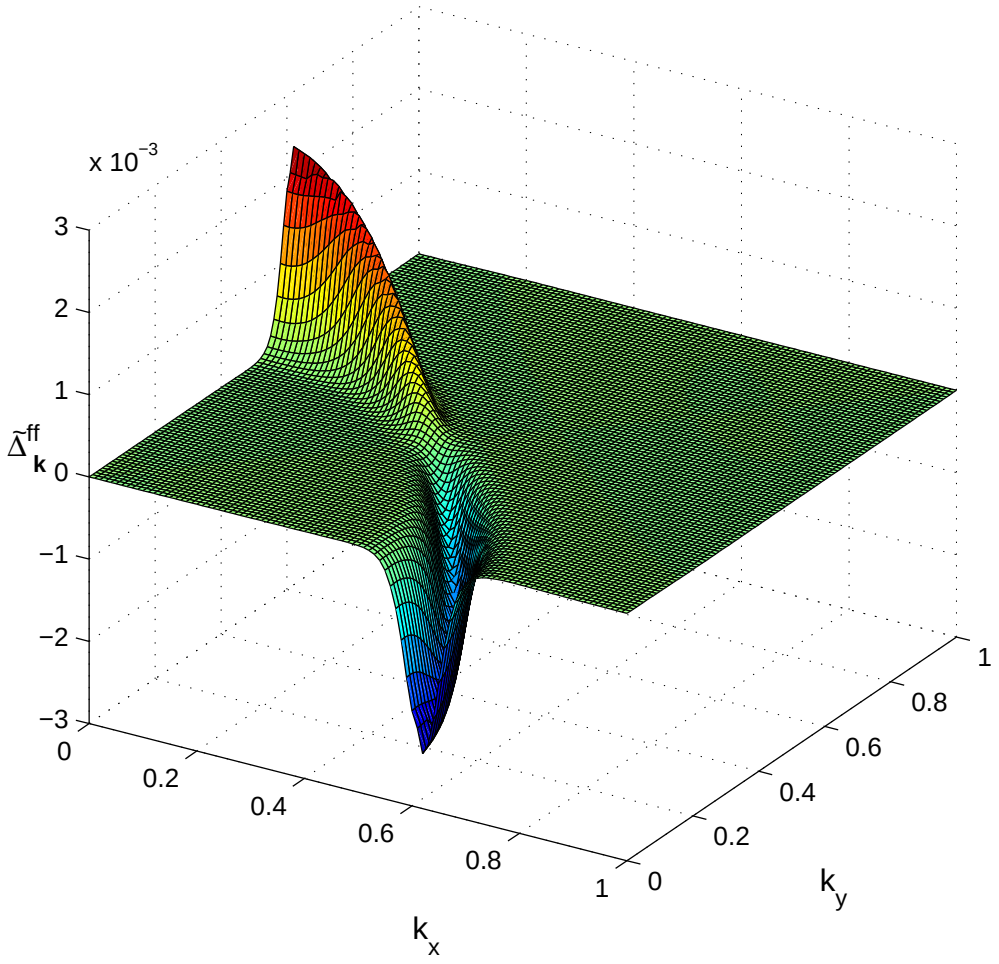

Figure 7.2: Superconducting energy gap, $\tilde{\Delta}^{ff}_{\mathbf{k}}$, with $d_{x^2-y^2}$-wave symmetry as a function of momentum $\mathbf{k}$ in the first quarter of the Brillouin zone at $\epsilon_f = -0.53$ for $U_{fc} = 1$, $V = 0.1$ and $T = 10^{-3}$.

of $\tilde{\Delta}^{ff}_{\mathbf{k}}$ are right in the diagonal direction of the Brillouin zone and the relation $\tilde{\Delta}^{ff}_{k_x k_y} = -\tilde{\Delta}^{ff}_{k_y k_x}$ if fulfilled. Here the result is shown only for the superconducting energy gap built

by the localized electrons. However, $d_{x^2-y^2}$ symmetry is also valid for the other possible

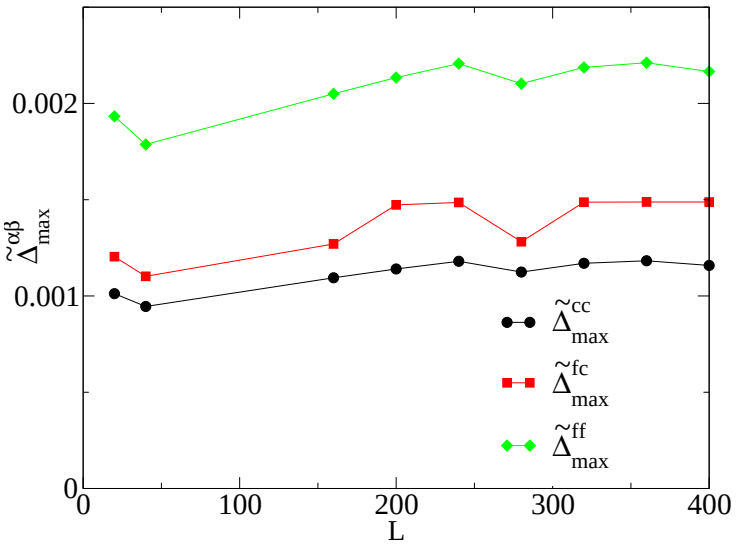

Figure 7.3: Maximum value of the superconducting energy gaps as a function of L for a two dimensional system with $N = L \times L$ lattice sites at $\epsilon_f = -0.53$ for $U_{fc} = 1$, $V = 0.1$ and $T = 10^{-3}$.

superconducting energy gaps $\tilde{\Delta}^{cc}_{\mathbf{k}}$, and $\tilde{\Delta}^{fc}_{\mathbf{k}}$ as well as for the superconducting pairing functions, $\langle c_{-\mathbf{k}\downarrow} c_{\mathbf{k}\uparrow} \rangle$, $\langle c_{-\mathbf{k}\downarrow} \hat{f}_{\mathbf{k}\uparrow} \rangle$, and $\langle \hat{f}_{-\mathbf{k}\downarrow} \hat{f}_{\mathbf{k}\uparrow} \rangle$. The maximum of the superconducting energy gap is located at the Fermi level which corresponds to the jump in the dispersion relation of the quasi-particle bands. In other words, the superconducting-state is dominant in the valence transition regime, in which some f-electrons become delocalized. The maximum position of the superconducting energy gap is shifted in correspondence to the shift of the jump position of the quasi-particle bands in momentum space. That means, if the Fermi line is a square with the corners at $(\pm\pi, 0)$ and $(0, \pm\pi)$, the maximum of the superconducting energy gap is located in the vicinity of $(\pm\pi, 0)$ or $(0, \pm\pi)$, which follows from the initial choice of the $d_{x^2-y^2}$ symmetry for the superconducting energy gap in self-consistent iteration. Furthermore, note that the SC-state is only found in a small region in the momentum space, where the values of the superconducting energy gap is

large. Therefore, the assumption we have used in (6.43) is applicable. The non-monotonic behavior in Fig. 7.2 of the superconducting energy gap as function of $\mathbf{k}$ is similar to that of the superconducting energy gap in the high temperature superconductors, which might be mediated by magnetic fluctuations [58, 59, 60, 61]. In the present study, the superconductivity is believed to be mediated by valence fluctuations.

By varying the number of lattice sites we have also examined the size effect of the superconducting energy gaps in our problem. For instance, the maximum values of $\tilde{\Delta}_{\mathbf{k}}^{\alpha\beta}$ (α and β denote c or f) are shown as functions of L ($N = L \times L$) in Fig. 7.3 for the same parameters as in Fig. 7.1 and Fig. 7.2. For small L, the maximum of each superconducting energy gap first somewhat decreases and then slowly increases till it reaches a size independent value as large L. Therefore, already a small system is able to mimic the thermodynamic limit.

7.2 Exact numerical results for a small lattice

As discussed in the previous section, we can already consider a small two-dimensional system to mimic the thermodynamic limit in the superconducting state of the EPAM by the use of the PRM. In this section, we discuss the self-consistent solutions of the superconducting energy gaps, as well as of the superconducting pairing functions, by applying the full PRM of section 6.2 to the EPAM. A system with $N = 16 \times 16$ lattice sites will be considered. In analogy to the one-dimensional problem in the normal state, in order to investigate the two-dimensional system by using PRM in the superconducting state, we start from some guess for the expectation values $\langle \hat{n}^f \rangle$, $\langle c_{\mathbf{k}m}^\dagger c_{\mathbf{k}m} \rangle$, and $\langle \hat{f}_{\mathbf{k}m}^\dagger c_{\mathbf{k}m} + \text{h.c.} \rangle$ as well as for the superconducting pairing functions $\langle c_{-\mathbf{k}\downarrow} c_{\mathbf{k}\uparrow} \rangle$, $\langle c_{-\mathbf{k}\downarrow} \hat{f}_{\mathbf{k}\uparrow} \rangle$, and $\langle \hat{f}_{-\mathbf{k}\downarrow} \hat{f}_{\mathbf{k}\uparrow} \rangle$. Solving the differential equations (4.32) and (6.17) with the initial conditions (4.13) and (6.3), we obtain the renormalized Hamiltonian of the EPAM in the superconducting state (6.18). Using the Bogolibov diagonalization, we can find the superconducting pairing functions by use of the renormalized Hamiltonian. The differential equations (4.51) are now used to determine the expectation values with the full Hamiltonian. This calculation procedure

of the expectation values has to be repeated until a self-consistent solution is achieved. The symmetry for the order parameters in the superconducting state is put in by hand by the chosen **k**-dependence of the initial superconducting pairing functions. For example, in order to find a $d_{x^2-y^2}$ wave symmetry we choose $\langle \alpha_{-\mathbf{k}\downarrow}\beta_{\mathbf{k}\uparrow}\rangle = A^0_{\alpha\beta}(\cos k_x - \cos k_y)$, where α, β denote the c or f-electron operators. If $\langle \alpha_{-\mathbf{k}\downarrow}\beta_{\mathbf{k}\uparrow}\rangle = A^0_{\alpha\beta}(\cos k_x + \cos k_y)$ is chosen, we have $s_{x^2+y^2}$-wave symmetry. Here, $A^0_{\alpha\beta}$ are constants. However, as concluded in the previous section, only d-wave superconductivity is a solution in our study. Therefore, only the d-wave symmetry is investigated in this section. Instead of showing all possible d-wave superconducting energy gaps and superconducting pairing functions at all positions in the Brillouin zone, we restrict ourselves to the ff-superconducting energy gap $\tilde{\Delta}^{ff}_{\mathbf{k}}$ as an illustration. Note that for a given set of the model parameters, the symmetries of all possible d-wave superconducting energy gaps and superconducting pairing functions are identical. The temperature dependence of their amplitudes will be left to a discussion at the end of this section.

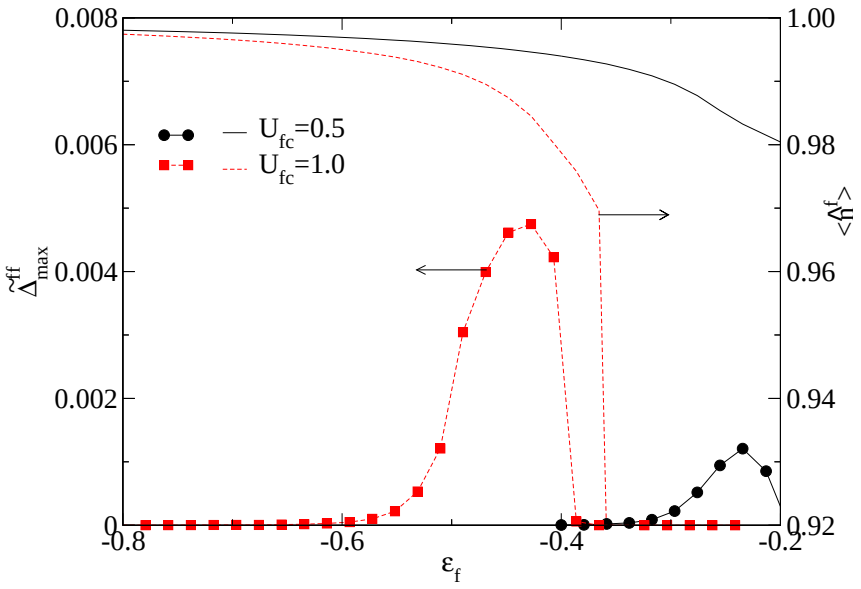

Figure 7.4: Maximum value of superconducting energy gap $\tilde{\Delta}^{ff}_{\mathbf{k}}$ and average f-electron occupation number $\langle \hat{n}^f \rangle$ as functions of the bare f-energy ϵ_f for two values of U_{fc} at $T = 10^{-3}$ and $V = 0.1$. Note that the scale of $\langle \hat{n}^f \rangle$ is restricted to values between $\langle \hat{n}^f \rangle = 1$ and $\langle \hat{n}^f \rangle = 0.92$.

Fig. 7.4 shows the behavior of the maximum value $\tilde{\Delta}^{ff}_{\max}$ of the superconducting energy gap $\tilde{\Delta}^{ff}_{\mathbf{k}}$ as well as the density of the localized electrons as function of the bare f-energy, ϵ_f. We see that similarly to the results of the one-dimensional EPAM, in the two-dimensional case, an increasing U_{fc} leads to a sharper valence transition. At the same time, for a regime which shows a rapid change of the average f-occupation $\langle \hat{n}^f \rangle$ also the superconducting energy gap becomes large. Thus, the regime where the superconducting state is stable, becomes enhanced by increasing U_{fc} which leads to a sharper valence transition. Moreover, note that superconductivity disappears in Fig. 7.4 for values of the f-occupation $\langle \hat{n}^f \rangle$ below 0.9. Therefore the approximation which leaves out the correlation between the localized electrons is applicable in the superconducting state. This result is agreement with the calculation in [21], in which the d-wave superconducting transition temperature for the three-dimensional EPAM has a peak at a value ϵ^*_f, which is slightly smaller than the value for ϵ_f, which corresponds to the steepest slope of the f-occupation (as function of ϵ_f). In [21], the transition temperature also drops down rapidly as $\epsilon_f > \epsilon^*_f$ and gradually decreases in the opposite direction. Note that from Fig. 7.4 one can conclude that the

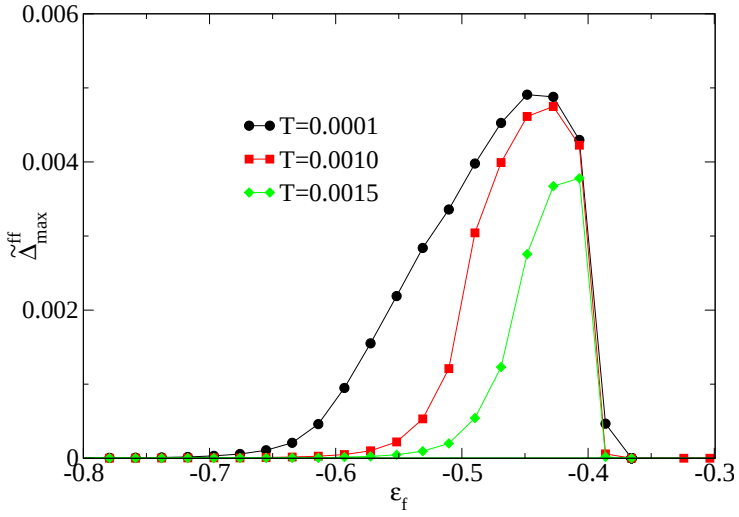

Figure 7.5: Maximum value of $\tilde{\Delta}^{ff}_{\mathbf{k}}$ as a function of the bare f-energy ϵ_f for several values of temperature T at $U_{fc} = 1$, $V = 0.1$.

valence transition regime and thus the superconducting regimes shift to smaller values of ϵ_f when U_{fc} is increased. This is not the case for the slave-boson mean-field treatment. The behavior for $\langle \hat{n}^f \rangle$ looks similar to the result in the one-dimensional EPAM. Our results affirm that superconductivity becomes more stable by the influence of valence fluctuations. Increasing U_{fc} in the EPAM is a crucial evidence for finding a sharp valence transition and d-wave superconductivity in the valence transition regime. This behavior can be explained by Eq. (6.54), where the effective pairing interaction $V^{\text{eff}}_{\mathbf{k},\mathbf{k}+\mathbf{q}}$ is linear dependent on U_{fc}.

Similarly to the one-dimensional EPAM (Fig. 5.8(a)), also for the two-dimensional EPAM a reduction of the temperature leads to a sharper valence transition. For the two-dimensional case, the dependence of maximum value of the superconducting energy gap $\tilde{\Delta}^{ff}_{\mathbf{k}}$ on the temperature is shown in Fig. 7.5. It once more demonstrates that the "window" of stable superconducting states broadens, when the valence transition becomes sharper.

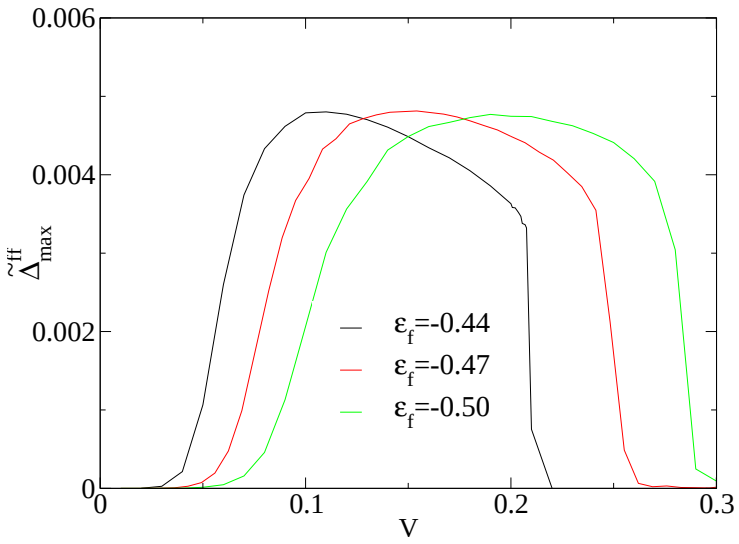

Figure 7.6: Maximum value of $\tilde{\Delta}^{ff}_{\mathbf{k}}$ as a function of the hybridization V for several values of the bare f-energy ϵ_f at $U_{fc} = 1$, $T = 10^{-3}$.

Increasing the hydrostatic pressure, the f-level is raised close to Fermi energy and the

hybridization between the localized electrons with the conduction electrons becomes enhanced. Therefore, in heavy fermion systems, besides the f-level ϵ_f, also the hybridization V can be considered as a parameter, which characterizes the applied external pressure. In Fig. 7.6, we can see the behavior of the maximum value of $\tilde{\Delta}^{ff}_{\mathbf{k}}$ as functions of the hybridization V at temperature $T = 10^{-3}$, Coulomb interaction $U_{fc} = 1$, for some values of the bare f-energy ϵ_f. For each value of ϵ_f, $\tilde{\Delta}^{ff}_{\mathbf{k}}$ first increases and then decreases as V is increased. This behavior can easily be understood in the picture of valence fluctuations which mediate the superconductivity. Indeed, by increasing the hybridization, the f-level comes close to the Fermi level and leads to more f-electron to jump to the conduction bands. It thus raises the chance of forming Cooper pairs between f-holes (see Fig. 1.3). Nevertheless, if V is large enough, a large number of holes in the f-level suppress the attractive pairing interaction of isolated pairs of $4f^0$ "holes" [20]. Furthermore, a "window" in which the superconductivity becomes stable is shifted to smaller V as ϵ_f is increased. When the f-level ϵ_f is located far below the Fermi level, the hybridization has to become larger in order to renormalize the f-level close to the Fermi level so that Cooper pairs can be formed. This behavior also can be understood by the simplified analytical expression for the effective pairing interaction in (6.54). Indeed, increasing the hybridization V leads to larger $V^{\text{eff}}_{\mathbf{k},\mathbf{k}+\mathbf{q}}$. Nevertheless, the factor $\tilde{A}_{\mathbf{k}}$ and $\tilde{A}_{\mathbf{k},\mathbf{k}+\mathbf{q}}$ increase as linear dependence of V. So when V is large, it makes some states which play a role to reduce the factor $\tilde{A}_{\mathbf{k}}$ be far from the Fermi level or the superconductivity is suppressed.

The behavior of the superconducting energy gaps as well as of the superconducting pairing functions for all possible combinations to form the Cooper pairs are shown in Fig. 7.7 as functions of temperature. As expected, the behavior of the superconducting energy gaps and the superconducting pairing functions are equivalent. Due to this result, we also can estimate the strength of an effective interaction between the Cooper pairs. Superconductivity only exists for f-occupations larger than $\langle \hat{n}^f \rangle = 0.9$. Thus, the density of f-holes is quite small, which leads to a small density $\langle \hat{f}_{-\mathbf{k}\downarrow} \hat{f}_{\mathbf{k}\uparrow} \rangle$ of the ff Cooper pairs created by coupling between the holes (green symbols in Fig. 7.7(b)). This physical picture results from the fact that the f-electrons are completely localized for $\langle \hat{n}^f \rangle =$

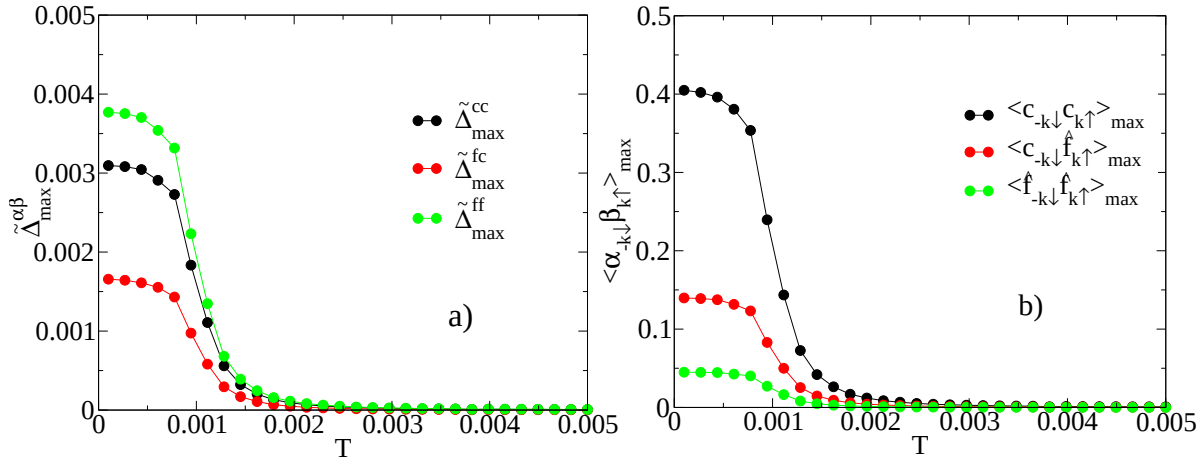

Figure 7.7: Maximum values of (a) the superconducting energy gaps and (b) of the superconducting pairing functions as functions of temperature for $U_{fc} = 1$, $V = 0.1$, and $\epsilon_f = -0.5$.

1. For $\langle \hat{n}^f \rangle > 0.9$ the density of f-holes is small, which means that it is difficult to find enough holes, which interact with each other. This is in contrast to the situation for the conduction electrons. The conduction electrons are delocalized. Therefore the probability for a pairing between conduction electrons is dominant as shown by the black symbols in Fig. 7.7(b). For the superconducting energy gaps the situation is reversed, Fig. 7.7(a). Fig. 7.7(b) shows that in order to break the Cooper pairs between the f-electrons, more energy has to be supplied than for pairs between conduction electrons. We can also realize that all possible Cooper pairs in the system will disappear simultaneously if the temperature is larger than a critical value. The critical temperature T_c can be determined by extrapolating the superconducting energy gaps or the superconducting pairing functions as functions of temperature close to the critical temperature value.

Chapter 8

Summary

Observations in $CeCu_2Si_2$ and related compounds showed that in the pressure-temperature phase diagram, there are two disconnected superconducting domes. The lower density superconducting dome is located close to antiferromagnetic order. Thus, the superconductivity in this dome might be mediated by spin fluctuations. In the higher density superconducting regime, the superconducting critical temperature is larger than that in the first dome. There are experimental evidences for these compounds that in the high pressure superconducting dome, a weakly first-order volume collapses, the residual resistivity enhances, and the coefficient of the T^2 law of the resistivity decreases. These evidences are related to an enhancement of valence fluctuations. The aim of this thesis was to discuss the possibility of superconductivity, which is induced by enhanced valence fluctuations in the heavy fermion systems under high pressure. The enhancement of the valence fluctuations is modeled by including a Coulomb repulsion term between the conduction and the localized electrons in the periodic Anderson model (PAM). This extended PAM (EPAM) was investigated by a recently developed projector-based renormalization method (PRM).

In chapter 2, we have presented the EPAM within representation which is useful for further calculations. In the case of infinite Coulomb repulsion between the localized electrons, the usual fermionic operators of the localized electrons were replaced by Hubbard

operators in order to restrict multiple occupied f-sites.

Chapter 3 was devoted to the basic ideas of the PRM. Instead of eliminating high energy states as in usual renormalization group methods, in the PRM high-energy transitions are successively eliminated. Thereby, a unitary transformation is used where all states of the unitary space of the interacting system are kept. The PRM starts from decomposing the Hamiltonian into two parts, a solvable unperturbed part and a perturbation, $\mathcal{H} = \mathcal{H}_0 + \mathcal{H}_1$, where the later part ($\mathcal{H}_1$) induces transitions between the eigenstates of $\mathcal{H}_0$. A renormalized Hamiltonian $\mathcal{H}_\lambda$, which only contains transitions with transition energies smaller than some given cutoff energy λ, has been constructed. In the following a further renormalization of $\mathcal{H}_\lambda$ is evaluated by reducing the cutoff λ to $\lambda - \Delta\lambda$. This is done by the unitary transformation, $\mathcal{H}_{\lambda-\Delta\lambda} = e^{X_{\lambda,\Delta\lambda}} \mathcal{H}_\lambda e^{-X_{\lambda,\Delta\lambda}}$, which guarantees that the eigenspectrum is not changed. The generator $X_{\lambda,\Delta\lambda}$ is specified by the condition $\mathbf{Q}_{\lambda-\Delta\lambda}\mathcal{H}_{\lambda-\Delta\lambda} = 0$, where $\mathbf{Q}_{\lambda-\Delta\lambda}$ is the projector on all transitions with energy differences larger than $\lambda - \Delta\lambda$. Note that only the corresponding part $\mathbf{Q}_{\lambda-\Delta\lambda}X_{\lambda,\Delta\lambda}$ of $X_{\lambda,\Delta\lambda}$ is fixed, whereas the orthogonal part $\mathbf{P}_{\lambda-\Delta\lambda}X_{\lambda,\Delta\lambda}$ can be chosen arbitrarily ($\mathbf{P}_{\lambda-\Delta\lambda} = \mathbf{1} - \mathbf{Q}_{\lambda-\Delta\lambda}$). In the thesis, $\mathbf{P}_{\lambda-\Delta\lambda}X_{\lambda,\Delta\lambda}$ is chosen to be nonzero. This additional freedom can be used, as in Wegner's flow equation method, to perform the unitary transformation continuously. In this case, the interaction parameters were chosen to decay exponentially. By proceeding the renormalization up to the final cutoff $\lambda = 0$, all transitions induced by $\mathcal{H}_1$, can be eliminated. The final Hamiltonian $\tilde{\mathcal{H}} = \mathcal{H}_{\lambda\to 0}$ is diagonal and allows to evaluate in principle any correlation function of physical interest. In particular, note that the one-particle excitations of $\tilde{\mathcal{H}}$ can be considered as quasiparticles of the coupled many-particle system since the eigenspectrum of the original interacting Hamiltonian $\mathcal{H}$ and of $\tilde{\mathcal{H}}$ are in principle the same.

By applying the present approach to the EPAM in the chapter 4, we obtained differential equations, which can be used to find the renormalized Hamiltonian. This Hamiltonian includes a new density-density interaction term between the f-electrons on different sites, which is generated during the renormalization procedure. Thus, we still can not straightforwardly determine the expectation values. Therefore, the second application of the PRM

to this Hamiltonian is used. Finally, the completely renormalized Hamiltonian permits us to evaluate the density of the localized electrons as well as its correlation function, $C^{ff}_{\rho,ij}$. However, this correlation function decays exponentially with the distance $\mathbf{R}_i - \mathbf{R}_j$ between the f-electrons. The decay becomes much faster when the temperature is increased. The largest value of $C^{ff}_{\rho,ij}$ is $\langle \hat{n}^f \rangle (1 - \langle \hat{n}^f \rangle)$ ($\langle \hat{n}^f \rangle$ is the density of localized electrons) at zero distance, $i = j$. Therefore, the density-density correlation function between the localized electrons can be left out in the case of large or small densities of the localized electrons. At high temperature it is replaced by a density-density correlation function on the same site. With this approximation, the second step in the renormalization procedure can be neglected, and it is very simple to calculate the expectation values. These simplifications were also used in chapter 6.

On the basic of the analytical results, in the one-dimensional case, at chapter 5, the numerical result for the renormalized dispersion relation of the conduction electrons and a physical picture of the valence transition is given. Due to the presence of the hybridization V and the Coulomb repulsion U_{fc} between localized and conduction electrons, various gaps are found in the dispersion relation. The number of gaps depends on the density of the localized electrons. It shows that in the case of large and of small $\langle \hat{n}^f \rangle$, the dispersion relations for the conduction electrons is not changed by the presence of $C^{ff}_{\rho,ij}$. The results for the valence transition are discussed as function of various model parameters such as U_{fc} and V or temperature T. For fixed total electron number, we find that the valence transition becomes sharper when U_{fc} is increased. On the other hand, the valence transition also becomes sharper when either the temperature T or the hybridization V becomes smaller, when U_{fc} is kept constant.

Chapter 6 contains the application of the PRM to the superconducting state of the EPAM. Small gauge symmetry breaking fields are included in the EPAM. The renormalized Hamilonian of the EPAM in the superconducting state is found in analogy to chapter 4. After being diagonalized by use of the Bogoliubov method, this Hamiltonian allows to determine the superconducting pairing functions of all possible Cooper pairs.

It was claimed by Miyake *et al.* that superconductivity in the heavy fermion material

$CeCu_2Si_2$ and in related compounds at high pressure may be described by the EPAM. However, only a three-dimensional system was considered by Miyake in a slave-boson mean field approach. The symmetry of the superconducting energy gaps were not explicitly described. Therefore, in chapter 6 we have discussed the self-consistent solution of the superconducting energy gaps for a two-dimensional EPAM model. By use of some additional simplifications, a BCS-like equation is found. The resulting effective pairing interaction depends strongly on momentum and becomes dominant in the valence transition regime. Our result verifies that superconductivity should have d-wave character and is mediated by valence fluctuations. The numerical evaluation for our analytical results is found for a two-dimensional system in chapter 7. First, we discuss the numerical solutions for a large system by use of some additional approximations, and then for a small system with $N = 16 \times 16$ lattice sites, where the original renormalization equations of section 6.1 were used. Our results once more show that d-wave superconductivity becomes important close to the valence transition.

Appendix A

The exact solvable Fano-Anderson model

In this appendix, we illustrate the renormalization approach for the case of a simple model, the Fano-Anderson model, which can be solved exactly [62].

A.1 Model

As simplification of the periodic Anderson model [49], the Fano-Anderson model consists of dispersionless f electrons, which hybridize with the conduction electrons. Thereby, all correlations are neglected. This model is given by

$$\begin{aligned} \mathcal{H} &= \mathcal{H}_0 + \mathcal{H}_1, \\ \mathcal{H}_0 &= \sum_{\mathbf{k},m} \epsilon_{\mathbf{k}} c^\dagger_{\mathbf{k}m} c_{\mathbf{k}m} + \epsilon_f \sum_{\mathbf{k},m} f^\dagger_{\mathbf{k}m} f_{\mathbf{k}m}, \\ \mathcal{H}_1 &= \sum_{\mathbf{k},m} V_{\mathbf{k}} (f^\dagger_{\mathbf{k}m} c_{\mathbf{k}m} + \text{h.c.}). \end{aligned} \tag{A.1}$$

Here $f^\dagger_{\mathbf{k}m}$ ($f_{\mathbf{k}m}$) and $c^\dagger_{\mathbf{k}m}$ ($c_{\mathbf{k}m}$) are creation (annihilation) operators of f-electrons and conduction electrons with wave vector $\mathbf{k}$ and angular momentum index m, respectively. Both types of electrons are assumed to have the same index m with ν_f values. By

introducing new fermion operators

$$\begin{aligned} \alpha^{\dagger}_{\mathbf{k}m} &= u_{\mathbf{k}} f^{\dagger}_{\mathbf{k}m} + v_{\mathbf{k}} c^{\dagger}_{\mathbf{k}m}, \\ \beta^{\dagger}_{\mathbf{k}m} &= -v_{\mathbf{k}} f^{\dagger}_{\mathbf{k}m} + u_{\mathbf{k}} c^{\dagger}_{\mathbf{k}m}, \end{aligned} \tag{A.2}$$

which satisfy

$$|u_{\mathbf{k}}|^2 + |v_{\mathbf{k}}|^2 = 1. \tag{A.3}$$

We can represent the model (A.1) in the following form with two hybridized bands

$$\mathcal{H} = \sum_{\mathbf{k},m} \omega^{(+)}_{\mathbf{k}} \alpha^{\dagger}_{\mathbf{k}m} \alpha_{\mathbf{k}m} + \sum_{\mathbf{k},m} \omega^{(-)}_{\mathbf{k}} \beta^{\dagger}_{\mathbf{k}m} \beta_{\mathbf{k}m}, \tag{A.4}$$

where

$$\begin{aligned} \omega^{(\pm)}_{\mathbf{k}} &= \frac{\epsilon_{\mathbf{k}} + \epsilon_f}{2} \pm \frac{1}{2} W_{\mathbf{k}}, \\ W_{\mathbf{k}} &= \sqrt{(\epsilon_{\mathbf{k}} - \epsilon_f)^2 + 4|V_{\mathbf{k}}|^2}, \end{aligned}$$

and

$$\begin{aligned} |u_{\mathbf{k}}|^2 &= \frac{1}{2}\left(1 - \frac{\epsilon_{\mathbf{k}} - \epsilon_f}{W_{\mathbf{k}}}\right), \\ |v_{\mathbf{k}}|^2 &= \frac{1}{2}\left(1 + \frac{\epsilon_{\mathbf{k}} - \epsilon_f}{W_{\mathbf{k}}}\right). \end{aligned} \tag{A.5}$$

So, the f occupation number, for instance, can be determined and its result is

$$\begin{aligned} \langle f^{\dagger}_{\mathbf{k}m} f_{\mathbf{k}m} \rangle &= |u_{\mathbf{k}}|^2 \langle \alpha^{\dagger}_{\mathbf{k}m} \alpha_{\mathbf{k}m} \rangle + |v_{\mathbf{k}}|^2 \langle \beta^{\dagger}_{\mathbf{k}m} \beta_{\mathbf{k}m} \rangle \\ &= |u_{\mathbf{k}}|^2 \frac{1}{1 + e^{\beta \omega^{(+)}_{\mathbf{k}}}} + |v_{\mathbf{k}}|^2 \frac{1}{1 + e^{\beta \omega^{(-)}_{\mathbf{k}}}}. \end{aligned} \tag{A.6}$$

The diagonalized Hamiltonian (A.4) contains two eigenmodes $\alpha^{\dagger}_{\mathbf{k}m}$ and $\beta^{\dagger}_{\mathbf{k}m}$, which change their character as function of the wave vector $\mathbf{k}$. Indeed, $\alpha^{\dagger}_{\mathbf{k}m}$ is a more f-like excitation for $\epsilon_{\mathbf{k}} < \epsilon_f$ and a more c-like excitation for $\epsilon_{\mathbf{k}} > \epsilon_f$, and vice versa for the $\beta^{\dagger}_{\mathbf{k}m}$ operators. Therefore, it is very difficult to distinguish the contribution of the conduction or of the localized electrons to the band structure.

A.2 Projector-based renormalization approach

In the renormalization approach, we integrate out the hybridization term between the localized and conduction electrons in order to obtain a diagonal effective Hamiltonian of free quasi-particles. The starting point of the method is to formulate a renormalized Hamiltonian $\mathcal{H}_\lambda$ which is obtained after all excitations with energies larger than cutoff λ have been eliminated. As discussed in the previous chapters, the renormalized Hamiltonian of the Fano Anderson model (A.1) at cutoff λ can be written as follows

$$\begin{aligned}\mathcal{H}_\lambda &= \mathcal{H}_{0,\lambda} + \mathcal{H}_{1,\lambda} \\ \mathcal{H}_{0,\lambda} &= \sum_{\mathbf{k},m} \epsilon_{\mathbf{k},\lambda} c^\dagger_{\mathbf{k}m} c_{\mathbf{k}m} + \sum_{\mathbf{k},m} \omega_{\mathbf{k},\lambda} f^\dagger_{\mathbf{k}m} f_{\mathbf{k}m} \\ \mathcal{H}_{1,\lambda} &= \sum_{\mathbf{k},m} V_{\mathbf{k},\lambda} (f^\dagger_{\mathbf{k}m} c_{\mathbf{k}m} + \text{h.c.}).\end{aligned} \tag{A.7}$$

Here, $\epsilon_{\mathbf{k},\lambda}$ and $\omega_{\mathbf{k},\lambda}$ are the dispersion relations of the conduction and the localized electrons at the cutoff λ. The excitation energies are determined by applying the non-interacting Liouville operator, $\mathcal{L}_{0,\lambda}$, to $\mathcal{H}_{1,\lambda}$

$$\mathcal{L}_{0,\lambda} f^\dagger_{\mathbf{k}m} c_{\mathbf{k}m} = (\epsilon_{\mathbf{k},\lambda} - \omega_{\mathbf{k},\lambda}) f^\dagger_{\mathbf{k}m} c_{\mathbf{k}m}. \tag{A.8}$$

In order to derive the renormalization equations for the parameters of the Hamiltonian, we compare the coefficients of the different operator terms in the two expressions of the renormalized Hamiltonian at cutoff $\lambda - \Delta\lambda$. They are obtained from (A.7) by two ways, the first one is

$$\begin{aligned}\mathcal{H}_{\lambda-\Delta\lambda} = &\sum_{\mathbf{k},m} \epsilon_{\mathbf{k},\lambda-\Delta\lambda} c^\dagger_{\mathbf{k}m} c_{\mathbf{k}m} + \sum_{\mathbf{k},m} \omega_{\mathbf{k},\lambda-\Delta\lambda} f^\dagger_{\mathbf{k}m} f_{\mathbf{k}m} \\ &+ \sum_{\mathbf{k},m} V_{\mathbf{k},\lambda-\Delta\lambda} (f^\dagger_{\mathbf{k}m} c_{\mathbf{k}m} + \text{h.c.}).\end{aligned} \tag{A.9}$$

The second one is deduced from the unitary transformation

$$\begin{aligned}\mathcal{H}_{\lambda-\Delta\lambda} = &\sum_{\mathbf{k},m} \epsilon_{\mathbf{k},\lambda} e^{X_{\lambda,\Delta\lambda}} c^\dagger_{\mathbf{k}m} c_{\mathbf{k}m} e^{-X_{\lambda,\Delta\lambda}} + \sum_{\mathbf{k},m} \omega_{\mathbf{k},\lambda} e^{X_{\lambda,\Delta\lambda}} f^\dagger_{\mathbf{k}m} f_{\mathbf{k}m} e^{-X_{\lambda,\Delta\lambda}} \\ &+ \sum_{\mathbf{k},m} V_{\mathbf{k},\lambda} e^{X_{\lambda,\Delta\lambda}} (f^\dagger_{\mathbf{k}m} c_{\mathbf{k}m} + \text{h.c.}) e^{-X_{\lambda,\Delta\lambda}},\end{aligned} \tag{A.10}$$

where an approximate generator $X_{\lambda,\Delta\lambda} = \sum_{\mathbf{k},m} \alpha_{\mathbf{k}}(\lambda, \Delta\lambda)(f^{\dagger}_{\mathbf{k}m} c_{\mathbf{k}m} - \text{h.c.})$ is chosen. In the limit of small $\Delta\lambda$, we can restrict ourselves to the first order contributions from the generator. Comparing the prefactors of corresponding operators in (A.9) and (A.10) and taking the limit $\Delta\lambda \to 0$, we find

$$\frac{d\epsilon_{\mathbf{k},\lambda}}{d\lambda} = 2V_{\mathbf{k},\lambda}\tilde{\alpha}_{\mathbf{k},\lambda}, \tag{A.11}$$

$$\frac{d\omega_{\mathbf{k},\lambda}}{d\lambda} = -2V_{\mathbf{k},\lambda}\tilde{\alpha}_{\mathbf{k},\lambda}, \tag{A.12}$$

$$\frac{dV_{\mathbf{k},\lambda}}{d\lambda} = (\omega_{\mathbf{k},\lambda} - \epsilon_{\mathbf{k},\lambda})\tilde{\alpha}_{\mathbf{k},\lambda}. \tag{A.13}$$

Here

$$\tilde{\alpha}_{\mathbf{k},\lambda} = \lim_{\Delta\lambda\to 0} \frac{\alpha_{\mathbf{k}}(\lambda, \Delta\lambda)}{\Delta\lambda}. \tag{A.14}$$

Substituting $\tilde{\alpha}_{\mathbf{k},\lambda}$ from (A.13) into (A.11), we have

$$(\omega_{\mathbf{k},\lambda} - \epsilon_{\mathbf{k},\lambda})\frac{d\epsilon_{\mathbf{k},\lambda}}{d\lambda} = 2V_{\mathbf{k},\lambda}\frac{dV_{\mathbf{k},\lambda}}{d\lambda}. \tag{A.15}$$

Comparing (A.11) and (A.12), we also obtain

$$\frac{d(\epsilon_{\mathbf{k},\lambda} + \omega_{\mathbf{k},\lambda})}{d\lambda} = 0, \tag{A.16}$$

or, $\epsilon_{\mathbf{k},\lambda} + \omega_{\mathbf{k},\lambda} = \epsilon_{\mathbf{k}} + \epsilon_f$. Therefore, we can rewrite (A.15) as

$$(\epsilon_{\mathbf{k}} + \epsilon_f - 2\epsilon_{\mathbf{k},\lambda})\frac{d\epsilon_{\mathbf{k},\lambda}}{d\lambda} = 2V_{\mathbf{k},\lambda}\frac{dV_{\mathbf{k},\lambda}}{d\lambda}, \tag{A.17}$$

or

$$(\epsilon_{\mathbf{k}} + \epsilon_f)\tilde{\epsilon}_{\mathbf{k}} - \tilde{\epsilon}^2_{\mathbf{k}} = (\epsilon_{\mathbf{k}} + \epsilon_f)\epsilon_{\mathbf{k}} - \epsilon^2_{\mathbf{k}} - V^2. \tag{A.18}$$

Here $\tilde{\epsilon}_{\mathbf{k}} = \epsilon_{\mathbf{k},\lambda\to 0}$ and $V_{\mathbf{k},\lambda\to 0} = 0$. So, we have found a quadratic equation which determine the completely renormalized dispersion relations of conduction and localized electrons. From Eq. (A.11), we realize that the derivations of $\epsilon_{\mathbf{k},\lambda}$ are changed through the intersection of $\epsilon_{\mathbf{k},\lambda}$ and $\omega_{\mathbf{k},\lambda}$. Therefore, $\tilde{\epsilon}_{\mathbf{k}}$ jumps between the two solutions of the quadratic equation

$$\tilde{\epsilon}_{\mathbf{k}} = \frac{\epsilon_{\mathbf{k}} + \epsilon_f}{2} - \frac{\text{sgn}(\epsilon_{\mathbf{k}} - \epsilon_f)}{2} W_{\mathbf{k}}, \tag{A.19}$$

where

$$W_{\mathbf{k}} = \sqrt{(\epsilon_{\mathbf{k}} - \epsilon_f)^2 + 4|V_{\mathbf{k}}|^2}. \tag{A.20}$$

From (A.16), we also obtain the second quasi-particle band

$$\tilde{\omega}_{\mathbf{k}} = \frac{\epsilon_{\mathbf{k}} + \epsilon_f}{2} + \frac{\mathrm{sgn}(\epsilon_{\mathbf{k}} - \epsilon_f)}{2} W_{\mathbf{k}}. \tag{A.21}$$

The fully renormalized Hamiltonian reads

$$\tilde{\mathcal{H}} = \sum_{\mathbf{k},m} \tilde{\epsilon}_{\mathbf{k}} c^\dagger_{\mathbf{k}m} c_{\mathbf{k}m} + \sum_{\mathbf{k},m} \tilde{\omega}_{\mathbf{k}} f^\dagger_{\mathbf{k}m} f_{\mathbf{k}m} + \tilde{E} \tag{A.22}$$

This final result corresponds to the diagonal Hamiltonian (A.4). However, in contrast to the eigenmodes $\alpha^\dagger_{\mathbf{k}m}$ and $\beta^\dagger_{\mathbf{k}m}$, the renormalized Hamiltonian (A.22) is diagonal in the eigenmodes $f^\dagger_{\mathbf{k}m}$ and $c^\dagger_{\mathbf{k}m}$, which do not change their character as function of the wave vectors. From the renormalized Hamiltonian (A.22), it is easy to evaluate the expectation values. Indeed, the free energy can be calculated as

$$F = -\frac{1}{\beta} \ln \mathrm{Tr} e^{-\beta \mathcal{H}} = -\frac{1}{\beta} \ln \mathrm{Tr} e^{-\beta \tilde{\mathcal{H}}}. \tag{A.23}$$

As an example, the f occupation number is found from the free energy by functional derivative

$$\begin{aligned} \langle f^\dagger_{\mathbf{k}m} f_{\mathbf{k}m} \rangle = \frac{1}{N} \frac{\partial F}{\partial \epsilon_f} = &\left(\frac{1}{2} + \mathrm{sgn}(\epsilon_{\mathbf{k}} - \epsilon_f) \frac{1}{2} \frac{\epsilon_{\mathbf{k}} - \epsilon_f}{W_{\mathbf{k}}} \right) \frac{1}{1 + e^{\beta \tilde{\omega}_{\mathbf{k}}}} \\ &+ \left(\frac{1}{2} - \mathrm{sgn}(\epsilon_{\mathbf{k}} - \epsilon_f) \frac{1}{2} \frac{\epsilon_{\mathbf{k}} - \epsilon_f}{W_{\mathbf{k}}} \right) \frac{1}{1 + e^{\beta \tilde{\epsilon}_{\mathbf{k}}}}. \end{aligned} \tag{A.24}$$

This result agrees with Eq. (A.6). The other expectation values and quantities, calculated by the two ways, are also identical. It follows that all static and dynamic quantitites, involving electron creation and annihilation operators, can be determined in the framework of the PRM.

Appendix B

Bogoliubov diagonalization

This appendix is devoted to the solution of the eigenvalue problem of $\tilde{\mathcal{H}}$ in Eq. (6.18). Here, we perform a Bogoliubov transformation [55] by introducing new fermionic operators

$$\mu_{\mathbf{k}}^{\dagger} = a_{\mathbf{k}}^{1*} c_{\mathbf{k}\uparrow}^{\dagger} - a_{\mathbf{k}}^{2*} c_{-\mathbf{k}\downarrow} + a_{\mathbf{k}}^{3*} \hat{f}_{\mathbf{k}\uparrow}^{\dagger} - a_{\mathbf{k}}^{4*} \hat{f}_{-\mathbf{k}\downarrow}, \tag{B.1}$$

which satisfy

$$[\mu_{\mathbf{k}}^{\dagger}, \mu_{\mathbf{k}'}]_{+} = \delta_{\mathbf{k}\mathbf{k}'}, \tag{B.2}$$

or

$$|a_{\mathbf{k}}^{1}|^2 + |a_{\mathbf{k}}^{2}|^2 + D|a_{\mathbf{k}}^{3}|^2 + D|a_{\mathbf{k}}^{4}|^2 = 1. \tag{B.3}$$

The yet unknown pre-factors $a_{\mathbf{k}}^{i}$ are found by using the relation

$$[\tilde{\mathcal{H}}, \mu_{\mathbf{k}}^{\dagger}] = E_{\mathbf{k}} \mu_{\mathbf{k}}^{\dagger}. \tag{B.4}$$

By evaluating the commutators, we obtain

$$\begin{aligned}[\tilde{\mathcal{H}}, \mu_{\mathbf{k}}^{\dagger}] = &\left(\tilde{\varepsilon}_{\mathbf{k}} a_{\mathbf{k}}^{1*} + \tilde{\Delta}_{\mathbf{k}}^{cc} a_{\mathbf{k}}^{2*} + D\tilde{\Delta}_{\mathbf{k}}^{cf} a_{\mathbf{k}}^{4*}\right) c_{\mathbf{k}\uparrow}^{\dagger} + \left(\tilde{\varepsilon}_{-\mathbf{k}} a_{\mathbf{k}}^{2*} - \tilde{\Delta}_{\mathbf{k}}^{cc,*} a_{\mathbf{k}}^{1*} - D\tilde{\Delta}_{\mathbf{k}}^{fc,*} a_{\mathbf{k}}^{3*}\right) c_{-\mathbf{k}\downarrow} \\ &+ \left(\tilde{\omega}_{\mathbf{k}} a_{\mathbf{k}}^{3*} + D\tilde{\Delta}_{\mathbf{k}}^{ff} a_{\mathbf{k}}^{4*} + \tilde{\Delta}_{\mathbf{k}}^{fc} a_{\mathbf{k}}^{2*}\right) \hat{f}_{\mathbf{k}\uparrow}^{\dagger} + \left(\tilde{\omega}_{\mathbf{k}} a_{\mathbf{k}}^{4*} - D\tilde{\Delta}_{\mathbf{k}}^{ff,*} a_{\mathbf{k}}^{3*} - \tilde{\Delta}_{\mathbf{k}}^{cf,*} a_{\mathbf{k}}^{1*}\right) \hat{f}_{-\mathbf{k}\downarrow},\end{aligned} \tag{B.5}$$

where $\tilde{\omega}_{\mathbf{k}} = \tilde{\mu}_f + D(\tilde{\gamma}_{\mathbf{k}} - \tilde{\bar{\gamma}})$. From (B.4), we find the linear equations for determining the pre-factors $a^i_{\mathbf{k}}$

$$\begin{cases} \tilde{\varepsilon}_{\mathbf{k}} a^{1*}_{\mathbf{k}} + \tilde{\Delta}^{cc}_{\mathbf{k}} a^{2*}_{\mathbf{k}} + D\tilde{\Delta}^{cf}_{\mathbf{k}} a^{4*}_{\mathbf{k}} = E_{\mathbf{k}} a^{1*}_{\mathbf{k}} \\ \tilde{\varepsilon}_{\mathbf{k}} a^{2*}_{\mathbf{k}} - \tilde{\Delta}^{cc,*}_{\mathbf{k}} a^{1*}_{\mathbf{k}} - D\tilde{\Delta}^{fc,*}_{\mathbf{k}} a^{3*}_{\mathbf{k}} = -E_{\mathbf{k}} a^{2*}_{\mathbf{k}} \\ \tilde{\omega}_{\mathbf{k}} a^{3*}_{\mathbf{k}} + D\tilde{\Delta}^{ff}_{\mathbf{k}} a^{4*}_{\mathbf{k}} + \tilde{\Delta}^{fc}_{\mathbf{k}} a^{2*}_{\mathbf{k}} = E_{\mathbf{k}} a^{3*}_{\mathbf{k}} \\ \tilde{\omega}_{\mathbf{k}} a^{4*}_{\mathbf{k}} - D\tilde{\Delta}^{ff,*}_{\mathbf{k}} a^{3*}_{\mathbf{k}} - \tilde{\Delta}^{cf,*}_{\mathbf{k}} a^{1*}_{\mathbf{k}} = -E_{\mathbf{k}} a^{4*}_{\mathbf{k}} \end{cases} . \tag{B.6}$$

These are homogeneous linear equations, which only has non-trivial solutions for

$$\det A = 0, \tag{B.7}$$

where

$$A = \begin{pmatrix} \tilde{\varepsilon}_{\mathbf{k}} - E_{\mathbf{k}} & \tilde{\Delta}^{cc}_{\mathbf{k}} & 0 & D\tilde{\Delta}^{cf}_{\mathbf{k}} \\ -\tilde{\Delta}^{cc,*}_{\mathbf{k}} & \tilde{\varepsilon}_{\mathbf{k}} + E_{\mathbf{k}} & -D\tilde{\Delta}^{fc,*}_{\mathbf{k}} & 0 \\ 0 & \tilde{\Delta}^{fc}_{\mathbf{k}} & \tilde{\omega}_{\mathbf{k}} - E_{\mathbf{k}} & D\tilde{\Delta}^{ff}_{\mathbf{k}} \\ -\tilde{\Delta}^{cf,*}_{\mathbf{k}} & 0 & -D\tilde{\Delta}^{ff,*}_{\mathbf{k}} & \tilde{\omega}_{\mathbf{k}} + E_{\mathbf{k}} \end{pmatrix}.$$

Setting the determinant equal to zero leads to an equation for the eigenvalues $E_{\mathbf{k}}$

$$|E_{\mathbf{k}}|^4 - u_{\mathbf{k}}|E_{\mathbf{k}}|^2 + v_{\mathbf{k}} = 0, \tag{B.8}$$

where

$$\begin{aligned} u_{\mathbf{k}} &= \tilde{\varepsilon}^2_{\mathbf{k}} + \tilde{\omega}^2_{\mathbf{k}} + |D\tilde{\Delta}^{ff}_{\mathbf{k}}|^2 + |\tilde{\Delta}^{cc}_{\mathbf{k}}|^2 + D(|\tilde{\Delta}^{fc}_{\mathbf{k}}|^2 + |\tilde{\Delta}^{cf}_{\mathbf{k}}|^2), \\ v_{\mathbf{k}} &= \left(\tilde{\varepsilon}^2_{\mathbf{k}} + |\tilde{\Delta}^{cc}_{\mathbf{k}}|^2\right)\left(\tilde{\omega}^2_{\mathbf{k}} + |D\tilde{\Delta}^{ff}_{\mathbf{k}}|^2\right) + D\tilde{\varepsilon}_{\mathbf{k}}\tilde{\omega}_{\mathbf{k}}\left(|\tilde{\Delta}^{fc}_{\mathbf{k}}|^2 + |\tilde{\Delta}^{cf}_{\mathbf{k}}|^2\right) \\ &\quad + |D\tilde{\Delta}^{cf}_{\mathbf{k}}|^2|D\tilde{\Delta}^{fc}_{\mathbf{k}}|^2 - D^2\left(\tilde{\Delta}^{cc}_{\mathbf{k}}\tilde{\Delta}^{cf,*}_{\mathbf{k}}\tilde{\Delta}^{fc,*}_{\mathbf{k}}\tilde{\Delta}^{ff}_{\mathbf{k}} + \tilde{\Delta}^{cc,*}_{\mathbf{k}}\tilde{\Delta}^{cf}_{\mathbf{k}}\tilde{\Delta}^{fc}_{\mathbf{k}}\tilde{\Delta}^{ff,*}_{\mathbf{k}}\right). \end{aligned} \tag{B.9}$$

Defining $\Phi_{\mathbf{k}} = u^2_{\mathbf{k}} - 4v_{\mathbf{k}}$, we have

$$\begin{aligned} E^{1,2}_{\mathbf{k}} &= \pm\sqrt{\frac{u_{\mathbf{k}} + \sqrt{\Phi_{\mathbf{k}}}}{2}}, \\ E^{3,4}_{\mathbf{k}} &= \pm\sqrt{\frac{u_{\mathbf{k}} - \sqrt{\Phi_{\mathbf{k}}}}{2}}. \end{aligned} \tag{B.10}$$

The eigenvectors $\mu^{\dagger}_{\mathbf{k}}$ are found from the condition (B.3) and three of the four equations in (B.6). For example, we have

$$\begin{cases} |a^1_{\mathbf{k}}|^2 + |a^2_{\mathbf{k}}|^2 + D|a^3_{\mathbf{k}}|^2 + D|a^4_{\mathbf{k}}|^2 = 1 \\ (\tilde{\varepsilon}_{\mathbf{k}} - E_{\mathbf{k}})a^{1*}_{\mathbf{k}} + \tilde{\Delta}^{cc}_{\mathbf{k}} a^{2*}_{\mathbf{k}} + D\tilde{\Delta}^{cf}_{\mathbf{k}} a^{4*}_{\mathbf{k}} = 0 \\ \tilde{\Delta}^{cc,*}_{\mathbf{k}} a^{1*}_{\mathbf{k}} - (\tilde{\varepsilon}_{\mathbf{k}} + E_{\mathbf{k}})a^{2*}_{\mathbf{k}} + D\tilde{\Delta}^{fc,*}_{\mathbf{k}} a^{3*}_{\mathbf{k}} = 0 \\ \tilde{\Delta}^{fc}_{\mathbf{k}} a^{2*}_{\mathbf{k}} + (\tilde{\omega}_{\mathbf{k}} - E_{\mathbf{k}})a^{3*}_{\mathbf{k}} + D\tilde{\Delta}^{ff}_{\mathbf{k}} a^{4*}_{\mathbf{k}} = 0 \end{cases}. \tag{B.11}$$

Solving this system of equations, we obtain

$$|a^i_{\mathbf{k}}|^2\Big|_{i=\overline{2,4}} = \left(\frac{\beta^i_{\mathbf{k}}}{\alpha^i_{\mathbf{k}}}\right)^2 |a^1_{\mathbf{k}}|^2, \tag{B.12}$$

where

$$\begin{aligned} \alpha^2_{\mathbf{k}} &= \alpha^3_{\mathbf{k}} = A = (\tilde{\varepsilon}_{\mathbf{k}} + E_{\mathbf{k}})(\tilde{\omega}_{\mathbf{k}} - E_{\mathbf{k}}) + D\tilde{\Delta}^{cf,*}_{\mathbf{k}}\tilde{\Delta}^{fc}_{\mathbf{k}}, \\ \alpha^4_{\mathbf{k}} &= D\tilde{\Delta}^{cf}_{\mathbf{k}} - \frac{D^2}{A}\tilde{\Delta}^{cf,*}_{\mathbf{k}}\tilde{\Delta}^{cc}_{\mathbf{k}}\tilde{\Delta}^{ff}_{\mathbf{k}}, \\ \beta^2_{\mathbf{k}} &= (\tilde{\omega}_{\mathbf{k}} - E_{\mathbf{k}})\tilde{\Delta}^{cc,*}_{\mathbf{k}} - D^{3/2}\tilde{\Delta}^{cf,*}_{\mathbf{k}} D\tilde{\Delta}^{ff}_{\mathbf{k}}\frac{\beta^4_{\mathbf{k}}}{\alpha^4_{\mathbf{k}}}, \\ \beta^3_{\mathbf{k}} &= -\sqrt{D}\Big[\tilde{\Delta}^{fc}_{\mathbf{k}}\tilde{\Delta}^{cc,*}_{\mathbf{k}} + \sqrt{D}\tilde{\Delta}^{ff}_{\mathbf{k}}(\tilde{\varepsilon}_{\mathbf{k}} + E_{\mathbf{k}})\frac{\beta^4_{\mathbf{k}}}{\alpha^4_{\mathbf{k}}}\Big], \\ \beta^4_{\mathbf{k}} &= \sqrt{D}\Big[E_{\mathbf{k}} - \varepsilon_{\mathbf{k}} - (\tilde{\omega}_{\mathbf{k}} - E_{\mathbf{k}})\frac{|\tilde{\Delta}^{cc}_{\mathbf{k}}|^2}{A}\Big], \end{aligned} \tag{B.13}$$

and

$$|a^1_{\mathbf{k}}|^2 = \left\{1 + \sum_{i=2}^{4}\left(\frac{\beta^i_{\mathbf{k}}}{\alpha^i_{\mathbf{k}}}\right)^2\right\}^{-1}. \tag{B.14}$$

For the four values of $E_{\mathbf{k}}$ we also obtain four values for the set of $\{a^i_{\mathbf{k}}\}$. The four eigenvectors $\{\mu^i_{\mathbf{k}}\}$ read

$$\begin{cases} \mu^{1\dagger}_{\mathbf{k}} = a^{11*}_{\mathbf{k}} c^{\dagger}_{\mathbf{k}\uparrow} - a^{12*}_{\mathbf{k}} c_{-\mathbf{k}\downarrow} + a^{13*}_{\mathbf{k}}\hat{f}^{\dagger}_{\mathbf{k}\uparrow} - a^{14*}_{\mathbf{k}}\hat{f}_{-\mathbf{k}\downarrow} \\ \mu^{2}_{\mathbf{k}} = a^{21}_{\mathbf{k}} c^{\dagger}_{\mathbf{k}\uparrow} - a^{22}_{\mathbf{k}} c_{-\mathbf{k}\downarrow} + a^{23}_{\mathbf{k}}\hat{f}^{\dagger}_{\mathbf{k}\uparrow} - a^{24}_{\mathbf{k}}\hat{f}_{-\mathbf{k}\downarrow} \\ \mu^{3\dagger}_{\mathbf{k}} = a^{31*}_{\mathbf{k}} c^{\dagger}_{\mathbf{k}\uparrow} - a^{32*}_{\mathbf{k}} c_{-\mathbf{k}\downarrow} + a^{33*}_{\mathbf{k}}\hat{f}^{\dagger}_{\mathbf{k}\uparrow} - a^{34*}_{\mathbf{k}}\hat{f}_{-\mathbf{k}\downarrow} \\ \mu^{4}_{\mathbf{k}} = a^{41}_{\mathbf{k}} c^{\dagger}_{\mathbf{k}\uparrow} - a^{42}_{\mathbf{k}} c_{-\mathbf{k}\downarrow} + a^{43}_{\mathbf{k}}\hat{f}^{\dagger}_{\mathbf{k}\uparrow} - a^{44}_{\mathbf{k}}\hat{f}_{-\mathbf{k}\downarrow} \end{cases}. \tag{B.15}$$

From Eqs. (B.15), we obtain the representation of c and f operators in terms of the operators $\{\mu^i_{\mathbf{k}}\}$

$$\begin{cases} c^\dagger_{\mathbf{k}\uparrow} = b^{11}_{\mathbf{k}}\mu^{1\dagger}_{\mathbf{k}} + b^{12}_{\mathbf{k}}\mu^{2}_{\mathbf{k}} + b^{13}_{\mathbf{k}}\mu^{3\dagger}_{\mathbf{k}} + b^{14}_{\mathbf{k}}\mu^{4}_{\mathbf{k}} \\ c_{-\mathbf{k}\downarrow} = b^{21}_{\mathbf{k}}\mu^{1\dagger}_{\mathbf{k}} + b^{22}_{\mathbf{k}}\mu^{2}_{\mathbf{k}} + b^{23}_{\mathbf{k}}\mu^{3\dagger}_{\mathbf{k}} + b^{24}_{\mathbf{k}}\mu^{4}_{\mathbf{k}} \\ \hat{f}^\dagger_{\mathbf{k}\uparrow} = b^{31}_{\mathbf{k}}\mu^{1\dagger}_{\mathbf{k}} + b^{32}_{\mathbf{k}}\mu^{2}_{\mathbf{k}} + b^{33}_{\mathbf{k}}\mu^{3\dagger}_{\mathbf{k}} + b^{34}_{\mathbf{k}}\mu^{4}_{\mathbf{k}} \\ \hat{f}_{-\mathbf{k}\downarrow} = b^{41}_{\mathbf{k}}\mu^{1\dagger}_{\mathbf{k}} + b^{42}_{\mathbf{k}}\mu^{2}_{\mathbf{k}} + b^{43}_{\mathbf{k}}\mu^{3\dagger}_{\mathbf{k}} + b^{44}_{\mathbf{k}}\mu^{4}_{\mathbf{k}} \end{cases}, \tag{B.16}$$

which satisfy $\sum_j |b^{ij}_{\mathbf{k}}|^2 = 1$. Substituting the above relations into the Hamiltonian (6.18), it can be rewritten as

$$\begin{aligned} \tilde{\mathcal{H}} &= \sum_{\mathbf{k},j=1}^{4} (-1)^{j-1} E^j_{\mathbf{k}} \mu^{j\dagger}_{\mathbf{k}} \mu^j_{\mathbf{k}} + \sum_{\mathbf{k}} \left[\tilde{\varepsilon}_{\mathbf{k}} + \tilde{\omega}_{\mathbf{k}} - (E^1_{\mathbf{k}} + E^3_{\mathbf{k}}) \right] + \sum_{\mathbf{k}} C_{\mathbf{k}} \\ &= \sum_{\mathbf{k}} \mathcal{E}^1_{\mathbf{k}} (\mu^{1\dagger}_{\mathbf{k}} \mu^1_{\mathbf{k}} + \mu^{2\dagger}_{\mathbf{k}} \mu^2_{\mathbf{k}}) + \sum_{\mathbf{k}} \mathcal{E}^2_{\mathbf{k}} (\mu^{3\dagger}_{\mathbf{k}} \mu^3_{\mathbf{k}} + \mu^{4\dagger}_{\mathbf{k}} \mu^4_{\mathbf{k}}) \\ &+ \sum_{\mathbf{k}} \left[\tilde{\varepsilon}_{\mathbf{k}} + \tilde{\omega}_{\mathbf{k}} - (\mathcal{E}^1_{\mathbf{k}} + \mathcal{E}^2_{\mathbf{k}}) \right] + \sum_{\mathbf{k}} C_{\mathbf{k}}, \end{aligned} \tag{B.17}$$

where, $\mathcal{E}^{1,2}_{\mathbf{k}} = \left[(u_{\mathbf{k}} \pm \sqrt{\Phi_{\mathbf{k}}})/2 \right]^{1/2}$. $u_{\mathbf{k}}$ and $\Phi_{\mathbf{k}}$ are defined in (B.9). From Hamiltonian (B.17), the free energy can straightforwardly be evaluated, which is used to determine the superconducting pairing functions of all possible Cooper pairs in the EPAM.

Bibliography

[1] H. K. Onnes, Investigations into the properties of substances at low temperatures, which have led, amongst other things, to the preparation of liquid helium, Nobel Lecture.

[2] M. Tinhkham, Introduction to superconductivity, McGraw-Hill, 1996.

[3] V. L. Ginzburg, L. Landau, On the theory of superconductivity, Zh. Eksperim. i Teor. Fiz. 20 (1950) 1064.

[4] A. A. Abrikosov, On the Magnetic Properties of Superconductors of the Second Group, Soviet Physics JETP 5 (1957) 1174.

[5] J. Bardeen, L. N. Cooper, J. R. Schrieffer, Theory of Superconductivity, Phys. Rev. 108 (1957) 1175.

[6] J. G. Bednorz, K. A. Müller, Possible highTc superconductivity in the BaLaCuO system, Z. Phys. B 64 (1986) 189.

[7] F. Steglich, J. Aarts, C. D. Bredl, W. Lieke, D. Meschede, W. Franz, H. Schäfer, Superconductivity in the Presence of Strong Pauli Paramagnetism: $CeCu_2Si_2$, Phys. Rev. Lett. 43 (1979) 1892.

[8] N. D. Mathur, F. M. Grosche, S. R. Julian, I. R. Walker, D. M. Freye, R. K. W. Haselwimmer, G. G. Lonzarich, Magnetically mediated superconductivity in heavy fermion compounds, Nature 394 (1998) 39.

[9] R. Movshovich, T. Graf, D. Mandrus, J. D. Thompson, J. L. Smith, Z. Fisk, Superconductivity in heavy-fermion $CeRh_2Si_2$, Phys. Rev. B 53 (1996) 8241.

[10] F. Thomas, J. Thomasson, C. Ayache, C. Geibel, F. Steglich, Precise determination of the pressure dependence of T_c in the heavy-fermion superconductor $CeCu_2Si_2$, Physica B 186-188 (1993) 303.

[11] A. T. Holmes, A. Demuer, D. Jaccard, Resistivity and AC-Calorimetric Measurements of the Superconducting Transition in $CeCu_2Si_2$ Under Very High Hydrostatic Pressure in a Helium-Filled Diamond Anvil Cell, Acta Phys. Pol. B 34 (2003) 567.

[12] A. T. Holmes, D. Jaccard, K. Miyake, Signatures of valence fluctuations in $CeCu_2Si_2$ under high pressure, Phys. Rev. B 69 (2004) 024508.

[13] D. Jaccard, H. Wilhelm, K. Alami-Yadri, E. Vargoz, Magnetism and superconductivity in heavy fermion compounds at high pressure, Physica B 259-261 (1999) 1.

[14] B. Bellarbi, A. Benoit, D. Jaccard, J. M. Mignot, H. F. Braun, High-pressure valence instability and T_c maximum in superconducting $CeCu_2Si_2$, Phys. Rev. B 30 (1984) 1182.

[15] Y. Onuki, R. Settai, K. Sugiyama, T. Takeuchi, T. C. Kobayashi, Y. Haga, E. Yamamoto, Recent Advances in the Magnetism and Superconductivity of Heavy Fermion Systems, J. Phys. Soc. Jpn. 73 (2004) 769.

[16] H. Q. Yuan, F. M. Grosche, M. Deppe, C. Geibel, G. Sparn, F. Steglich, Observation of Two Distinct Superconducting Phases in $CeCu_2Si_2$, Science 302 (2003) 2104.

[17] A. Onodera, S. Tsuduki, Y. Ohishi, T. Watanuki, K. Ishida, Y. Kitaoka, Y. Onuki, Equation of state of $CeCu_2Ge_2$ at cryogenic temperature, Solid State Communications 123 (2002) 113.

[18] T. M. Rice, K. Ueda, Gutzwiller method for heavy electrons, Phys. Rev. B 34 (1986) 6420.

[19] K. Miyake, H. Maebashi, Huge Enhancement of Impurity Scattering due to Critical Valence Fluctuations in a Ce-Based Heavy Electron System, J. Phys. Soc. Jpn. 71 (2002) 1007.

[20] A. T. Holmes, Exotic Superconducting Mechanisms in Fe and $CeCu_2Si_2$ under Pressure, Ph.D. thesis, University of Geneva (2004).

[21] Y. Onishi, K. Miyake, Enhanced Valence Fluctuations Caused by f-c Coulomb Interaction in Ce-Based Heavy Electrons: Possible Origin of Pressure-Induced Enhancement of Superconducting Transition Temperature in $CeCu_2Ge_2$ and Related Compounds, J. Phys. Soc. Jpn. 69 (2000) 3955.

[22] S. Watanabe, M. Imada, K. Miyake, Superconductivity Emerging near Quantum Critical Point of Valence Transition, J. Phys. Soc. Jpn. 75 (2006) 043710.

[23] C. M. Varma, S. Schmitt-Rink, Charge transfer excitations and superconductivity in ionic metals, Solid State Communications 62 (1987) 681.

[24] M. Grilli, R. Raimondi, C. Castellani, C. D. Castro, G. Kotliar, Superconductivity, phase separation, and charge-transfer instability in the $U = \infty$ limit of the three-band model of the CuO_2 planes, Phys. Rev. Lett. 67 (1991) 259.

[25] D. S. Hirashima, Y. Ono, T. Matsuura, Y. Kuroda, Charge Fluctuation and Superconductivity in the d- p Model, J. Phys. Soc. Jpn. 61 (1992) 649.

[26] K. Miyake, O. Narikiyo, Y. Onishi, Superconductvity of Ce-based heavy fermions under pressure: Valence fluctuation mediated pairing associated with valence instability of Ce, Physica B 259-261 (1999) 676.

[27] A. T. Holmes, D. Jaccard, K. Miyake, Valence Instability and Superconductivity in Heavy Fermion Systems, J. Phys. Soc. Jpn. 76 (2007) 051002.

[28] Y. Saiga, T. Sugibayashia, D. Hirashima, Valence instability in an extended periodic Anderson model, Physica B: Condensed Matter 403 (2008) 808.

[29] T. Sugibayashi, Y. Saiga, D. S. Hirashima, Charge Fluctuations and Superconductivity in an Extended Periodic Anderson Model: A Weak Coupling Theory, J. Phys. Soc. Jpn. 77 (2008) 024716.

[30] K. W. Becker, A. Hübsch, T. Sommer, Renormalization approach to many-particle systems, Phys. Rev. B 66 (2002) 235115.

[31] A. Hübsch, K. W. Becker, Valence transition in the periodic Anderson model, Eur. Phys. J. B 52 (2006) 345.

[32] A. Mai, V. N. Phan, K. W. Becker, Application of the Continuous Projector based Renormalization method to the Periodic Anderson model, to be published.

[33] A. Hübsch, S. Sykora, K. W. Becker, Projector-based renormalization method (PRM) and its application to many-particle systems, to be published.

[34] K. S. Burch, S. V. Dordevic, F. P. Mena, A. B. Kuzmenko, D. van der Marel, J. L. Sarrao, J. R. Jeffries, E. D. Bauer, M. B. Maple, D. N. Basov, Optical signatures of momentum-dependent hybridization of the local moments and conduction electrons in Kondo lattices, Phys. Rev. B 75 (2007) 054523.

[35] S. Danzenbächer, Y. Kucherenko, D. V. Vyalikh, M. Holder, C. Laubschat, A. N. Yaresko, C. Krellner, Z. Hossain, C. Geibel, X. J. Zhou, W. L. Yang, N. Mannella, Z. Hussain, Z.-X. Shen, M. Shi, L. Patthey, S. L. Molodtsov, Momentum dependence of 4f hybridization in heavy-fermion compounds: Angle-resolved photoemission study of $YbIr_2Si_2$ and $YbRh_2Si_2$, Phys. Rev. B 75 (2007) 045109.

[36] D. Khomskii, A. Kocharjan, Virtual levels, mixed valence phase and electronic phase transitions in rare-earth compounds, Solid State Communications 18 (1976) 985.

[37] A. Hewson, P. Riseborough, An exact limit of a local mixed valence model, Solid State Communications 22 (1977) 379.

[38] I. Singh, A. K. Ahuja, S. K. Joshi, Role of hybridization in phase transition in the Falicov-Kimball model, Solid State Communications 34 (1980) 65.

[39] K. W. Becker, S. Sykora, V. Zlatic, Static and dynamic properties of the spinless Falicov-Kimball model, Phys. Rev. B 75 (2007) 075101.

[40] F. Wegner, Flow-equations for Hamiltonians, Ann. Physik 3 (1994) 77.

[41] S. D. Głazek, K. G. Wilson, Renormalization of Hamiltonians, Phys. Rev. D 48 (1993) 5863.

[42] S. D. Głazek, K. G. Wilson, Perturbative renormalization group for Hamiltonians, Phys. Rev. D 49 (1994) 4214.

[43] A. Hübsch, K. W. Becker, Renormalization of the electron-phonon interaction: a reformulation of the BCS-gap equation, Eur. Phys. J. B 33 (2003) 391–396.

[44] S. Sykora, A. Hübsch, K. Becker, Analytical approach to the quantum-phase transition in the one-dimensional spinless Holstein model, Eur. Phys. J. B 51 (2006) 181.

[45] A. Hübsch, K. Becker, Renormalization of the periodic Anderson model: an alternative analytical approach to heavy fermion behavior, Phys. Rev. B 71 (2005) 155116.

[46] P. Coleman, New approach to the mixed-valence problem, Phys. Rev. B 29 (1984) 3035.

[47] S. Sykora, A. Hübsch, K. Becker, Dominant particle-hole contributions to the phonon dynamics in the spinless one-dimensional Holstein model, Europhys. Lett. 76 (2006) 644.

[48] P. W. Anderson, A poor man's derivation of scaling laws for the Kondo problem, J. Phys. C: Solid State Phys. 3 (1970) 2436.

[49] P. W. Anderson, Localized Magnetic States in Metals, Phys. Rev. 124 (1961) 41.

[50] P. Farkaovsk, Falicov-Kimball model and the problem of valence and metal-insulator transitions, Phys. Rev. B 51 (1995) 1507.

[51] P. Lemberger, Segregation in the Falicov-Kimball model, J. Phys. A: Math. Gen. 25 (1992) 715.

[52] N. W. Ashcroft, N. D. Mermin, Solid State Physics, Brooks Cole, 1976.

[53] H. Fröhlich, Interaction of Electrons with Lattice Vibrations, Proc. R. Soc. London A 215 (1952) 291.

[54] S. Sykora, A. Hübsch, K. W. Becker, Coexistence of superconductivity and charge-density waves in a two-dimensional Holstein model at half-filling, to be published.

[55] N. N. Bogoliubov, On a new method in the theory of superconductivity, Nuovo Cim. 7 (1958) 794.

[56] K. Miyake, New trend of superconductivity in strongly correlated electron systems, J. Phys.: Condens. Matter 19 (2007) 125201.

[57] D. Manske, Theory of unconventional superconductors: Cooper-pairing Mediated by Spin-Excitations, Springer-Verlag, 2004.

[58] D. Manske, I. Eremin, K.-H. Bennemann, Theory for electron-doped cuprate superconductors: d-wave symmetry order parameter, Phys. Rev. B 62 (2000) 13922.

[59] I. Eremin, E. Tsoncheva, A. V. Chubukov, Signature of the nonmonotonic d-wave gap in electron-doped cuprates, Phys. Rev. B 77 (2008) 024508.

[60] H. Yoshigama, D. S. Hirashima, Angular Dependence of the Superconducting Order Parameter in Electron-doped High-Temperature Superconductors, J. Phys. Soc. Jpn. 73 (2004) 2057.

[61] X.-S. Ye, J.-X. Li, Asymmetric d-wave superconducting gap in orthorhombic high-T_c superconductors, Phys. Rev. B 76 (2007) 174503.

[62] U. Fano, Effects of Configuration Interaction on Intensities and Phase Shifts, Phys. Rev. 124 (1961) 1866.

Acknowledgements

I would like to express my sincerest appreciation and deep gratitude to my thesis advisor, Prof. Klaus W. Becker. I am greatly indebted to what he has done for me. He concerned not only on my work but also on my life during staying in Dresden. He did always encourage and help me step by step overcome various problems to accomplish my PhD thesis.

I am grateful to Mrs. Gudrun Latus for her kindly help as soon as the first day I came to Institute for theoretical physics, Dresden University of Technology. Without her help, I could not concentrate on my work properly.

I wish to thank all my colleagues in the Institute for theoretical physics, Dresden University of Technology, for their timely help and friendly atmosphere. Specially, I am grateful to: Mr. Alexander Mai for his sharing numerical tricks, friendly discussions; Dr. Arnd Huebsch, Dr. Steffen Sykora, Dr. Dietmar Lehmann, and Dr. Dmitri Efremov for their useful discussions.

Also, I would like to take this opportunity to thank all my colleagues in the Institute of Physics and Electronic, Hanoi-Vietnam and Vietnamese friends in Dresden for their encouragements and assistances during the time living far from home.

Most importantly, this work is dedicated to the memory of my grandfather, grandmother. I wish to express my gratitude to my parents, brother, sister, and Nguyen Thi Ha for their love, care, patience and encouragement, without that the thesis could not be finished on time.

Finally, I would like to thank the International Max-Planck Research School "Dynamical Processes in Atoms, Moleculars and Solids" for the financial support of this work.

Diese Arbeit wurde unter der Betreuung von Herrn Prof. Klaus W. Becker am Institut für Theoretische Physik der Technischen Universität Dresden angefertigt.

Versicherung

Hiermit versichere ich, dass ich die vorliegende Arbeit ohne unzulässige Hilfe Dritter und ohne Benutzung anderer als der angegebenen Hilfsmittel angefertigt habe; die aus fremden Quellen direkt oder indirekt übernommenen Gedanken sind als solche kenntlich gemacht. Die Arbeit wurde bisher weder im Inland noch im Ausland in gleicher oder ähnlicher Form einer anderen Prüfungsbehrde vorgelegt.

Dresden, 05.02.2009

Phan Van Nham